Spring 2010

Synthesis of transition-metal polyphosphides

Brian Michael Barry
University of Iowa

SYNTHESIS OF TRANSITION-METAL POLYPHOSPHIDES

by

Brian Michael Barry

An Abstract

Of a thesis submitted in partial fulfillment
of the requirements for the Doctor of
Philosophy degree in Chemistry
in the Graduate College of
The University of Iowa

May 2010

Thesis Supervisor: Associate Professor Edward G. Gillan

ABSTRACT

This dissertation describes the synthesis of several transition-metal polyphosphides including orthorhombic FeP_2, cubic CoP_3, cubic NiP_2, monoclinic PdP_2 and monoclinic CuP_2. The investigation of these materials was initiated by the discovery of MP_x formation upon reacting a metal halide with molecular yellow P_4 in superheated toluene. When these MP_x products were annealed at moderate temperatures (350-500 °C), crystalline phosphorus-rich phases were produced. We found that these phases have been previously synthesized from high-temperature elemental reactions and that low temperature routes to these phase-pure polyphosphides using at least one non-elemental source were not found in the literature. The absence of low-temperature, "bottom up" routes to these materials encouraged us to investigate our initial findings further, as such methods provide unique chemical and structural flexibility in materials synthesis.

Metal-rich counterparts to the aforementioned polyphosphides have been successfully produced via molecular solvothermal reactions. These reports consistently used an excess of phosphorus in their reactions but still afforded metal-rich products, and often produced materials with a combination of metal-rich and phosphorus-rich phases. These routes show the inability to dial in the phosphorus content of the produced MP_x phases and so they were unable to use balanced stoichiometry to rationalize the chemistry, and rarely attempted to identify reaction byproducts. This prompted us to design a synthesis in which discrete amounts of a phosphorus reagent could be used to target specific compositions and phases and allow for byproduct identification.

In order to determine reaction byproducts, a metal halide and yellow P_4 were reacted in together without solvent in sealed ampoules. The clear liquid byproduct was identified as PCl_3 or PBr_3, indicating that stoichiometric and balanced reactions were possible. In these reactions, metal halides and phosphorus (red or yellow) were balanced such that the chloride was ideally removed has PCl_3 and any remaining phosphorus was

used to form targeted, phase-pure MP_x phases. Using this stoichiometry in solid-state reactions, all of the aforementioned polyphosphide phases were synthesized as phase pure products at moderate temperatures (500-700 °C). By pelletizing the metal halide reagents in reactions with yellow P_4 or by co-pelletizing the metal halide with red phosphorus, porous pellet products reminiscent of the reagent pellet could be afforded.

The reaction stoichiometries used in solid-state reactions were adapted to solvothermal reactions. In these reactions, amorphous MP_x products were synthesized from metal halides and yellow P_4 in various solvents (superheated toluene, 1-octadecene and hexadecane), and upon annealing (350-500 °C), targeted phase -pure CoP_3, NiP_2 and CuP_2 were produced. Reactions substituting red phosphorus for yellow P_4 in hexadecane reactions also yielded the same crystalline phases.

Solvothermal reactions were modified by the addition of Lewis base surfactants that led to lower reaction temperatures and in certain systems afforded nanoparticles (10-30 nm). In these reactions, a metal acetylacetonate or halide was complexed with a Lewis base, activating the metal halide or acetylacetonate bond and increasing their solubility and reactivity with yellow P_4. The Lewis-base surfactants also acted to stunt particle growth. These systems afforded phase-pure NiP_2 and CuP_2 nanoparticles for the first time. In some cases, crystalline MP_2 was produced directly from the solvothermal reaction.

Abstract Approved: _____
Thesis Supervisor

_____
Title and Department

_____
Date

SYNTHESIS OF TRANSITION-METAL POLYPHOSPHIDES

by

Brian Michael Barry

A thesis submitted in partial fulfillment
of the requirements for the Doctor of
Philosophy degree in Chemistry
in the Graduate College of
The University of Iowa

May 2010

Thesis Supervisor: Associate Professor Edward G. Gillan

Graduate College
The University of Iowa
Iowa City, Iowa

CERTIFICATE OF APPROVAL

_____

PH.D. THESIS

_____

This is to certify that the Ph.D. thesis of

Brian Michael Barry

has been approved by the Examining Committee
for the thesis requirement for the Doctor of Philosophy
degree in Chemistry at the May 2010 graduation.

Thesis Committee: _____
Edward G. Gillan, Thesis Supervisor

_____
Johna Leddy

_____
F. Christopher Pigge

_____
Jan-Uwe Rohde

_____
John W. Schweitzer

To Mom and Dad

ACKNOWLEDGMENTS

I would first and foremost like to thank Ed. He has gone above and beyond to impart his knowledge of chemistry to me, and I owe my growth as a chemist primarily to him. Ed was always, kind, patient and thorough, and always had an open door. The gratitude that I have for the support that he has given me through the years cannot easily be expressed, but I humbly say thank you so much.

Next I would like to thank my family for always being there for me and believing in me. Mom and Dad, I could not have managed getting to this point with out your support and unconditional love. Hugh John, Pat and Sean I want to thank you all for being the best group of brothers anyone could have. I am so grateful to have three unique brothers that all put in things into perspective for me in their own way.

I would also like to thank the following current and former group members: Dale, C.J., Sujith, James, Miller, Andrew and Nate. I would especially like to thank James for being a great friend and roommate; I have missed sportscoat Fridays for some time now. I would also like to thank Miller for his contibutions to my research and I would like to wish him the best as he continues his graduate career.

I would also like to thank the following people for their help over the years: Dale Swenson for maintaining the XRD machine that I used just a little, Peter Hatch for his great help with all of my glass needs, Randy, Jean and Jonas for the help they gave me with microscopy, Tim and Andy for their help in procuring chemicals in a timely fashion, and to Santana and Robert for their help with NMR.

The following professors I would like to thank for being great teachers as well: Darrell, Russell, Jan-Uwe, Ned, Norb, and Lou. I have learned a great deal from each of you.

Lastly I would like to thank Shonda, Brian, and Earlene for being great co-workers, I enjoyed working with each of you thoroughly. Sharon, Janet, and Betty I

would like to thank for taking care of all of the paperwork through the years, everything always went without hiccups and that has been invaluable.

ABSTRACT

This dissertation describes the synthesis of several transition-metal polyphosphides including orthorhombic FeP_2, cubic CoP_3, cubic NiP_2, monoclinic PdP_2 and monoclinic CuP_2. The investigation of these materials was initiated by the discovery of MP_x formation upon reacting a metal halide with molecular yellow P_4 in superheated toluene. When these MP_x products were annealed at moderate temperatures (350-500 °C), crystalline phosphorus-rich phases were produced. We found that these phases have been previously synthesized from high-temperature elemental reactions and that low temperature routes to these phase-pure polyphosphides using at least one non-elemental source were not found in the literature. The absence of low-temperature, "bottom up" routes to these materials encouraged us to investigate our initial findings further, as such methods provide unique chemical and structural flexibility in materials synthesis.

Metal-rich counterparts to the aforementioned polyphosphides have been successfully produced via molecular solvothermal reactions. These reports consistently used an excess of phosphorus in their reactions but still afforded metal-rich products, and often produced materials with a combination of metal-rich and phosphorus-rich phases. These routes show the inability to dial in the phosphorus content of the produced MP_x phases and so they were unable to use balanced stoichiometry to rationalize the chemistry, and rarely attempted to identify reaction byproducts. This prompted us to design a synthesis in which discrete amounts of a phosphorus reagent could be used to target specific compositions and phases and allow for byproduct identification.

In order to determine reaction byproducts, a metal halide and yellow P_4 were reacted in together without solvent in sealed ampoules. The clear liquid byproduct was identified as PCl_3 or PBr_3, indicating that stoichiometric and balanced reactions were possible. In these reactions, metal halides and phosphorus (red or yellow) were balanced such that the chloride was ideally removed has PCl_3 and any remaining phosphorus was

used to form targeted, phase-pure MP_x phases. Using this stoichiometry in solid-state reactions, all of the aforementioned polyphosphide phases were synthesized as phase pure products at moderate temperatures (500-700 °C). By pelletizing the metal halide reagents in reactions with yellow P_4 or by co-pelletizing the metal halide with red phosphorus, porous pellet products reminiscent of the reagent pellet could be afforded.

The reaction stoichiometries used in solid-state reactions were adapted to solvothermal reactions. In these reactions, amorphous MP_x products were synthesized from metal halides and yellow P_4 in various solvents (superheated toluene, 1-octadecene and hexadecane), and upon annealing (350-500 °C), targeted phase -pure CoP_3, NiP_2 and CuP_2 were produced. Reactions substituting red phosphorus for yellow P_4 in hexadecane reactions also yielded the same crystalline phases.

Solvothermal reactions were modified by the addition of Lewis base surfactants that led to lower reaction temperatures and in certain systems afforded nanoparticles (10-30 nm). In these reactions, a metal acetylacetonate or halide was complexed with a Lewis base, activating the metal halide or acetylacetonate bond and increasing their solubility and reactivity with yellow P_4. The Lewis-base surfactants also acted to stunt particle growth. These systems afforded phase-pure NiP_2 and CuP_2 nanoparticles for the first time. In some cases, crystalline MP_2 was produced directly from the solvothermal reaction.

TABLE OF CONTENTS

LIST OF TABLES

LIST OF FIGURES

CHAPTER 1

INTRODUCTION AND BACKGROUND

1.1 Extended Solid State Materials: An Introduction to the Field

This section will briefly describe the different general types of known solid materials classified in a very general manner by structural or physical properties; while I may generalize a material group as exhibiting a certain property or characteristic, there are often exceptions to such broad property descriptions. Emphasis in this chapter is placed on details about the considerations that must be made when examining inorganic, extended solid state materials, particularly with respect to the materials that will be the focal point of this thesis. This chapter begins with a broad scope of the solid-state field and successive sections will narrow the scope, concluding with a description of transition-metal polyphosphides and phosphorus, which are the central focus of this thesis.

Solid state chemistry encompasses the study of the synthesis, structure and physical properties of solid materials. Solids may be molecular in nature, where discrete molecules composed of covalently bonded atoms, typical for organic compounds, are held together by weak intermolecular forces such as hydrogen bonds or van der Waals forces. These weak interactions are revealed in their physical properties as they have relatively low melting or sublimation temperatures. In contrast, extended solid state materials, typically inorganic, are non-molecular and have interatomic forces that extend in up to three dimensions. These interatomic forces are much stronger than their intermolecular counterparts and may include covalent, ionic or metallic bonding; as such, these solids typically have higher melting temperatures than molecular solids.

Inorganic, solid-state materials have bonding that spans a spectrum from ionic to covalent to metallic. At the ionic extreme of the spectrum, the atoms' electrons are

confined to the atoms' orbits and exhibit little overlap with neighboring atoms, albeit the atoms' orbits may be polarized to point towards a neighboring atom. The classic example of an ionic solid is NaCl. These atoms' valence electrons follow the octet rule such that they take on noble gas configurations. Because of this, the individual atoms are ionized, either having more or less electrons than protons depending on where the atom appears on the periodic table. These materials rely on electrostatic attractions to maintain structural integrity. Ionic solids are often electrically insulating materials with large optical band gaps due to the localization of the valence electrons.[1]

On the other end of the spectrum lie solids with metallic bonding, which include metals and metal alloys. In these materials the atoms live in a "sea of electrons." The valence electrons of these materials have the freedom to move easily through the crystal structure from atom to atom. Because of this high mobility, these materials are good electric conductors. The individual atoms in simple metals are roughly neutral in charge, meaning that, over time, the average number of electrons residing within that atoms' orbits is the same as the number of protons the atom possesses. These materials do not have an optical band gap and usually absorb in the infrared region.[1]

Covalent solids, with directional bonding and slightly polar or non-polar bonds, lie somewhere between metals and ionic solids. Many electrical semiconductors fall into this class of solid-state structures. These compounds can contain covalent bonds, as in silicon or germanium, in which neighboring atoms share valence electrons. Elements with covalently bonded networks generally contain non-polar bonds. Semiconductors can alternatively be comprised of a mixture of atoms, the most common of these materials are known as 13-15 semiconductors, GaAs being an example. These types of semiconductors have polarized bonds and their atoms are commonly described as having partially ionized or polar-covalent bonds. The degree of polarization is manifested in the size of the material's optical band gap; lower ionicity or polarity and high covalent overlap leads to smaller band gaps, while higher ionicity or polarity with little to no

covalent overlap leads to larger band gaps. Semiconductors may also have a combination of bonding, for instance a covalently-bonded, infinite anionic network may be paired with cations regularly dispersed throughout, leading to both covalent and partially ionic bonds in the extended structure.[2]

Because semiconductors fall with in a wide range between ionic and metallic and have a large diversity of bonding moieties, they offer a varied array of properties that may be tuned for specific needs. They may be tuned by varying composition, as is evident in doped materials or solid solutions.[3] They may also be tuned when the crystal size is reduced into the nanometer regime and quantum confinement effects are operative. This effect allows for properties to be altered simply by changing the size of the crystal and number of interacting atoms, and is a phenomenon that is partially responsible for driving the "nano"-materials movement that we see in the scientific community today.[4-6]

Semiconductors are used in many applications, most notably in electronics, but also in photovoltaics, recording media, catalysis, and ceramics to name a few. The potential of this class of materials is extensive, and the opportunity for improvement and new material discovery drives the scientific study of these materials.

1.2 Metal/Non-Metal Binary Phases

Many inorganic materials are composed of a mixture of a metal and a non-metal atoms, and are called binary phases as they contain two constituents. The metal can be a main group metal like Ga, or a transition-metal like Fe, and the non-metal is typically a chalcogen (O, S, Se, Te), pnictogen (N, P, As) or carbon. Within this class of binary solids are some of the most technologically useful and capable materials to date. Transition-metal oxides represent a class of compounds which have found utility in many different areas. For example, titanium dioxide (TiO_2), one of the most diverse oxide semiconductors, is a widely used pigment in both paints and cosmetics.[7] It is also used in photoinduced processes where light energy is absorbed, creating energy-rich electron-

hole pairs[8] that can be used electrically (solar cells)[9] or chemically (photocatalysis).[10] Another significant material is cobalt oxide, which forms the anode material in current Li-ion batteries that are present in most modern laptop computers and cell phones.[11]

Other prominent metal chalcogenides include 12-16 semiconductors which are comprised of Zn, Cd or Hg and S, Se or Te, as in CdSe for example. Since these compounds contain larger anions and more covalency than their oxide counterparts, their band gaps are reduced and they are able to absorb visible light. Their band gaps may also be tuned by reducing the particle size of these crystalline phases into the nanoregime (< *ca.* 20 nm);[4] nearly all work on these materials is performed targeting nanocrystals. Nanocrystalline particles of these phases, also known as quantum dots, show promise as materials for nanoelectronics[4] and for visible-light absorbers in photovoltaic cells.[12] Since these nanoparticles are able to form aqueous colloidal solutions when coated with hydrophilic capping ligands, they are also at the forefront of bioimaging and biosensing.[13,14]

Metal nitrides are another class of binary compounds which have made their mark in society as ceramic and catalytic materials. For example, TiN is used as a hard protective coating in many industrial settings due to its thermal stability, hardness, low friction coefficient and good adhesion to substrates.[15] The main-group nitrides, Si_3N_4 and BN, have low compressibility and high hardness making them ideal for cutting and grinding applications.[16,17] GaN and InN are used as visible and ultraviolet light emitting diodes in the field of optoelectronics.[18,19] Nitrides of Mo and W can adsorb and activate hydrogen allowing them to catalytically react with nitrogen and sulfur-containing compounds found in crude transportation fuels, which form undesirable byproducts when combusted.[20] It is clear that the diversity of properties and applications for metal nitrides and other metal/non-metal binary phases is vast and have been well-examined. Another class of binary, metal pnictides are comprised of metal phosphides. These will be discussed in more detail below as they are a major synthetic focus of this thesis.

1.3 Metal Phosphides

There are over 170 known binary phases of metal phosphides and they have compositions that range from metal-rich to phosphorus-rich (~M_6P to MP_4).[21] This range is, to a large extent, derived from phosphorus' ability to exist as isolated anions or larger polyphosphide network anions with direct P-P bonding.[22] These binary phosphides are split into three classes; metal-rich (MP_x where $x<1$), monophosphides (MP_x where $x=1$) and polyphosphides (MP_x where $x>1$). The wide range in composition, along with the fact that phosphides will form with almost all metals, make for a diverse class of metal/non-metal binary materials. Because of their variety of compositions and structures, phosphides exhibit a wide array of magnetic and electric properties. For instance, metal-rich phosphides such as Ni_2P are typically metallic,[23] while main-group monophosphides such as InP and GaP are semiconductors (E_g= 1.25 and 2.25 eV respectively) and polyphosphides such as FeP_2 are often small bandgap semiconductors (E_g= 0.4 eV).[24] The phosphides, particularly those of transition-metals with d orbital valence electrons, can show a variety of magnetic properties as well. For instance, Fe_2P is ferromagnetic, Mn_2P is antiferromagnetic, Ni_2P is paramagnetic and Re_2P_5 is diamagnetic.[25,26]

Because of their diverse properties, phosphides have attracted attention for many different applications. Although metal-rich phosphides' physical and chemical properties resemble those of carbides and nitrides, their crystal structures are quite different since phosphorus is larger than carbon and nitrogen. Their similar physical properties are demonstrated as they are also used as corrosion-resistant, oxidation-resistant, and wearproof materials.[27,28] However, phosphides are often more catalytically active than their carbide and nitride counterparts, which is attributed to their difference in structure.[29] The high stability and catalytic activity has made Ni_2P a strong candidate for a catalyst in the hydrodesulfurization of transportation fuels.[29,30] The efficiency of this process must be improved to keep up with the continually increasing restrictions on automotive

emissions. Another metal-rich phosphide, Cu_3P, is used industrially as a fine solder and is an important additive in metal alloys.[31]

Monophosphides also have utility in many different areas. For instance, GaP and InP are used in high-speed digital circuits and optoelectronic devices,[32] and are being explored as host lattices for dilute magnetic semiconductors in the field of spintronics.[33] Monophosphides frequently have useful magnetic properties as well; MnP is ferromagnetic below room temperature and is used for magnetic refrigeration, which can achieve temperatures below 1 K.[34] In magnetic recording media, the magnetically pinned regions are stabilized by being sandwiched between two antiferromagnetic layers, a property which, although they have not been reported as being utilized in this manner, is observed in YbP, UP and FeP.[35-37] Iron monophosphide (FeP) is also being investigated as a candidate for use as an anode material in Li-ion batteries.[38,39]

Transition-metal polyphosphides are typically small band-gap semiconductors or semimetals[22] and are often diamagnetic.[40,41,42] They also have interesting structures as their polyphosphide anions can be found in an array of forms. This class of materials encompasses the phases that are targeted in this thesis, as such the properties and structures of the target transition-metal polyphosphides will be discussed in further detail in the following section. The most common application that polypyhosphides are being investigated for is their capability as anode materials for Li-ion batteries. Some phases that have been investigated for this purpose so far are MoP_2,[43] CoP_3,[44,45] MnP_4,[46,47] FeP_2,[48,49] CuP_2,[50] NiP_2,[51,52] and ZnP_2[53] to name a few. CoP_3 has also shown promise for thermoelectric applications.[41,54-56] Since most of these materials have small band gaps, they may also be employed as IR-absorbers in photovoltaic cells; CuP_2 (E_g= 1.5 eV) has been investigated for this purpose.[57] It is apparent that polyphosphides and binary metal phosphides in general, have value in many different technological areas and are a worthwhile class of compounds to target for new and flexible synthetic methodology developments.

1.4 Introduction to the Target Phases: FeP_2, CoP_3, NiP_2, PdP_2 and CuP_2

This section will preview the principal phases that are targeted in this thesis, which is heavily focused on improved synthetic techniques towards these materials. Detailed backgrounds of previous syntheses will be presented in the introduction of subsequent chapters; however brief conventional methods will be mentioned here. Alternative phases are observed and discussed in the relevant chapters. Also, it should be noted that the five aforementioned phases are all targeted in the second chapter, but after that the focus will remain on CoP_3, NiP_2 and CuP_2.

Iron diphosphide (FeP_2) is a diamagnetic *n*-type semiconductor with a band gap of 0.37 eV.[58] Its unit cell is orthorhombic in the *Pnnm* space group with a marcasite-type structure, and has a density of 5.107 g/cm^3. The polyphosphide anions can be described as finite P_2^{4-} dumbbells. Bulk FeP_2 can be synthesized by first heating stoichiometric amounts of iron powder and red phosphorus in an evacuated, sealed ampoule to form a feedstock. This feedstock can then be used in a chemical transport reaction where the feedstock is kept at 880 °C and the growth zone at 865 °C with I_2 as the transport agent. This method takes a week to grow 0.5 mm single-crystals.[58]

Cobalt triphosphide (CoP_3) is a diamagnetic semiconductor with a band gap of 0.45 eV.[41] Its unit cell is cubic in the *Im*3 space group with a skutterudite-type structure, and has a density of 4.406 g/cm^3. The polyphosphide anions can be described as P_4^{4-}, nearly square-planar rings occupying 75% of the octahedral holes in the Co simple cubic sublattice. Bulk CoP_3 can be synthesized by a Sn flux method where stoichiometric amounts of cobalt powder and red phosphorus are heated with tin in an evacuated ampoule for one week at 780 °C.[56]

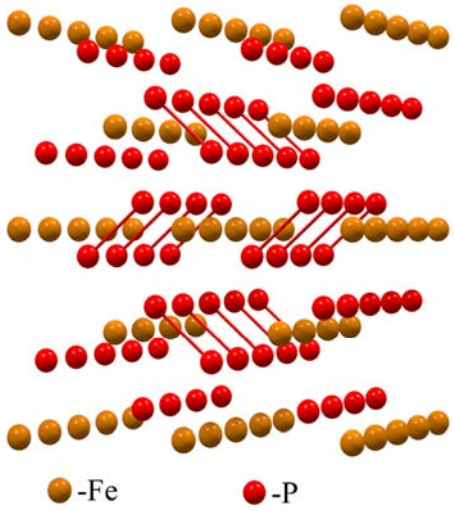

Figure 1.1 Structural representation of orthorhombic FeP_2.

There are two reported phases for nickel diphosphide (NiP_2), one being monoclinic,[59,60] and the other being cubic.[61] The phase that was synthesized in this work is the cubic, pyrite-type structure. It is important to note that the cubic, pyrite NiP_2 has been previously reported as the high-pressure phase[61,62] and was initially synthesized at 65 kbars and 1200 °C. Cubic NiP_2, with a density of 4.895 g/cm^3, has mixed reports as exhibiting weak Pauli paramagnetism,[61] or being diamagnetic.[40] The latter report states it is an *n*-type semiconductor with a band gap of 0.73 eV.[40] The polyphosphide anions can be described as finite P_2^{4-} dumbbells. Bulk, pyrite-type NiP_2 can be synthesized from a Sn flux method where stoichiometric amounts of nickel powder and red phosphorus are heated with tin in an evacuated ampoule for 15h at 1150 °C.[40]

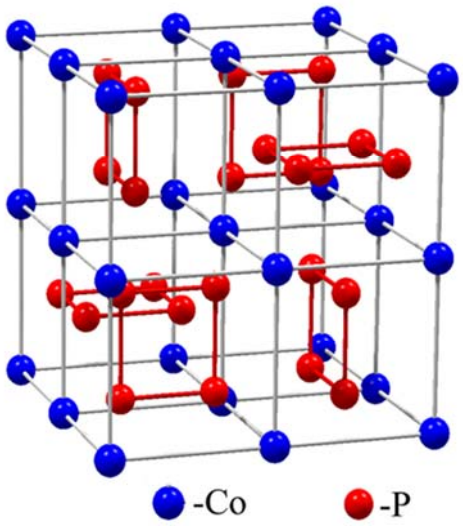

Figure 1.2 Structural representation of cubic CoP_3.

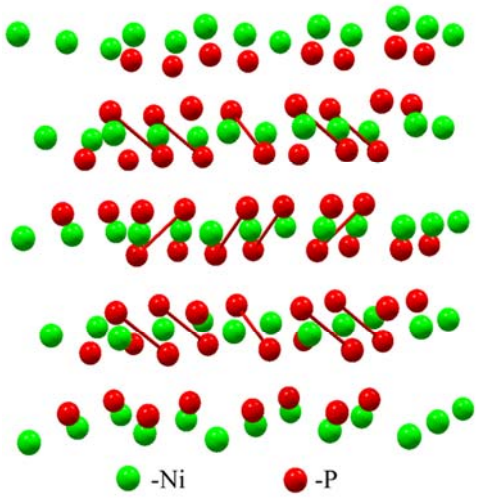

Figure 1.3 Structural representation of cubic NiP_2.

Palladium diphosphide (PdP_2) is a diamagnetic semiconductor with a band gap of 0.65 eV.[63] Its unit cell is monoclinic in the *I*2/*a* space group with a marcasite-type structure, and has a density of 5.640 g/cm^3. The polyphosphide anions can be described as infinite, zigzag, 1D chains. Bulk PdP_2 can be synthesized simply by heating a mixture palladium powder and red phosphorus in an evacuated ampoule at 800-1100 °C; unfortunately more detailed descriptions of the synthesis can not be found in the literature.[59]

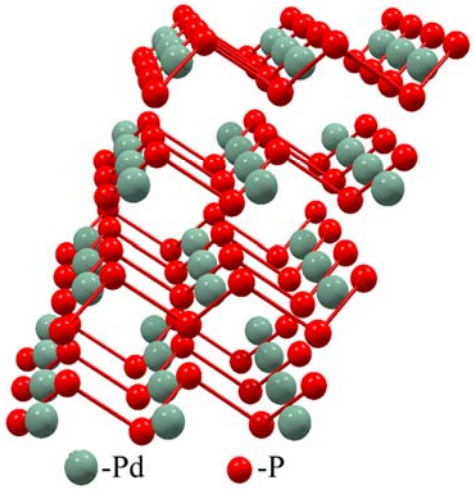

Figure 1.4 Structural representation of monoclinic PdP_2.

Copper diphosphide (CuP_2) is a diamagnetic *p*-type semiconductor with a band gap of 1.53 eV.[40] Its unit cell is monoclinic in the $P2_{1/c}$ space group with a unique crystal structure only observed for CuP_2 and AgP_2, and has a density of 4.306g/cm^3. The polyphosphide anions can be described as infinite, corrugated, 2D sheets of fused P_{10}^{5-} rings, and the copper exists as covalently bonded Cu-Cu dumbbells. Bulk CuP_2 can be synthesized by a chemical transport method in which a mixture of stoichiometric amounts of copper powder and red phosphorus are heated in a sealed ampoule with 50 mTorr of

Cl_2, which acts as the transporting agent. The mixture is kept at 815 °C while the growth zone is at 835 °C for one day.

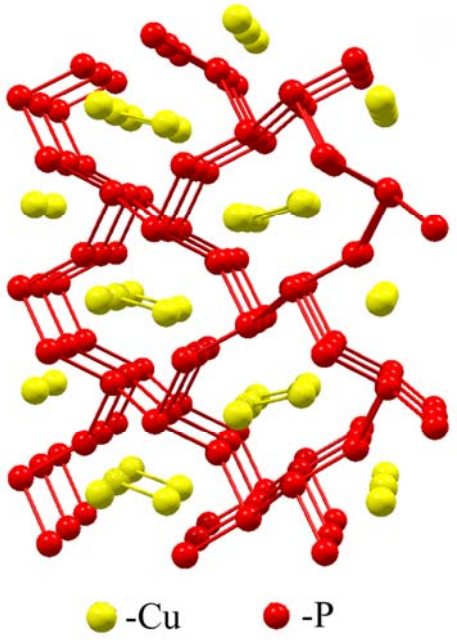

Figure 1.5 Structural representation of monoclinic CuP_2.

1.5 Elemental Phosphorus

In this section I would like to introduce elemental phosphorus as it is the major phosphorus source used in the syntheses that will be presented in this work. The discussion in this section is primarily taken almost exclusively from two books dedicated to phosphorus, one by John R. Van Wazer,[64] and the other by D.E.C. Corbridge.[21] this section includes some historical background on the element and then moves on to discuss the properties of the different allotropes and how they apply to our synthetic methods.

Phosphorus is element 15 on the periodic table and has an atomic weight of 30.97. It belongs to the Group 15 family along with nitrogen, arsenic, antimony and bismuth; this group is referred to as the pnictides or pnictogens. The chemistry of nitrogen and

phosphorus are by far the most important of the pnictides as they play important roles in life processes and in the environment. The chemistry of phosphorus, however, is far more similar to that of arsenic than that of nitrogen. The isotopic abundance of phosphorus is nearly all ^{31}P, which has a nuclear spin of ½ making it easily detectable by NMR techniques.

Elemental phosphorus was first discovered by Hennig Brand of Germany in 1669, who discovered it by distilling urine, thinking that the yellow appearance was attributed to the presence of gold. The substance would glow in the dark and burst into flames when exposed to air, a property which gave phosphorus its name, which means 'light bearing.' Urine remained the only source for obtaining the element for 100 years after its discovery, but by the 18th century the primary source became bones. In the early 1800's, strike matches were the main use of phosphorus, but were quickly replaced as the main use when it was found that elemental phosphorus could be converted into useful phosphate fertilizers. As the need for phosphorus grew in the agricultural sector, a more abundant source for phosphorus became desired. In Europe in 1850, phosphate minerals were found in ore and quickly replaced bones as the main source for industrial phosphorus.

There are three main allotropes of phosphorus: yellow (or white), red and black. These allotropes are successively denser and less reactive. The simplest form is yellow phosphorus, and was the form first discovered by Brand. Yellow phosphorus is molecular in nature and exists as a P_4 tetrahedron, with P-P bond lengths of 2.21 Å. When pure, this compound is colorless, but almost always appears yellow due to small amounts of polymerization between P_4 units caused by UV exposure.[65] Yellow phosphorus is a soft, waxy substance with a density of 1.83 g/cm^3 and is soluble in many non-polar organic solvents (e.g. hexanes, toluene). It has a melting point of 44 °C, a boiling point of 280 °C, and can be sublimed at room temperature under reduced

pressures. Yellow phosphorus is extremely reactive and will burst into flames on exposure to oxygen in air (Equation 1.1).

$$P_4 + 5\ O_2 \rightarrow P_4O_{10} \quad (1.1)$$

The high reactivity of P_4 can be attributed to the high ring strain in the tetrahedron, where the P-P-P bond angles are 60 °, and to the reactive lone pair on each phosphorus atom in the tetrahedron. These two features facilitate reactions by breaking labile P-P bonds or by coordinating to P_4 via the lone pairs. Extreme care must be taken when working with yellow phosphorus as it is highly toxic when ingested. Yellow phosphorus is stable when stored under water as it forms a P_4O_{10} coating by slowly reacting with dissolved O_2. Because of this coating, the surface must be removed to expose fresh P_4 prior to use. Reaction equipment must also be cleaned by oxidizing any P_4 residue with aqueous bleach. Yellow phosphorus is produced industrially by first reacting mineral phosphates from ore with silica forming P_4O_{10}, and then reducing P_4O_{10} with carbon (Equation 1.2)

$$2\ Ca_3(PO_4)_2 + 6\ SiO_2 \rightarrow 6\ CaSiO_3 + P_4O_{10} \quad (1.2a)$$

$$P_4O_{10} + 10\ C \rightarrow P_4 + 10\ CO \quad (1.2b)$$

Red phosphorus is a polymeric allotrope of phosphorus and is stable in air and far less reactive than yellow P_4. There are many forms of red phosphorus, most being crystalline but some are amorphous. The most common form of red phosphorus is crystalline and is comprised of infinite (1D), tubular chains. This form of red phosphorus is also referred to as violet phosphorus or Hittorf's phosphorus. It can be obtained by heating yellow phosphorus to temperatures above 260 °C in inert atmospheres. This form of phosphorus is insoluble in all organic solvents, and has a density of 2.36 g/cm^3. Polymeric red phosphorus will sublime at 416 °C, giving off P_4 vapor. This process can be used to obtain yellow phosphorus as it is no longer available commercially unlike red phosphorus. Yellow phosphorus is no longer available due to its use in the production of illicit drugs. On an interesting side note, the famous 'red spot' on Jupiter is likely due to the presence of red phosphorus.

Black phosphorus is the most thermodynamically stable form of phosphorus and exists in three different crystalline forms: orthorhombic, rhombohedral and cubic. It is insoluble, inert and practically non-flammable. It can be made by heating white or red phosphorus at high pressures (50-100 kbar) under an inert atmosphere. Orthorhombic black phosphorus can be described structurally as infinite (2D), double-layer sheets with P-P-P bond angles of 100 ° and is a flaky solid not unlike mica. At higher pressures, the orthorhombic phase can be converted to the slightly denser rhombohedral and cubic phases. The rhombohedral phase (density of 3.53 g/cm^3) consists of infinite (2D), corrugated sheets of fused P_6 rings, and is a semiconductor with a band gap of 0.34 eV. In the cubic phase (density 3.83 g/cm^3), all phosphorus atoms are in an octahedral environment with P-P-P bond angles of 90 °, forming a simple cubic lattice. Some structural representations of phosphorus are shown in Figure 1.6.

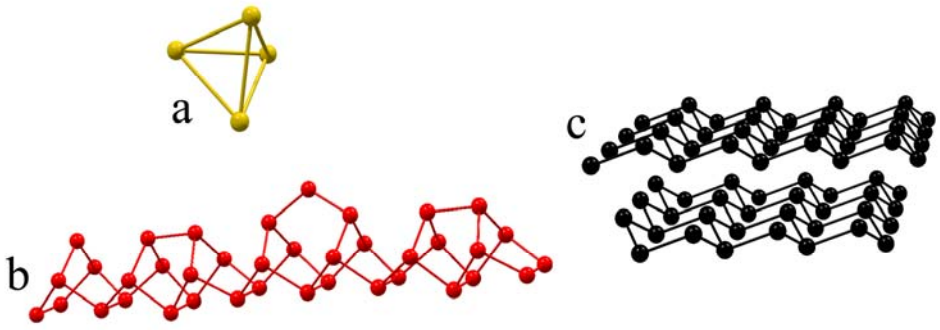

Figure 1.6 Structural representations of a) yellow P_4, b) red (Hittorf's) phosphorus and c) rhombohedral black phosphorus.

1.6 Thesis Synopsis

The following chapters will describe the synthesis and characterization of several transition-metal polyphosphides. These polyphosphides are synthesized in several ways, including a solid-state method (FeP_2, CoP_3, NiP_2, PdP_2 and CuP_2) and multiple

solvothermal routes (CoP_3, NiP_2 and CuP_2). The syntheses developed in this work provide significant advances in the production of polyphosphides. They introduce flexible, low-temperature routes that show the ability to discretely produce targeted polyphosphides. Previous works frequently produce a mixture of metal-rich and phosphorus-rich phases, unable to afford phase-pure products. This work will also reveal the production of nanosized particles for phases in which they have not been previously observed.

CHAPTER 2

A GENERAL AND FLEXIBLE, SOLVENT-FREE SYNTHESIS OF TRANSITION-METAL POLYPHOSPHIDES VIA PCl_3 ELIMINATION*

2.1 Introduction and Background

Traditional solid-state syntheses of metal/non-metal phases are performed by simply heating intimate mixtures of the elemental components at high temperatures in inert atmospheres or in fluxes. Transition-metal polyphosphides are no exception to this rule and have been successfully synthesized by either heating a mixture of the powdered metal and red phosphorus at high temperatures (700-1200 °C) in sealed ampoules under inert atmospheres, or at moderate temperatures for extended periods of time in tin fluxes (~550 °C, > 10 days).[40,66-68] They can also be made by heating the elements in the presence of a chemical transport agent (Cl_2 or I_2) in sealed ampoules (~600-800 °C).[40,68,69] Less conventional methods such as high energy ball-milling and high-pressure anvil syntheses have also been used to produce phosphorus-rich structures.[53,70,71] All of these routes lack morphological and size control and most require a large energy input and long reaction times.

Frequently elemental phosphide reactions require an excess of phosphorus to synthesize the desired phosphorus-rich phase.[66,68] Considering the variety of binary metal phosphide phases that exist, using non-stoichiometric amounts of reagents makes targeting phases with specific metal to phosphorus ratios problematic. And since these reaction techniques are typically performed at high-temperatures for long periods of time, the more thermodynamically stable phases are favored in the resulting product. To circumvent this problem, a lower temperature approach is desirable. If the reaction

* A majority of this work was recently published in *Chem. Mater.* **2009,** *21*(19) 4454-4461.

temperature is lowered, a more reactive metal source is required as elemental metals are relatively inert. Also, a stoichiometric reaction would be required in order to target specific polyphosphide phases.

This chapter describes the discovery of a simple, solvent-free, moderate-temperature, route to several phosphorus-rich structures (FeP_2, CoP_3, NiP_2, CuP_2, and PdP_2). This synthetic approach involves the direct thermal reaction of pellets of metal dichloride powders with P_4 vapor or the direct reaction of intimately mixed composite pellets containing red phosphorus and the metal chloride powders. It notably uses a compositionally simple and stoichiometric reaction to produce these metal phosphides, including a high-temperature/pressure NiP_2 phase. Both of these reaction strategies involve the evolution of a volatile PCl_3 byproduct and produce crystalline MP_x ($x \geq 2$) at moderate temperatures of 500-700 °C. The pellets remain intact throughout the synthesis and the macrostructure of the MP_x products resembles that of the reactant pellets. By varying the phosphorus source, the percentage of the pellet precursor mass that is retained in the final metal phosphide pellet products changes, which influences the morphology and microstructure of the final phosphide pellet.

2.2 Experimental Section

2.2.1 Metal phosphide syntheses using molecular yellow P_4

Metal halides used were anhydrous $FeCl_2$, $CoCl_2$, $NiCl_2$, $CuCl_2$, and $PdCl_2$ (Alfa-Aesar, 99.5%, 99.7%, 98.0%, 98.0%, and 99.9% respectively), the only other reagent used was elemental white/yellow P_4 (Aldrich, stick, yellow phosphorus 99^+% stored in water). Low level impurities in white P_4 frequently give it a light yellow appearance. These impurities have been ascribed to traces of polymeric red phosphorus that form on exposure to UV light.[65] All metal halides were dried under dynamic vacuum at 250 ºC

for a minimum of four hours to remove any adsorbed water and stored in an argon-filled glovebox prior to use. Schlenk flasks loaded with sticks of yellow P_4 were briefly evacuated (2 min.) and then loaded into the glovebox. Yellow P_4 can sublime at room temperature and low pressures so care must be taken to avoid its sublimation into vacuum systems.

In each experiment, the metal dichloride was ground with an agate mortar and pestle in an argon-filled glovebox and then pressed into 2 or 3 cylindrical pellets (7 mm diameter and 2-3 mm thick) using a standard KBr die set. The pellets were carefully ejected from the steel collars and weighed. In a typical NiP_2 reaction, a total mass of $NiCl_2$ pellets was targeted as 156 mg (1.2 mmol). Other reactions were typically conducted with ~1-1.5 mmol of metal halide. The pellets were then loaded into a Pyrex or silica tube that was sealed on one end (12 mm O.D., 9 mm I.D. and ~30 cm in length) being careful not to disrupt the pellet integrity as they were positioned at the closed end of the ampoule. Yellow P_4 was prepared by first shaving off any noticeable oxidized surface material with a razor blade and then cutting off an appropriate amount of P_4 from the stick (99 mg or 0.8 mmol P_4 for a NiP_2 experiment using 1.2 mmol of $NiCl_2$). The MCl_2:P_4 ratios were chosen such that all chloride forms a PCl_3 byproduct and all remaining phosphorus is used to form the metal phosphide (MCl_2:P_4 molar ratios are 3:2 for MP_2 and 3:2.75 for MP_3). The pieces of P_4 were then added to the tube containing the pellets. The open end of the glass tube was fitted with a Cajon connector and a closed Kontes needle valve, removed from the glovebox, and attached to a Schlenk line. The precursor-containing end of the tube was vertically submerged in liquid N_2 and then evacuated to ~80 mTorr. Liquid N_2 cooling was required to prevent P_4 from subliming

away during evacuation and altering the reagent stoichiometry. After a short (~2 min.) evacuation, the tube was sealed to a length of ~10 cm with a methane-oxygen torch. Light tapping was used to assure that the pellets at one end of the sealed ampoule were not touching each other. This ampoule was carefully placed in the center of a horizontal tube furnace and the two ends of the furnace are stuffed with glass wool cloth to prevent heat loss and minimize undesirable temperature gradients across the ampoule. The ampoule was then heated linearly over 3 h to 500-700 °C and held there ~40 h. With the furnace still at its maximum temperature, the empty end of the ampoule was carefully moved to the cooler outside opening of the furnace, leaving the pellet-containing end in the furnace. The ampoule was left in this state for ~20 min to allow the PCl_3 byproduct to condense in the cool end of the ampoule. The ampoule was then cooled to room temperature outside the furnace at an angle such that the pellets and the PCl_3 remain separated. The ampoule was then gently scored and cracked open, being careful to avoid the liquid PCl_3 from contacting the pellets. The isolated product pellets were stored in the glovebox.

2.2.2 Metal phosphide syntheses using red phosphorus

Metal halides used were the same as described in the previous section, the only other reagent used was red phosphorus (Aldrich, powder, 99%). In an argon-filled glovebox, stoichiometric amounts of the metal halide and red phosphorus (MCl_2:P molar ratio is 3:8 for MP_2 and 3:11 for MP_3) were thoroughly ground together with an agate mortar and pestle. This powder mixture was then pressed into 2 or 3 cylindrical pellets (7 mm diameter and 2-3 mm thick) using a standard KBr die set. The pellets were ejected from the steel collars and weighed. In a typical NiP_2 reaction, the total composite pellet

mass was targeted as 250 mg, consisting of 153 mg (1.17 mmol) of $NiCl_2$ and 97 mg (3.13 mmol) of red phosphorus. The pellets were then loaded into Pyrex or silica tubes that were sealed on one end (12 mm O.D., 9 mm I.D. and ~30 cm in length), being careful not to disrupt the pellet integrity as they were positioned at the closed end of the tube. The tube was then sealed in the same manner described in the previous section except that no liquid N_2 was required. The evacuated ampoule's orientation in the furnace, the PCl_3 separation, and product pellet isolation and storage were all performed in the same manner described in the previous section. The heating profiles for the PdP_2, CuP_2, and NiP_2 were also the same as described in the previous section. To limit metal halide attack on ampoule walls, the higher temperature CoP_3 and FeP_2 reactions were performed using slower linear heating ramps over 12 h to 600 and 700 °C, respectively, and were held at those temperatures for 40 h.

Safety Notes. Molecular yellow P_4 is stable when stored under water; however it is very pyrophoric and burns with a flame immediately on contact with oxygen/air. Care should be taken to work with this material in small quantities and to carefully clean all experimental equipment of phosphorous residue by oxidizing it with aqueous bleach. One must also calculate the ideal internal pressure that could be produced from the moles of PCl_3 gas produced in the sealed ampoule at the maximum reaction temperature. In this work, calculated gas pressures below 10 atm did not result in ampoule explosions.

2.2.3 Product characterization

Solution ^{31}P NMR of the liquid byproducts in C_7D_8 was performed on a 400 MHz Bruker DRX-400. An external reference sample of H_3PO_4 ($\delta = 0.0$ ppm) was used for calibration. The phase and crystallinity of the products were analyzed by powder X-ray

diffraction (XRD) using a Siemens D5000 diffractometer (Cu K_α radiation) for the Cu, Ni, and Pd samples. The Fe and Co samples can absorb Cu K_α X-rays resulting in low intensity peaks and an unacceptable fluorescence background, so a Rigaku MiniFlex II diffractometer with a Co K_α radiation souce was used for the Fe and Co samples. The two theta values for all data are plotted based on Cu K_α radiation for consistency. Standard patterns were generated by inputting known crystallographic data into the PowderCell computer program.[72, 73] Thermogravimetric-differential thermal analysis (TG-DTA) was run on a Seiko Exstar 6300 system in alumina pans under argon flow with a 10 °C/min heating rate. Very small samples (< 5 mg) were used as gaseous P_4 is generated that can react with and corrode platinum components of the TGA system. SEM analyses were performed on a Hitachi S-4800 on pellet shards affixed to aluminum sample stubs with carbon paint. Elemental analyses were performed on a Hitachi S-3400N with EDS capabilities. Bulk elemental analysis of selected samples was performed using ICP-AE spectroscopy (Varian ICP-OES 720-ES). Samples were first dissolved in hot concentrated HNO_3 and then diluted with D.I. H_2O to 5% HNO_3 by volume.

2.3 Results and Discussion

2.3.1 Metal phosphide formation via PCl_3 elimination

In this study, we investigated the direct reaction of metal dichlorides (M = Fe, Co, Ni, Cu, and Pd) with either gaseous molecular yellow P_4 or with solid polymeric red phosphorus in sealed, evacuated glass ampoules. In the molecular P_4 reactions, the metal chloride was finely ground and formed into lightly pressed pellets. In the red phosphorus reactions, the metal chloride and the red phosphorus were ground together and pressed

into well-mixed composite pellets. In contrast to most prior metal phosphide precursor reactions, the chemical exchange reactions in this research study were *stoichiometrically balanced* such that all chlorine was ideally removed as PCl_3 and any remaining phosphorus (yellow P_4 or red phosphorus) formed the metal phosphide product.

$$3MCl_2 + (2 + 3x)\ P \rightarrow 3MP_x + 2\ PCl_3 \qquad (2.1)$$

The evacuated sealed ampoules were slowly heated in a tube furnace to maximum temperatures ranging from 500-700 °C. Optimal maximum reaction temperatures were determined as the temperature necessary to crystallize the products within ~2 days. For example, CuP_2 and NiP_2 will crystallize at 350 °C; however, durations of 4 days were required for reaction completion (see Table 2.1 for reaction temperatures). The higher temperature red phosphorus reactions targeting FeP_2 and CoP_3 at 600 °C and 700 °C, respectively, required a slower heating ramp (12 h) versus all other experiments (3 h) because ampoule etching and silica contamination in the phosphide products was observed when a 3 h ramp was used. The synthesis of FeP_2 and CoP_3 from yellow P_4 did not show evidence of SiO_2 contamination or etching even with the faster heating ramp, likely due to the high reactivity of yellow P_4 compared to red phosphorus. Our working hypothesis is that reactions with red phosphorus are incomplete after a fast 3 hr ramp and unreacted metal halide can attack the silica ampoule resulting in SiO_2 contamination in the product pellets. By slowing the heating ramp, the metal halide is given the needed time to completely react with red phosphorus, which prevents its high temperature reaction with the ampoule.

In all reactions, the metal chloride or metal chloride/phosphorus composite pellets showed a distinct color change to grey/black by 250 °C, indicating initial phosphorus

reaction with the metal halide. When one end of the ampoule was pulled out of the 250 °C furnace, a small amount of colorless liquid condensed at the cool end, indicating that PCl_3 formation was beginning. After the reactions were finished, the identity of the clear liquid byproduct was determined to be PCl_3 in all reactions by ^{31}P NMR (δ 220 ppm). We also detected some $POCl_3$ in all ^{31}P NMR spectra (δ -2.25 ppm), which is not surprising as the PCl_3 is briefly in contact with air during its separation from the pellet product and can oxidize by reacting with O_2.

Pressed reagent pellets were utilized to demonstrate this approach's ability to form microstructured metal phosphide monoliths though vapor infiltration or intimate solid-state reactions between the powdered metal halide and phosphorus reagents. The integrity of the pellets was retained when the metal chloride was converted to its corresponding metal phosphide and the overall size and shape of the pellet was unchanged (~7 mm diam. before and after reaction). Phosphide product pellets from the yellow P_4 reactions appear silver with a metallic luster, with the exception of the yellow P_4 CuP_2 reaction that produced a slightly expanded pellet with a rough flakey surface. In contrast, the pellets from the red phosphorus reactions appear black and matted (Figure 2.1). This difference in pellet appearance is attributed to the increase in voids in the red phosphorus products because of significant loss in pellet mass during the reaction. The pellets from the yellow P_4 reactions forming MP_2 from MCl_2 exchange two chlorines (~71 amu) for two phosphorus atoms (~62 amu) resulting in a minimal net loss in pellet weight; except in the CoP_3 case, where the product pellet is slightly heavier than the initial $CoCl_2$ pellet. In contrast, the red phosphorus reactions eliminate PCl_3 from the pellets leading to significantly greater net pellet mass loss than in the corresponding

yellow P_4 reactions because red phosphorus is part of the pellet's initial mass (see Table 2.1). For example, the ideal CuP_2 pellet's product mass, assuming complete reaction, as a percentage of initial starting pellet mass is 93.3 % for a yellow P_4 reaction and only 57.8 % for a red phosphorus reaction. Table 2.1 pellet product mass data is consistent with essentially quantitative conversion for each reaction studied (assuming phosphide product pellets), indicating that the ideal proposed reactions in Eq. 2.1 is efficiently taking place in these phosphide syntheses. Chemical yields can also be seen in Table 2.1.

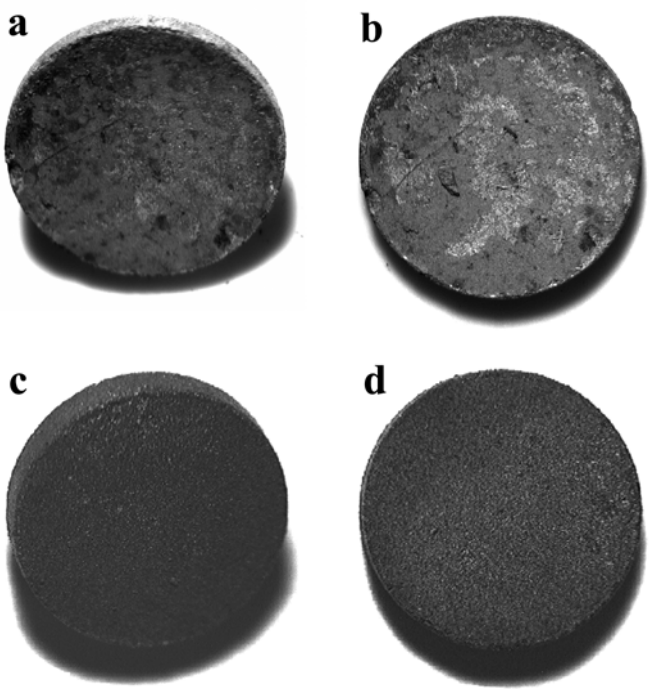

Figure 2.1 Optical micrographs of MP_x product pellets of (a) CoP_3 synthesized from yellow P_4, (b) NiP_2 synthesized from yellow P_4, (c) PdP_2 synthesized from red phosphorus, and (d) CuP_2 synthesized from red phosphorus. Product pellet diameters from all reactions were 7.0 mm ± 0.5 mm.

Table 2.1 Phosphorus-Rich MP_x Synthesis and Product Analysis.

target phase	P source	reaction temp. (°C)	% of orig. mass[a](yield %)[b]	MP_x analysis (M:P:Cl)[c]	TGA decomp. temp. (°C)[d]
FeP_2	yellow P_4	700	92.0 (99%)	1:2.00:<0.01	735 (828)
FeP_2	red P	700	56.3 (97%)	1:1.98:<0.01	750 (849)
CoP_3	yellow P_4	600	117 (100%)	1:3.06:<0.01	815 (920)
CoP_3	red P	600	62.4 (100%)	1:2.79:<0.01	780 (876)
NiP_2	yellow P_4	500	95.9 (103%)	1:2.00:0.01	595 (660)
NiP_2	red P	500	59.7 (105%)	1:1.89:0.04	575 (660)
CuP_2	yellow P_4	500	93.3 (100%)	1:1.96:0.01	555 (647)
CuP_2	red P	500	57.2 (99%)	1:1.83:0.03	520 (627)
PdP_2	yellow P_4	500	94.9 (100%)	1:2.16:0.01	770 (865)
PdP_2	red P	500	66.1 (102%)	1:2.17:0.02	760 (874)

[a]Experimental results for: (product pellet mass)/(reagent pellet mass) x 100. [b]Yield based on MCl_2 used in accordance with eq. 2.1. [c]Molar ratios from EDS data. [d]Data from TG-DTA analysis, decomposition temperature onset (temperature of 10% weight loss).

2.3.2 Phase determination and elemental analysis

Upon cooling, the pellet containing ampoules were carefully cracked to avoid PCl_3 contact with the final pellets. The pellets were analyzed with no further processing or workup to avoid potential surface reactions. Powder XRD patterns of ground pellets were taken to determine the bulk crystalline phases contained in each product pellet (Figure 2.2). The patterns revealed the presence of the crystalline phosphides corresponding to compositions targeted in Eq. 2.1 for both the yellow P_4 and red phosphorus reactions: specifically, orthorhombic FeP_2,[72] cubic CoP_3,[72] cubic NiP_2,[72] monoclinic CuP_2,[72] and monoclinic PdP_2.[73] The cubic NiP_2 phase was obtained in both the yellow P_4 and red phosphorus reactions, which is unexpected since this structure is

not commonly observed and has previously been described as a high temperature and high-pressure phase (1200 °C, 6.5 GPa).[61] The ambient pressure form of NiP_2 is the monoclinic structure, which is closely related to the PdP_2 phase observed in this work.[59]

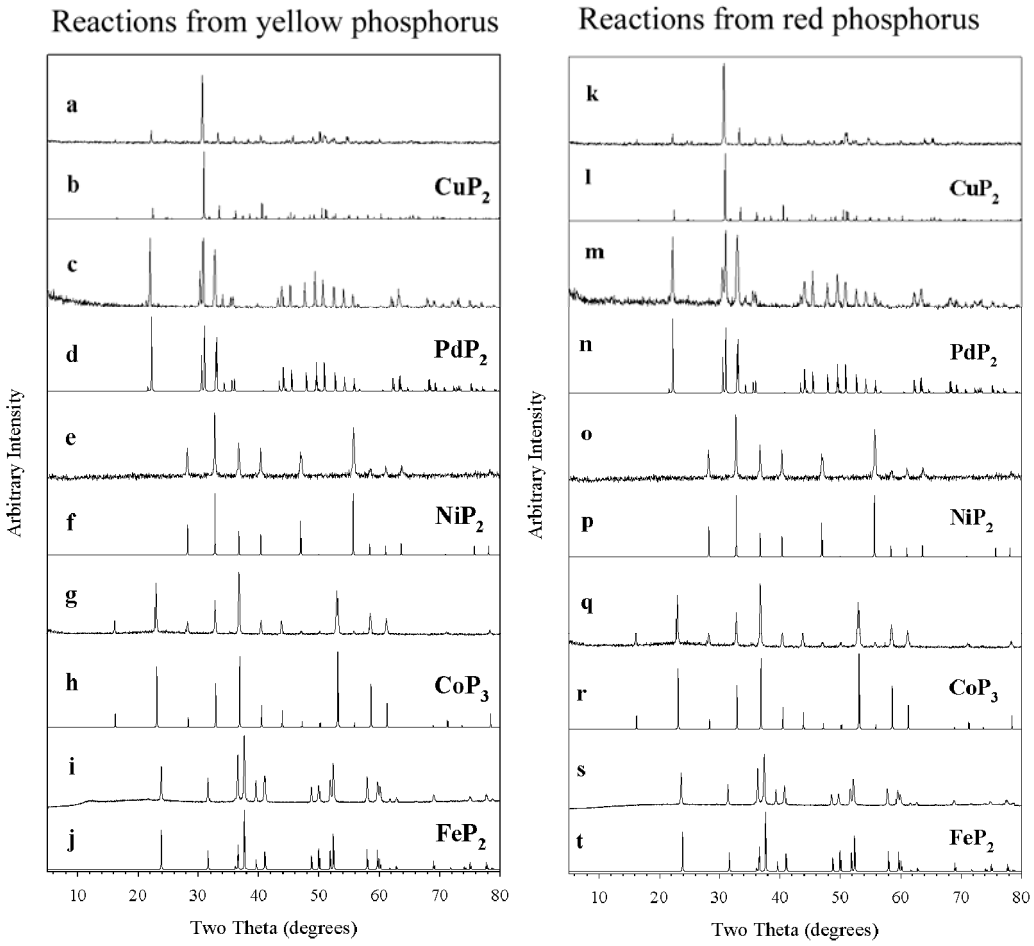

Figure 2.2 Experimental XRD patterns for MP_x products from both the yellow P_4 and red phosphorus reactions: (a, k) monoclinic CuP_2, (c, m) monoclinic PdP_2, (e, o) cubic NiP_2, (g, q) cubic CoP_3, and (i, s) orthorhombic FeP_2. The patterns just below each of the experimental patterns (b, d, f, h, j, l, n, p, r and t) are the calculated patterns for the respective phase.

Energy dispersive spectroscopy (EDS) analysis of the isolated metal phosphides revealed that products had M:P molar ratios near their expected 1:2 or 1:3 values and little or no detectable chlorine residue (Table 2.1). Products from yellow P_4 reactions targeting Cu, Ni, and Co phosphides have slightly higher phosphorus contents than their red phosphorus counterparts, which may indicate more efficient phosphorus incorporation using yellow P_4 in these reactions. Bulk ICP-AE elemental analysis of the CuP_2 and NiP_2 from reactions with red phosphorus revealed the M:P ratios to be 1:1.848 and 1: 2.020 respectively which confirmed the EDS M:P molar ratio results. The bulk weight percentages of Ni and P in the NiP_2 sample were found to be 44.9 and 47.9% respectively, accounting for 92.8 % of the total pellet mass. The remaining weight may be due to oxygen from surface oxidation. The bulk weight percentages of Cu and P in the CuP_2 sample were found to be 52.0 and 46.8 % respectively accounting for 98.8% of the total pellet mass. This result may indicates that little oxidation has occurred in this sample.

2.3.3 Phosphide pellet morphologies

Each phosphide pellet from the syntheses outlined in Table 2.1 has distinct morphological features as determined by scanning electron microscopy (SEM). For example, the CuP_2 product from the red phosphorus reaction is comprised of similarly-shaped, fused, faceted polyhedra which range in size from 10-20 μm along their longest edge (Figures 2.3a and 2.4b). A lower magnification view of a cross-section of the CuP_2 product from red phosphorus can be seen in Figure 2.4a. The CuP_2 product from the yellow P_4 reaction consists of large faceted domains that contain sharp crags and pinholes scattered on their surface (Figures 2.3b and 2.4d). The yellow P_4 product appears to have less void space than CuP_2 from red phosphorus, consistent with earlier discussion of pellet mass loss being larger for the red phosphorus composite reagent pellets. A lower

magnification view of a fragment of a CuP_2 product from yellow phosphorus shows the aforementioned large faceted domains with sizes ranging from 50-200μm (Figure 2.4c).

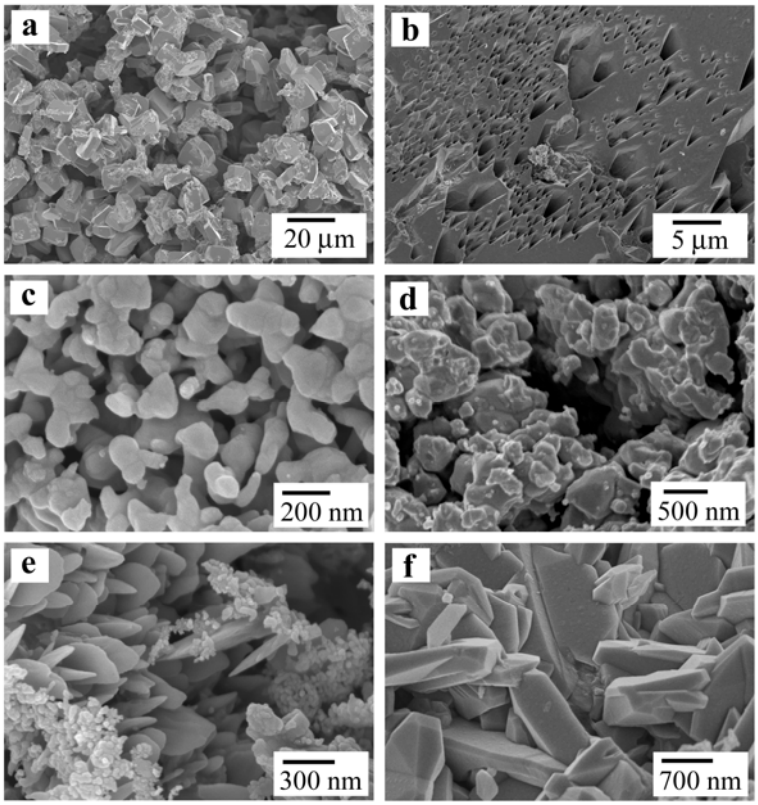

Figure 2.3 SEM images of (a) CuP_2 synthesized from red phosphorus, (b) CuP_2 synthesized from yellow P_4, (c) NiP_2 synthesized from red phosphorus, (d) NiP_2 synthesized from yellow P_4, (e) PdP_2 synthesized from red phosphorus, and (f) FeP_2 synthesized from yellow P_4.

The NiP_2 products from red phosphorus and yellow P_4 reactions both consist of fused masses of irregular particles with smooth surfaces and features ranging from 50-200 nm for the red phosphorus product to larger 100-600 nm sizes for the yellow P_4 product (Figures 2.3c, d). Lower magnification images of NiP_2 from both red phosphorus and yellow P_4 can be seen in Figure 2.5 and clearly show that the particle domains from

the red phosphorus reactions are much smaller than from the yellow P_4 product counterparts.

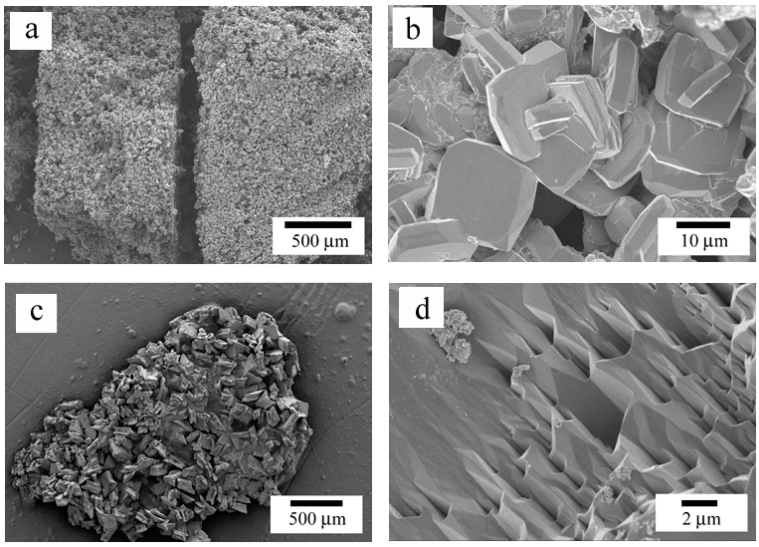

Figure 2.4 SEM images of CuP_2 synthesized from red phosphorus at low magnification (a) and high magnification (b), and of CuP_2 synthesized from yellow P_4 at low magnification (c) and high magnification (d)

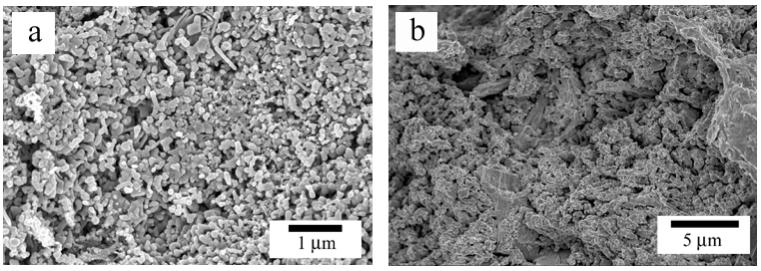

Figure 2.5 Low magnification SEM images of NiP_2 from red phosphorus (a) and yellow P_4 (b).

The PdP_2 pellet synthesized from red phosphorus shows fused clusters of spherical particles ranging from ~20-300 nm in size along with thin plates (~30 nm in

thickness and ~ 500 nm in diameter) that appear to be growing from the fused spherical particles (Figure 2.6a). Figure 2.3e shows a slightly higher magnification image, showing the plates more clearly. The PdP_2 products from yellow P_4 reactions have a variety of morphologies; the most common feature can be described as irregular, fused, smooth particles which range in size from 100-500 nm (Figure 2.6b, c), and the other, more interesting, feature is the appearance of rods (~100nm in diameter and ~2 μm in length) that are growing on the surface of a larger mass (Figure 2.6d).

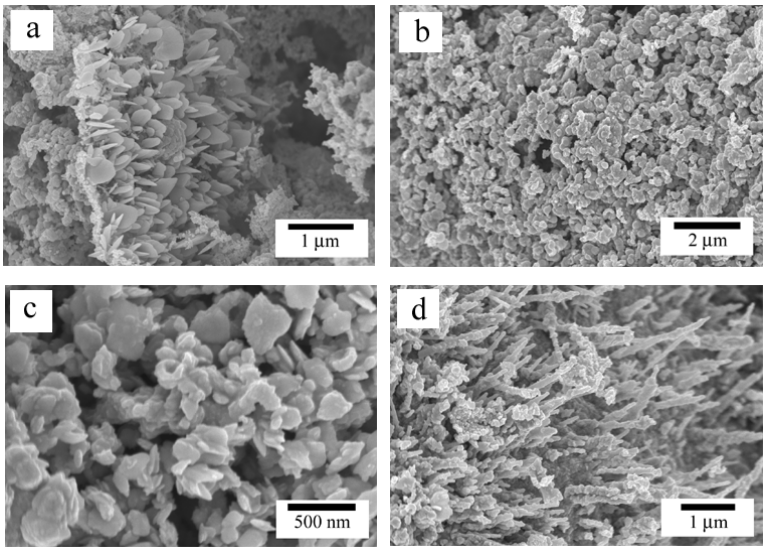

Figure 2.6 SEM images of PdP_2 from red phosphorus (a) and from yellow P_4 (b, c, and d).

The FeP_2 products from both the yellow and red phosphorus reactions contained fused, faceted large particles with a variety of shapes and sizes (submicron to ~5μm, Figures 2.3f and 2.7a). Images of a cross-sectioned pellet of FeP_2 from yellow P_4 at low and high magnifications can be seen in Figure 2.10b and 2.10c respectively. When comparing the particle sizes in products from the red phosphorus and yellow P_4 (Figures

2.3f and 2.7c respectively) it is clear to see that the red phosphorus products yield smaller faceted particles.

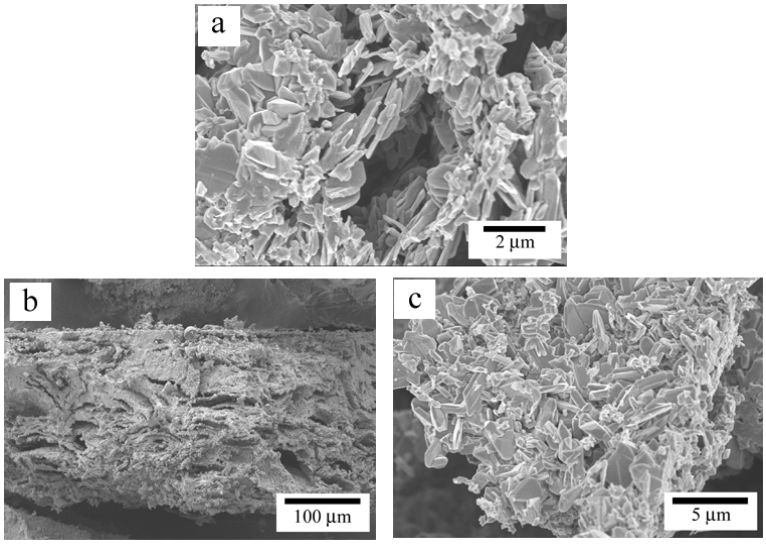

Figure 2.7 SEM images of FeP_2 from red phosphorus (a) and yellow P_4 (b and c).

The CoP_3 product from yellow P_4 is different from the other reactions in that the pellet gains weight during the reaction, which leads to a pellet with no visible voids (Figures 2.8a) and smooth fused surface features at various magnifications (Figure 2.9a, b). In contrast, the CoP_3 product from red phosphorus has smooth, fused, particle-like features ranging from 150-500 nm in size (Figures 2.8b and 2.9c). When the CoP_3 reaction with yellow P_4 was performed at a lower 500 °C temperature and held for only one day as opposed to two, the product is morphologically different. This CoP_3 product pellet, which consists of poorly crystalline CoP_3 by XRD analysis, has a clear morphological contrast between the pellet crust and its interior (Figures 2.8c,d). Under a continuous surface, there are numerous fused rod-shaped particles (~400 nm in diameter

by 2 μm in length). When these pellets are heated at 600 °C for 1 additional day, they convert to a non-porous, solid mass similar to that shown in Figure 2.8a.

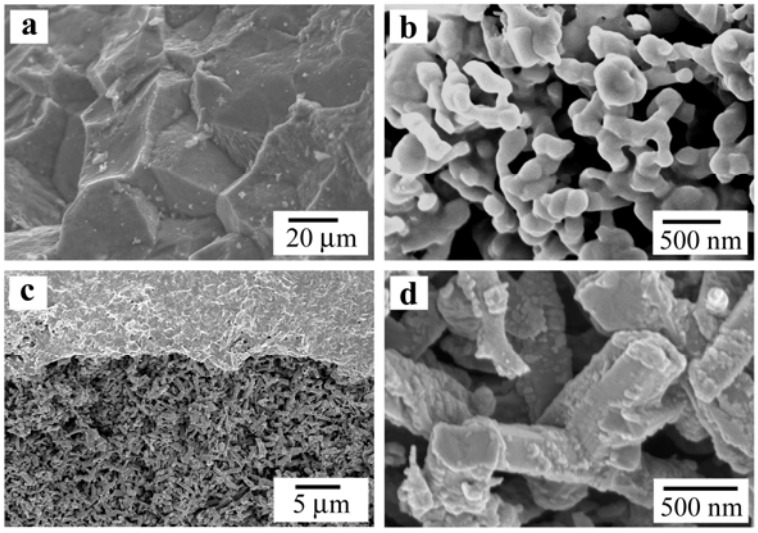

Figure 2.8 SEM images of (a) CoP_3 synthesized from yellow P_4 at 600 °C for 2d, (b) CoP_3 synthesized from red phosphorus at 600 °C for 2d, and (c, d) CoP_3 synthesized from yellow P_4 at 500 °C for 1d.

Although control of pellet porosity was not targeted in this study, even the visibly porous pellets appear to have interconnected structures. As a qualitative test, all phosphide pellets register a measurable 2-probe resistance value across the pellet surface (~10 Ω to 300 Ω), indicating the presence of conducting interparticle pathways. The exceptions were the CuP_2 samples that showed higher ~20-80 kΩ values. This may be a result of CuP_2 having a semiconducting band gap (E_g = 1.5 eV)[74] that is twice that of any of the other phosphides in this study.[42,56,58,75]

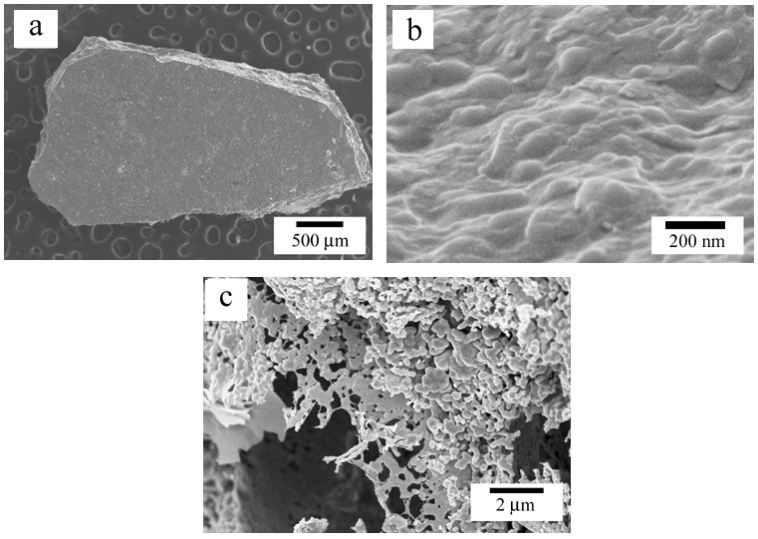

Figure 2.9 Additional SEM images of CoP_3 synthesized from yellow P_4 (a and b) and red phosphorus (c) at 600°C.

2.3.4 Metal phosphide thermal stabilities

The thermal stability of each phosphide product was studied by thermogravimetric-differential thermal analysis (TG-DTA). The samples were heated up to 1000 °C under an argon flow and their decomposition temperatures are listed in Table 1 as estimated weight loss onset and 10% weight loss temperatures (Figure 2.10). All sample weights after TG-DTA decomposition were greater than those expected if the samples decomposed to the metallic elements, suggesting that the remaining products were metal-rich phosphides. When feasible, the TG-DTA residue was analyzed by XRD. XRD data showed that FeP_2 and CoP_3 decomposed to FeP and CoP respectively, with theoretical weight losses for these transformations that were in good agreement with the experimental results (26.3% and 40.8% for FeP_2 and CoP_3).

Since TG-DTA utilizes an argon flow and our synthetic conditions are static vacuum, an experiment was conducted to determine if the phosphorus-rich pellets decompose in evacuated ampoules at temperatures similar to the TG-DTA results.

Pellets of CuP_2 and NiP_2 from red phosphorus were resealed in evacuated silica ampoules (similar size and furnace orientation as described for phosphide synthesis) and heated to 600 and 650 °C, respectively, for ~ 15 hrs.

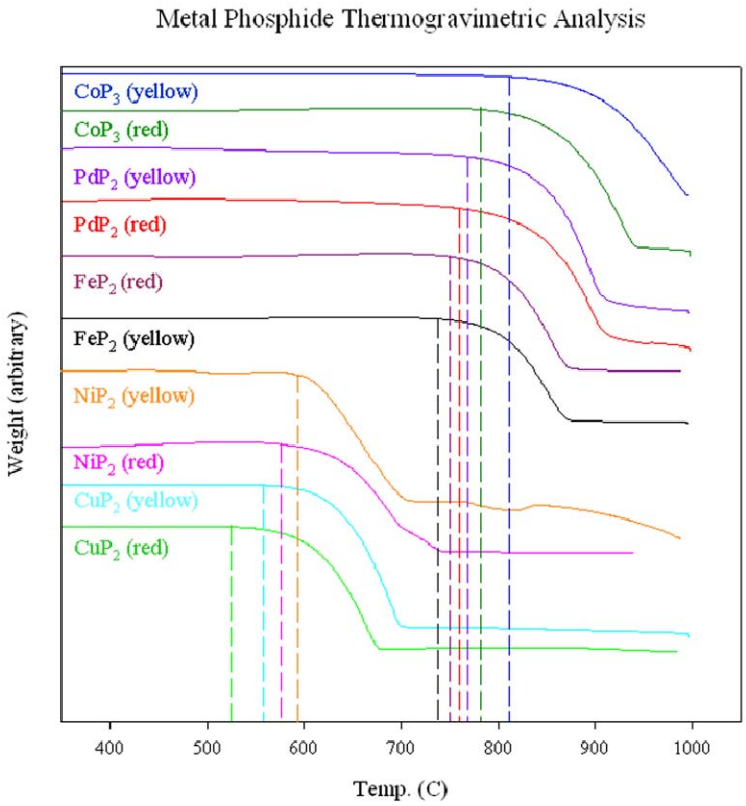

Figure 2.10 Stack plot of TGA weight loss events from synthesized MP_x from either yellow molecular P_4 or polymeric red phosphorus. All experiments were conducted in flowing argon gas.

After heating, one end of the tube was pulled out of the furnace to transport any evolved yellow P_4 away from the pellets. The condensation of yellow P_4 at the cool end of the tube was evident, and upon cracking the ampoules in air, the substance would spontaneously ignite, confirming that it was likely pyrophoric yellow P_4. The resulting pellets were crystalline Cu_3P and Ni_2P by XRD (Figure 2.11), confirming that the

polyphosphide decomposition temperatures are consistent with TG-DTA results. Overall, the thermal decomposition data shows that phosphorus-rich metal phosphide phases require relatively low synthetic conditions, <600 °C in some cases, as higher reaction temperatures will lead to their decomposition to metal-rich phosphide phases. Previous elemental synthesis approaches to CuP_2 have shown that excess phosphorus vapor is necessary to heat such systems to above 900 °C where CuP_2 melts, otherwise Cu_3P forms.[76,77] Systems using excess phosphorus to encourage phosphorus-rich phase formation may produce pyrophoric molecular yellow phosphorus byproducts that require more careful handling than the PCl_3 byproducts in the current strategy.

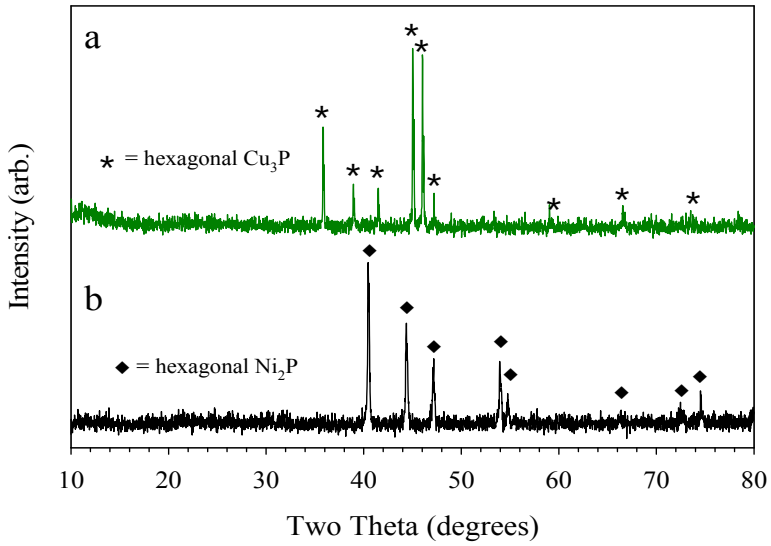

Figure 2.11 XRD data for products after annealing crystalline metal phosphide pellets in evacuated ampoules to higher temperatures: (a) a CuP_2 pellet product annealed at 600 °C and (b) a NiP_2 pellet annealed at 650 °C.

2.3.5 Phosphorus reactions and product formation

As this study shows, crystalline phosphorus-rich metal phosphides are easily synthesized via direct reaction of metal chloride pellets with elemental phosphorus (molecular P_4 vapor or intimate contact with polymeric red phosphorus) resulting in volatile PCl_3 elimination. Figure 2.12 is a cartoon schematic diagram of the reaction/elimination processes that likely occur during these elemental phosphorus to phosphide transformations. Given the significant mass changes that occur in the red phosphorus reagent pellet during the reaction, more open porous structures generally result. An inert, removable template additive may be a useful tool for converting these phosphide pellets to higher surface area, porous phosphide structures or composites. While pressed pellets were used in this study, their use with volatile molecular yellow phosphorus is not required for this synthetic method. This is demonstrated by reactions with lightly ground $CuCl_2$ and $NiCl_2$ powders with yellow P_4 that produced crystalline CuP_2 and NiP_2 under the same heating conditions used for the pellet reactions (Figure 2.13). The CuP_2 powder product has a faceted particle microstructure that is similar to that observed for pellet products (Figure 2.14a and b), while the NiP_2 product reveals a distinct crystal shard appearance at low magnifications (Figure 2.14c) which upon examining at higher magnifications shows to be comprised of fused, sub-micron particle domains (Figure 2.14d). The crystal shard morphology seen in the macrostructure of NiP_2 at low magnifications may be indicative of the $NiCl_2$ precursor shape.

As was discussed earlier, many metal phosphide syntheses produce metal-rich phases or mixtures of phases, even when phosphorus-rich metal phosphides are targeted by reaction stoichiometry. In our reaction system, phosphorus-rich phases are very accessible and even appear to be favored over metal-rich MP_x formation. For example, Co_2P or Cu_3P were targeted using the modifications in reagent stoichiometry according to Eq. 2.1 and the same experimental conditions as described above for the phosphorus-rich metal phosphides.

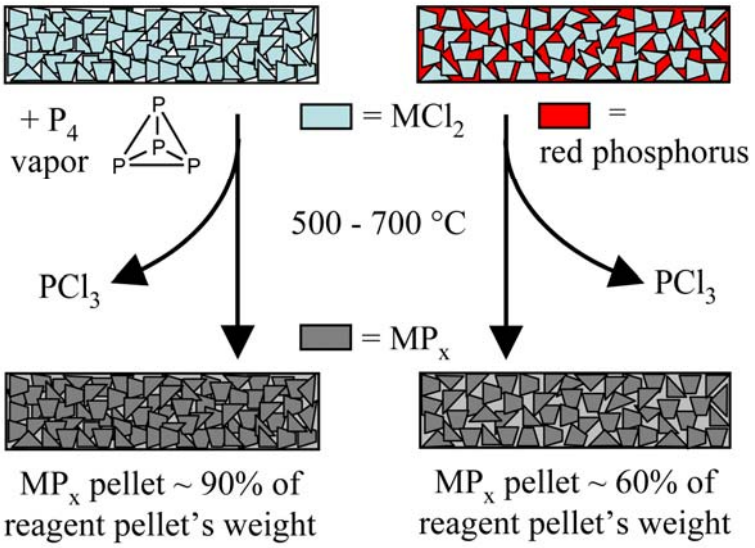

Figure 2.12 A schematic diagram of MCl_2 pressed pellet reactions with either molecular P_4 vapor or intimate solid-state mixtures with polymeric red phosphorus. The product forms emphasize the overall macrosopic shape retention and relative weight loss during PCl_3 byproduct elimination.

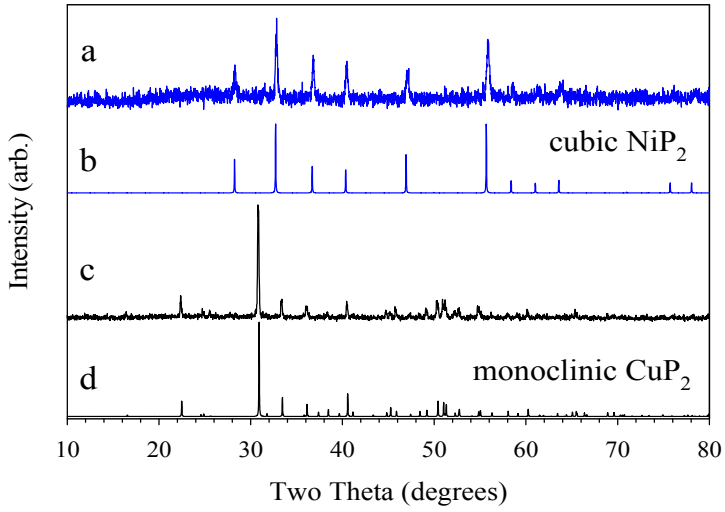

Figure 2.13 XRD data for 500 °C sealed ampoule reactions between powdered metal halide and yellow P_4: (a) $NiCl_2$ reaction product, (c) $CuCl_2$ reaction product and calculated patterns for (b) cubic NiP_2 and (d) monoclinic CuP_2.

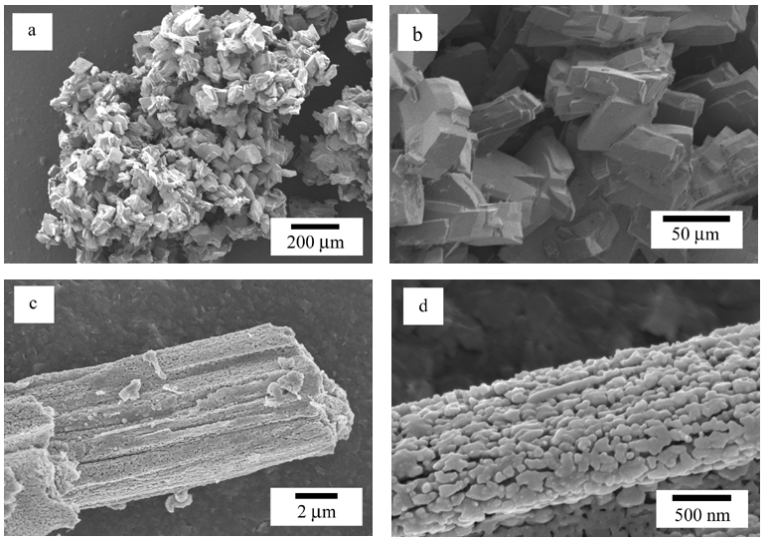

Figure 2.14 SEM images of products from loose powder metal halide ($CuCl_2$ and $NiCl_2$) reactions with yellow P_4 performed at 500 °C using the same experimental conditions described for pressed pellets. CuP_2 products are shown in a and b while NiP_2 products are shown in c and d.

The isolated crystalline products in these Co_2P and Cu_3P syntheses were CoP_3 with significant unreacted $CoCl_2$ and CuP_2 with reduced CuCl, respectively. These results were surprising since both crystalline metal-rich phases have been previously synthesized at low temperatures (~140 °C).[78]

An examination of reaction thermochemistry for the Co-P and Cu-P systems shows that the formation of phosphorus-rich phases is thermodynamically favored over their metal-rich counterparts in our reactions. The calculated ΔH_{rxn} (298 K) for the cobalt and copper phosphide formation reactions (Eq.2.1), based on the moles of metal in the final product, were found to be exothermic for CoP_3 (-109 kJ/mol) and CuP_2 (-86 kJ/mol) versus being comparably less exothermic (or endothermic) for Co_2P (+6.7 kJ/mol) and Cu_3P (-35 kJ/mol). In both cases, reaction enthalpy favors formation of phosphorus-rich phases over their metal rich counterparts. Note that these calculated enthalpies are room

temperature values that ignore additional entropy energy changes at higher temperatures primarily due to gaseous PCl_3 vapor production.

The use of elemental phosphorus sources with pre-formed P-P bonds may also play an important role in facilitating the formation of polyphosphide anions in these solid-state syntheses. Several structural examples that emphasize P-P networks produced in this study are shown in Chapter 1 (Figures 1.1-1.5). In contrast, using yellow P_4 or red phosphorus to form metal-rich phases requires the breaking of several reagent P-P bonds in order to afford small P^{3-} phosphide anions. Thermochemical reaction preferences and P-P precursor bonding effects may also play a role in explaining why previous studies that used alkylphosphines (PR_3, P-R bond breaking required) as "P" reagents most readily produce metal-rich phosphides over their phosphorus-rich counterparts.

2.4 Conclusions

The reaction of transition-metal dichlorides (M = Fe, Co, Ni, Cu, and Pd) with either yellow P_4 vapor or with intimately mixed red phosphorus in the solid state at temperatures ranging from 500-700 °C, leads to the formation of crystalline phosphorus-rich MP_x (x = 2, 3) phases. In the case of nickel, a high temperature/pressure cubic NiP_2 phase is formed at moderate temperatures. This phosphorus-rich phosphide formation reaction is facilitated by thermochemically favorable processes that include the elimination of a PCl_3 byproduct. The solid powdered reagents were pressed into pellets and retained their macroscopic shape after reaction. The pellet morphologies generally consist of fused particles with smooth to faceted shapes ranging from nanometer to micrometer dimensions. This method represents a rare moderate temperature and stoichiometric synthetic approach to a range of phosphorus-rich metal phosphides.

CHAPTER 3

SOLVOTHERMAL SYNTHESIS OF MP_X (M= Co, Ni AND Cu X= 2 OR 3) IN SUPERHEATED AND SUPERCRITICAL TOLUENE†

3.1 Introduction and Background

Traditionally, metal phosphides have been synthesized by directly combining the elements in high-temperature reactions,[79-81] relying on bulk diffusion to afford polycrystalline products. These syntheses often require performing the following steps repeatedly: grinding, heating, and cooling. This 'shake and bake' technique typically produces small crystallites and often requires heating at elevated temperatures for weeks to ensure a complete reaction. Bulk metal phosphides have also been synthesized from the elements using fluxes as a solvent; usually salts like NaCl or low-melting metals like Sn are used.[26,40,56,82] The flux method has many advantages over the 'shake and bake' method. Fluxes can dissolve elemental reagents at relatively low temperatures (500-800 °C) which allows for lower temperature reactions, increased diffusion, and lower activation energy barriers.[66] This method also produces larger crystal domains, and often even single crystals, and can circumvent thermodynamic traps, which can lead to phases not attainable by the 'shake and bake' method. The drawbacks of the flux method is that the flux can often be reactive and not behave as a true solvent, and that when metal fluxes are used, separating the product from the metal by acid digestion can be difficult. Both of these 'top-down' methods can result in bulk products with large particles (>1 μm). Current research on metal phosphide synthesis is predominately focused on solvothermal or hydrothermal routes with the aim of decreasing particle size.

Solvothermal reactions are inherently low-temperature routes as the reaction temperature is limited by the boiling point of the solvent when performed at atmospheric

† A portion of this work was recently published in *Chem. Mater.* **2008,** *20*(8) 2618-2620.

pressures. Because of this, more reactive precursors are required and successful reactions are often driven by the formation of thermodynamically favorable byproducts. In typical reactions, separate metal and phosphorus sources are dissolved or suspended in a solvent and upon heating, form M-P nuclei which grow in a snowball-like manner producing MP_x particles. An example of this is the exchange reaction between $InCl_3$ and $(Me_3Si)_3P$, which forms InP and Me_3SiCl.[83,84] In this reaction, $InCl_3$ is suspended in toluene and reacted at room temperature with a solution of $(Me_3Si)_3P$, also in toluene. The amorphous InP_x product is then isolated and heated to 650 °C to achieve fused nanocrystalline InP. In another route, a metal halide (halide = Cl or Br) is reacted with Na_3P in refluxing toluene producing MP_x and NaCl or NaBr.[85-88] This reaction is very exothermic as it gives off considerable heat when forming the stable NaCl or NaBr byproduct. These nanoparticle products are crystalline as prepared. Both of the routes just described are considered metathesis (exchange) routes and the oxidation states of the metal and phosphorus do not change in the transformation from reagent to product.

The temperature range of solvothermal or hydrothermal reactions can be elevated by using autoclave reactors in which solvents are heated above their boiling points (superheated), generating an internal pressure above atmospheric. Several metal phosphides have been synthesized using superheated solvents in autoclaves. For example when a $MCl_2 \cdot xH_2O$ (M= Co, Ni and Cu) is heated with excess yellow P_4 in ethylenediamine (b.p. 118 °C) at 140 °C, nanocrystalline Ni_2P, Co_2P and Cu_3P is produced.[78] In a similar reaction a $MCl_2 \cdot xH_2O$ (M= Ni and Cu) is heated with excess yellow P_4 in a dilute aqueous ammonia to 140 °C producing nanocrystalline Ni_2P and Cu_3P.[89] In a different reaction, $CuSO_4 \cdot 5H_2O$ is reacted with excess yellow P_4 in a solvent mixture of glycol, ethanol and water at 180 °C, producing hollow nanospheres of crystalline Cu_3P.[31] Another example is a reaction between a copper halide ($CuX_{1 \text{ or } 2}$, where X = Cl or I) and excess amorphous red phosphorus in superheated H_2O at 200 °C, producing bulk, polycrystalline Cu_3P.[90] These are all redox reactions, as the oxidation

state of the phosphorus, and sometimes the metal, changes going from reactant to products. Unlike the metathesis reactions, these are not driven by large thermodynamic gains, and as such, typically require a larger energy input (higher reaction temperature) to drive the reaction to completion.

If superheated solvents can not achieve the desired reaction temperature, then reactions may also be performed in supercritical fluids. Supercritical fluids are achieved when the temperature, pressure and volumes are elevated above their critical values. Critical temperature, T_c, is defined as the temperature above which a gas can no longer be liquefied no matter how high the pressure. Critical pressure, P_c, is defined as the lowest pressure which will liquefy a gas at its critical temperature. Critical volume, V_c, is defined as the volume of 1 mol at the critical temperature and critical pressure. Critical volume can be calculated using the critical density, ρ_c, and molecular weight:

$$\text{MW (g·mol}^{-1}\text{)} / \rho_c \text{ (g·cm}^{-3}\text{)} = V_c \text{ (cm}^{-3}\text{·mol}^{-1}\text{)} \qquad (3.1)$$

When a solvent is heated in a sealed autoclave, the density of the liquid decreases with increases in temperature and the density of the vapor (gas) in the headspace increases with increases in temperature; so as the temperature is increased the density of the headspace vapors and liquid start to approach the same values. When the densities are equal, the two phases (liquid and gas) are no longer separate and a supercritical fluid is achieved, occupying the entire container. If we compare the densities of gaseous toluene and liquid toluene at standard conditions (298 °K, 1 atm) we will find that the density of the gas is 0.0038 g·cm^{-3} and the liquid is 0.87 g·cm^{-3}. The critical density of toluene is 0.27 g·cm^{-3}, so supercritical toluene has a density that is far closer to the liquid than that of the gas, meaning that a supercritical fluid resembles a liquid more than a gas. The critical values for some solvents commonly used as supercritical fluids are listed in Table 3.1 along with values for toluene used in this work.

Supercritical fluids are a far less common reaction environment for synthesizing metal phosphides, in fact there has only been one report of such a synthesis. In this

reaction $(tBu)_3Ga$ and $(Me_3Si)_3P$ were reacted in supercritical hexanes (500 °C, 365 atm) in the presence of gold nanoparticles, producing GaP nanowires.[91] Other semiconducting materials have been produced in superheated or supercritical fluids such as oxides and nitrides. In one reaction TiO_2 nanoparticles were produced from $Ti(SO_4)_2$ in superheated H_2O.[92] In another reaction CeO_2 was synthesized from $Ce(NO_3)_3$ also in superheated H_2O.[93] Ta_3N_5 has been synthesized from $TaCl_5$ and $LiNH_2$ in superheated benzene or mesitylene (500-550 °C).[94] GaN has also been synthesized in several syntheses in supercritical ammonia, where ammonia is the nitrogen source and solvent.[95,96]

Table 3.1 Critical values of common solvents.[97]

Solvent	T_c, °C	P_c, psi	V_c, $cm^3 \cdot mol^{-1}$
Carbon dioxide	31.2	1069	94.0
Ammonia	133	1635	72.5
Water	374	3197	56.0
Ethanol	241	925	167
Hexane	234	430	370
Benzene	289	710	259
Toluene	319	596	316

When examining the solvothermal syntheses of metal phosphides, it is clear that the vast majority of the products produced are metal-rich phosphides; this is surprising since in most reactions a large excess of phosphorus is used. The need for excess phosphorus is likely due to its consumption by hydrolysis or oxidation side reactions.[30,98-100] There are only two solvothermal syntheses that produce phosphorus-rich metal phosphides; one converted metal nanoparticles into metal phosphides using

trioctylphosphine as the solvent and as the phosphorus source at 360 -370 °C (Au_2P_3, PdP_2, and PtP_2)[100,101] and another used phosphorus-containing organometallic complexes that were incorporated into silica xerogels and subsequently decomposed at elevated temperatures of 700 °C (PtP_2).[102] In this chapter we will present a facile, solvothermal, low-temperature synthesis of three phase-pure, phosphorus-rich metal phosphides (CoP_3, NiP_2 and CuP_2) from the reaction of anhydrous, divalent metal chlorides ($CoCl_2$, $NiCl_2$, $CuCl_2$) with yellow P_4 in either superheated (275 °C) or supercritical toluene (350-400 °C, CuP_2 and NiP_2).

3.2 Experimental Section

3.2.1 Reagents used

Metal halides used were anhydrous $CoCl_2$, $NiCl_2$, $NiBr_2$ and $CuCl_2$ (Alfa-Aesar, 99.7%, 98.0%, 98.0% and 98.0% respectively) and other reagents and solvents used were elemental white/yellow P_4 (Aldrich, yellow phosphorus 99+% stored in water), PCl_3 (Aldrich, 98%), PBr_3 (Aldrich, 98%), toluene (Fisher Scientific, 99.9%), and methanol (Fisher Scientific, 99.9%). Low level impurities in white P_4 frequently give it a light yellow appearance. These impurities have been ascribed to traces of polymeric red phosphorus that form on exposure to UV light.[65] **Caution**: Elemental molecular white phosphorous is stable when stored under water; however it is very pyrophoric and exothermically burns with a flame immediately on contact with oxygen/air. Care should be taken to work with this material in small quantities and carefully clean all experimental equipment of phosphorous residue by oxidizing it with aqueous bleach.

3.2.2 Metal phosphide (CoP_3, NiP_2 and CuP_2) synthesis in superheated toluene

In a typical experiment, 4.46 mmol of the anhydrous metal halide ($CoCl_2$, $NiBr_2$, $NiCl_2$,or $CuCl_2$, vacuum dried at 250 °C, 4h) and stoichiometric molar amounts of P_4 to

produce PCl_3 and the desired MP_x phase (e.g., 2.97 mmol of P_4 for MP_2, and 4.09 mmol of P_4 for MP_3) were loaded into a 125 ml stainless steel autoclave reactor (Parr Instruments Model 4752) in an inert atmosphere argon-filled glovebox. The P_4 was cut from a monolith that was stored under water and dried under vacuum prior to use. Any visible surface oxidized material was shaved from the P_4 block in the glovebox using a razor blade. The resulting yellow/white P_4 was shiny yellow. The closed Parr reactor with solid reagents was removed from the glovebox and toluene (85 ml distilled from sodium, degassed with N_2) was then added to the reactor via canula transfer. The reactor was fitted with a reactor head containing a thermocouple and an analog pressure gauge, and flushed and filled with 1 atm N_2. Reactions were heated with constant stirring in heating mantles to 130 °C (internal temp. reading) over 2h and held overnight (~15 h), and then heated to 275 °C over 2h and held for two days (~40h) before being cooled to room temperature. The lower temperature step was necessary to ensure the volatile P_4 did not sublime out of the solution prior to reacting with the metal chloride. Reactor contents were transferred to a 250 ml Schlenk flask where the black powders settled out and the supernatant was removed by canula transfer. The products were washed with toluene and methanol to remove any unreacted reagent or byproduct and then dried *in vacuo* at room temperature. Selected samples were sealed in evacuated pyrex or silica ampoules and placed in a horizontal tube furnace for annealing and crystallization studies.

3.2.3 Metal phosphide (NiP_2 and CuP_2) synthesis in supercritical toluene

In a typical experiment, 1.32 mmol (178 mg $CuCl_2$ or 171 mg $NiCl_2$) of the anhydrous metal chloride (vacuum dried at 250 °C, 4h) and stoichiometric molar amounts of P_4 (0.880 mmol, 109 mg) were loaded into a 75 cm^3 stainless steel autoclave reactor (Parr Instruments Model 4740CH) in an inert atmosphere argon-filled glovebox. The autoclave had a custom glass lining, reducing the reactor volume to ~60 cm^3. The P_4 was

cut from a monolith that was stored under water and dried under vacuum prior to use. Any visible surface oxidized material was shaved from the P_4 block in the glovebox using a razor blade. The resulting yellow/white P_4 was shiny yellow. The closed Parr reactor with solid reagents was removed from the glovebox and toluene (40 ml distilled from sodium, degassed with N_2) was then added to the reactor via canula transfer. The reactor was fitted with a reactor head (graphite gasket) containing an analog pressure gauge, and flushed and filled with 1 atm N_2. Reactions were heated with constant stirring (custom, pyrex-coated stirbar) in heating mantles to 130 °C (external temp. only) over 2h and held overnight (~15 h), and then heated to 350-400°C over 10h and held for 1 day ($CuCl_2$ reactions, 15h) or 2 days ($NiCl_2$ reactions, 40h) before being cooled to room temperature. The lower temperature step was necessary to ensure the volatile P_4 did not sublime out of the solution prior to reacting with the metal chloride. Once cooled, the reactor was opened up (on benchtop) and the glass liner, containing products and supernatant, was carefully lifted out of the reactor bottom. The product had settled to the bottom of the liner by the time the reactor cooled (~3h), and the supernatant was carefully decanted. The product (fine black powder) was transferred to a centrifuge tube with the aid of an additional fresh 40 ml of toluene. The tube was then centrifuged (5 min, 3000 RPM), and the supernatant was decanted again. Methanol was then added to the centrifuge tube as a wash solvent, and the product was shaken with methanol for 5 minutes, followed by centrifugation and decanting. The washed product was then air-dried.

3.2.4 Control experiments: PCl_3, PBr_3 and P_4 in superheated toluene

In the glovebox, 15 mg of freshly cut yellow P_4 was loaded into an open-ended, pyrex tube (9 mm O.D., ~30 cm in length), sealed with a suba and brought out of the box. On the benchtop, 1 ml of toluene (distilled from sodium, degassed with N_2) was added via canula transfer. On the benchtop, solutions of PCl_3 or PBr_3 in toluene (200 μl of PX_3

diluted to 1 mL with toluene) were added to similar, separate pyrex tubes. Each of these three solutions were then sealed separately in the following manner: The tubes were first connected to a Cajon connector and a Kontes needle valve and then the solution-containing end of the tube was vertically submerged in liq. N_2, freezing the solutions in the tube. The tubes were then evacuated to ~80 mTorr, and were then sealed with a methane-oxygen torch to a length of ~10 cm. These three tubes were then placed in the previously-described, 125 ml autoclave reactor and filled to a total volume of 85 ml (70 ml toluene + 15 ml for volume of three ampoules). The reactor was then sealed and heated identically to the experiments in Section 3.2.2. Once the reaction had cooled the ampoules were carefully scored and cracked and the reaction solutions were transferred into scintillation vials on the benchtop for future analysis.

3.2.5 Product characterization

Supernatants from reactions in Section 3.2.2 and reaction solutions from Section 3.2.4 were analyzed by ^{31}P NMR. In these cases ~200 µl of sample was diluted to 600 µl with C_7D_8, placed in an NMR tube and analyzed by ^{31}P NMR on a 400 MHz Bruker DRX-400. An external reference sample of H_3PO_4 (δ = 0.00 ppm) was used for calibration. SEM analyses were performed on a Hitachi S-4800 or a Hitachi S-3400N microscope with EDS analysis capabilites. XRD data was obtained from a Siemens D5000 XRD system (CuK_α, 0.04 step size and 4 sec/step acquisition times). XRD FWHM peak widths were used for crystallite size calculations (Scherrer-Warren method) and were corrected for instrumental broadening using a crystalline LaB_6 standard. Thermogravimetric-differential thermal analysis (TG-DTA) was run on a Seiko Exstar 6300 system in alumina pans under argon flow with a 10 °C/min heating rate. Very small samples (6-10 mg) were used as gaseous P_4 is generated that can react with and corrode platinum components of the TGA system. Electron ionization mass spectroscopy (EI-

MS) analysis was performed on a high-resolution Waters Autospec double-focusing magnetic-sector mass spectrometer.

3.3 Results and Discussion

3.3.1 Metal phosphide (CoP_3, NiP_2 and CuP_2) synthesis in superheated toluene

In this study, we investigated the direct reaction of a suspended metal halide ($CoCl_2$, $NiBr_2$, $NiCl_2$ or $CuCl_2$) with dissolved yellow P_4 in superheated toluene. Unlike most precursor routes to metal phosphides, reactions were *stoichiometrically balanced* such that all halide was ideally removed as PX_3 and the remaining "P" was used to form the metal phosphide product (Equation 3.2).

$$3MX_2 + [(3y + 2)/4]P_4 \rightarrow 3MP_y + 2PX_3 \quad (3.2)$$

The autoclave reaction was heated and held at 130 °C overnight; this was done because benchtop observations of dissolved, yellow P_4 in other non-halogenated organic solvents (e.g. hexadecane or 1-octadecene) showed that P_4 would transport out of the solution at elevated temperatures (> 140 °C). By keeping the temperature at 130 °C overnight, the P_4 was given an adequate chance to react or coordinate to the metal halide, which ensured that the stoichiometric balance of Eq. 3.2 would not be disturbed by P_4 sublimation out of the reaction solution. After being held at 130 °C overnight, reactions were heated to 275 °C and held for 2 days. Reactions were performed in autoclaves that utilized Teflon-coated stirbars and gaskets and could only be heated to 275 °C as Teflon will deform at temperatures >300 °C. All as-synthesized products were washed with fresh toluene and methanol to remove any unreacted reagent and byproducts.

All washed products required post-reaction annealing to achieve crystallinity. By annealing the washed products (in evacuated ampoules) at various temperatures overnight, we found that CuP_2 and NiP_2 would crystallize by 350 °C and that CoP_3 could crystallize by 500 °C. The CoP_3 samples annealed at 500 °C were poorly crystalline, but

by increasing the annealing temperature to 600 °C, a much more crystalline product could be attained (Figure 3.1). For annealing temperatures ≤500 °C, pyrex ampoules were used and for higher temperatures silica ampoules were used.

Reactions durations of 2 days at 275 °C were required to ensure complete reactions. For instance, in reactions targeting CuP_2, when reactions were only held overnight at 275 °C, CuCl could be detected by XRD in the crude product. Also reactions targeting NiP_2 that were only maintained at 275°C overnight would reveal Ni_2P, a metal-rich phase, even after annealing at 500 °C. It was also revealed to be critical that the reaction environment be strictly anhydrous. Metal halides are typically hygroscopic, but can be purchased as anhydrous reagents. We found that the as-purchased "anhydrous" metal halide reagents still contain surface water that is likely adsorbed during packaging and shipping. For the above MP_2 and MP_3 reactions to be successful using stoichiometric amounts of reactive yellow phosphorus, it was critical to vacuum-dry the as-purchased "anhydrous" metal chlorides. For example, the stoichiometric NiP_2 reaction using as-received anhydrous $NiCl_2$ produced solely metal-rich Ni_2P after annealing with a poor 15% yield. After the $NiCl_2$ was vaccuum-dried at 250 °C, the same solvothermal reaction produced NiP_2 after annealing with an 85% yield. This result is not surprising considering the aforementioned syntheses where metal sources were reacted with elemental phosphorus in aqueous environments, always producing metal-rich phases.

3.3.2 Phase determination and elemental analysis (superheated toluene)

All crude, washed (toluene and methanol) and annealed products were analyzed by XRD to determine which crystalline phases were present in the powders. XRD patterns of the washed products targeting CoP_3 and CuP_2 were amorphous, but contained broad regions of diffraction intensity consistent with the most intense peak positions of crystalline CoP_3 and CuP_2. In contrast, the products targeting NiP_2 (from both $NiBr_2$ and

$NiCl_2$), had XRD patterns that showed evidence of some poorly crystalline metal-rich Ni_2P along with broad peaks indicative of NiP_2 (Fig. 3.2). Upon annealing (350 °C for CuP_2 and NiP_2 and 600 °C for CoP_3) XRD revealed the presence of the targeted crystalline phases: cubic CoP_3, cubic NiP_2, and monoclinic CuP_2. As in Chapter 2, the cubic phase of NiP_2, which has been previously described as the high temperature/pressure phase, was afforded.[61,62] The XRD patterns of the crystalline products along with calculated patterns based on their known structures can be seen in Figure 3.1.

Energy dispersive spectroscopy (EDS) analysis shows that the overall M:P ratios in the washed products are consistent with those targeted in the CoP_3 and CuP_2 syntheses; however the M:P ratio for the washed product targeting NiP_2 from $NiCl_2$ showed an excess of phosphorus (~23%). The amount of halide residue in the washed products varied from sample to sample. The chlorine residue was minimal for washed CoP_3 (1:0.04 M:Cl molar ratio), was higher for washed NiP_2 from $NiCl_2$ (1:0.15) and was significant for washed CuP_2 (1:0.39). After annealing, the EDS analysis revealed that the M:P and M:Cl ratios had dropped in all cases. The chlorine residue dropped significantly in all samples to the point of being below detection limits (<2 wt %). The M:P ratios of the annealed CoP_3 and CuP_2 were slightly phosphorus deficient and the M:P ratio of the NiP_2 from $NiCl_2$ was slightly phosphorus rich, but all M:P ratios were, however, with in 15 % of their ideal values, which is within semi-quantitative EDS relative percent sampling error for particulate samples. A summary of EDS atomic ratio data are listed in Table 3.2 and a summary of average atomic percentages used to calculate the atomic ratios are listed in Table 3.3.

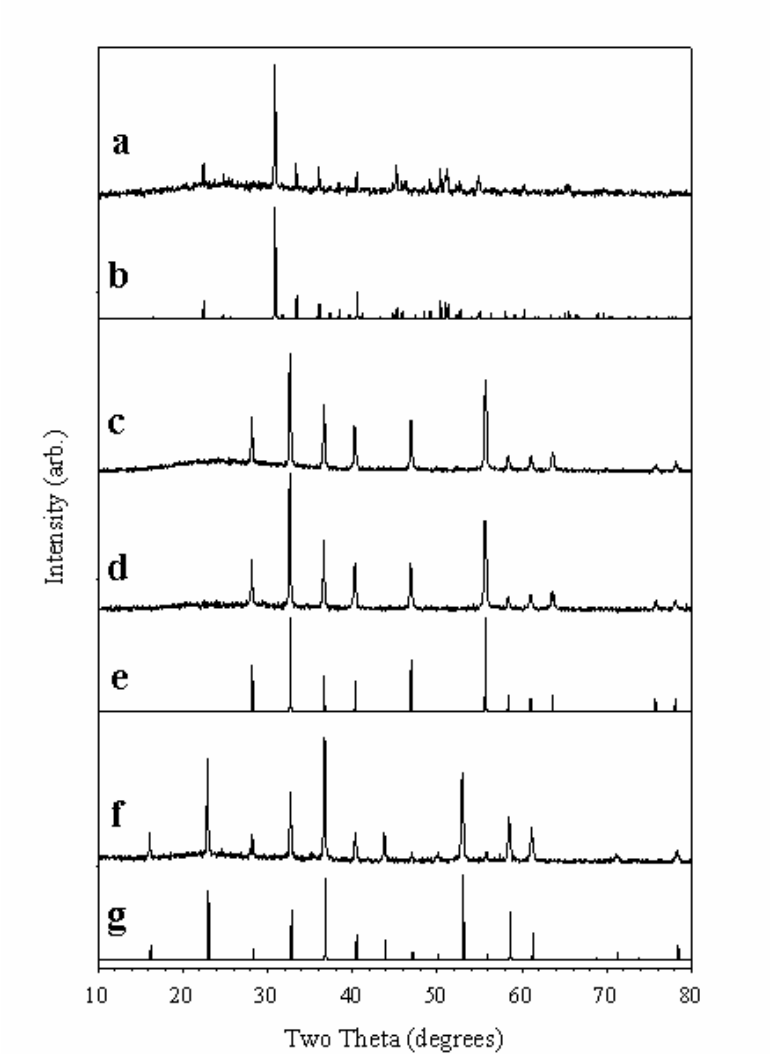

Figure 3.1 Experimental XRD patterns of annealed products of CuP_2 (a), NiP_2 from $NiBr_2$ (c), NiP_2 from $NiCl_2$ (d) and CoP_3 (f). Below the experimental patterns are the calculated patterns for monoclinic CuP_2 (b), cubic NiP_2 (e) and cubic CoP_3 (g). Lattice parameters: cubic CoP_3 (a = 7.7073 Å), cubic NiP_2 (a = 5.4706 Å) and monoclinic CuP_2 (a = 5.8004 Å, b = 4.8063 Å, c = 7.5263 Å, β = 112.70 °).

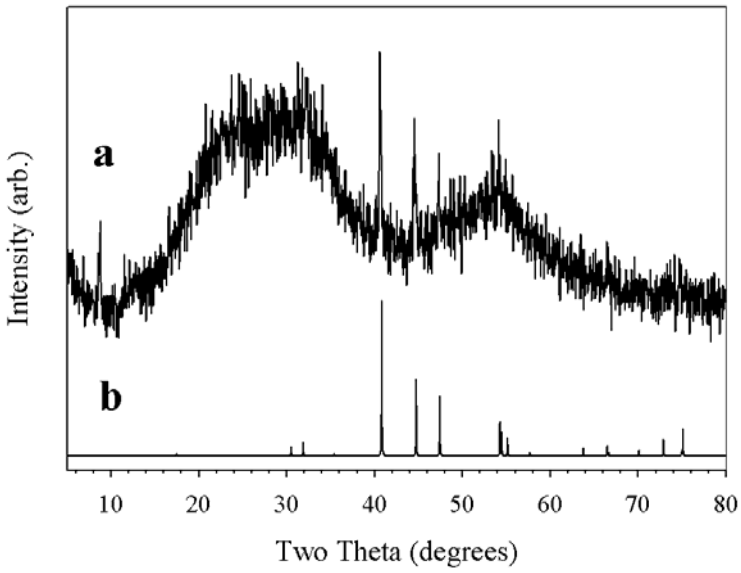

Figure 3.2 Experimental XRD of the washed product targeting NiP_2 synthesized from $NiBr_2$ (a) and the calculated pattern for hexagonal Ni_2P (b).

Table 3.2 Summary of data for solvothermal phosphorus-rich MP_x synthesis.

targeted phase	**MCl_2 : P_4 molar ratio**	**Chemical yield based on MCl_2**	**TGA wt loss[1]**	**as-synthesized MP_x analysis (M:P:Cl)[2]**	**annealed MP_x analysis (M:P:Cl)[2]**	**XRD annealed phase (crystallite size, nm)**
CoP_3	1:0.93	82 %	9.1 %	1:2.97:0.04	1:2.60:0.0	cubic CoP_3 (99 nm)
NiP_2 [3]	1:0.67	85 %	6.4 %	1:2.46:0.15	1:2.15:0.0	cubic NiP_2 (46 nm)
CuP_2	1:0.67	84 %	8.6 %	1:1.99:0.38	1:1.87:0.0	monoclinic CuP_2 (102 nm)

1) Weight loss during heating in argon from 25 °C to crystallization temperature (350 - 500 °C).
2) Atomic ratios calculated from EDS data.
3) NiP_2 synthesized form $NiCl_2$.

Table 3.3 Summary of EDS (M, P, Cl) relative atomic percent values.

	Washed Products (Atomic %)			Annealed Products		
	M	**P**	**Cl**	**M**	**P**	**Cl**
CoP_3	24.9(1.4)	74.0(1.4)	1.1(0.3)	27.8(2.4)	71.8(2.4)	0.41(0.04)
NiP_2	27.8(2.1)	68.0(2.3)	4.2(0.4)	31.3(3.0)	66.7(5.7)	2.0(0.4)
CuP_2	29.6(0.4)	59.1(0.3)	11.4(0.2)	34.9(2.5)	64.9(2.4)	0.28(0.04)

Average relative atomic % values for data from 2-3 sample regions from 2 mm^2 - 100 μm^2, with data's standard deviation from average value noted in parentheses. NiP_2 data is from products synthesized from $NiCl_2$.

3.3.3 Product morphologies (superheated toluene)

Scanning electron microscopy (SEM) analysis revealed that the washed amorphous phosphides are spherical particles with a variety of sizes, with the largest being CoP_3 (~150-250 nm, Figure 3.3a), as compared to NiP_2 (~75-150 nm from $NiBr_2$, Figure 3.5a) and CuP_2 (~20-60 nm, Figure 3.6a). After annealing, the CuP_2 nanoparticles form into a fused structure at 350 °C with ~100-300 nm features (Figure 3.6b) that eventually grow into large micron-sized plates by 500 °C (Figure 3.6 c, d). In contrast, the particles of NiP_2 generally retained their shape and size through the annealing process (~75-150 nm from $NiBr_2$, Figure 3.5b and ~50-100 nm from $NiCl_2$, Figure 3.4). The annealed CoP_3 products retained their spherical shape but grew slightly larger (~200-350 nm, Figure 3.3b) when they were annealed. It is important to note that SEM images of annealed products, even when general shape was retained, clearly show increased fusion between particles.

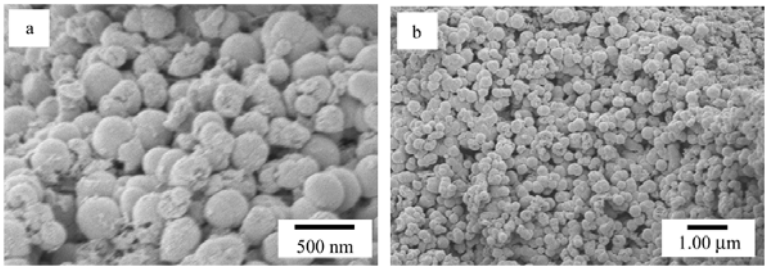

Figure 3.3 SEM images of washed CoP_3 (a) and 600 °C annealed CoP_3 (b).

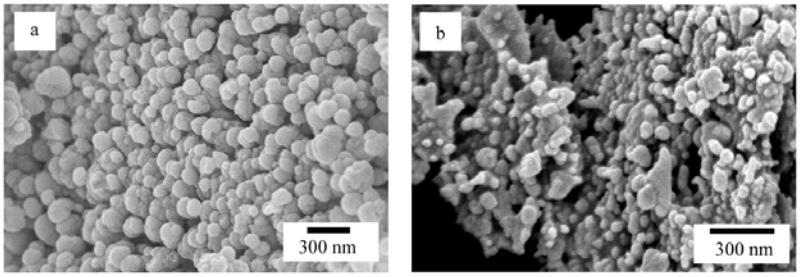

Figure 3.4 SEM images of washed NiP_2 (a) and 350 °C annealed NiP_2 (b) synthesized from $NiCl_2$.

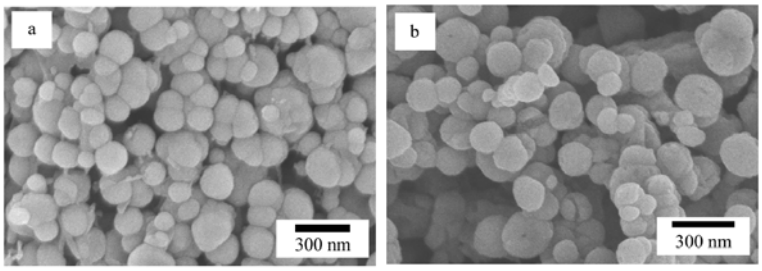

Figure 3.5 SEM images of washed NiP_2 (a) and 350 °C annealed NiP_2 (b) synthesized from $NiBr_2$.

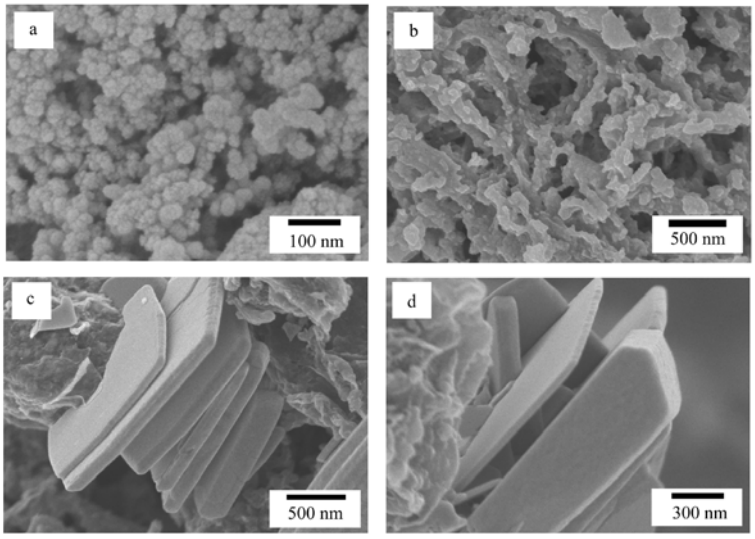

Figure 3.6 SEM images of washed CuP_2 (a), 350 °C annealed CuP_2 (b) and 500 °C annealed CuP_2 (c and d).

3.3.4 ^{31}P NMR analysis of reaction supernatants and control experiments

Our proposed mechanism calls for the formation of PX_3 (X = Cl or Br), as was detected by ^{31}P NMR in our solid-state reactions from Chapter 2. In attempts to confirm that PX_3 was again being generated in our solvothermal reactions, the supernatant was saved from selected reactions and subjected to ^{31}P NMR analysis. In these cases, 200 µl of supernatant (mainly toluene with soluble byproducts) was added to a quartz NMR tube and diluted to 600 µl with C_7D_8. Spectra from all samples revealed multiple singlet peaks across a wide range of the ^{31}P NMR spectrum along with PCl_3 (220 ppm), PBr_3 (230 ppm) and traces of reagent P_4 (-521 ppm). This result is not completely surprising since PX_3 is a very reactive compound that is used as a precursor in many organic syntheses targeting organophosphorus compounds;[21] it could very well react with toluene once it is formed, especially at 275 °C which is well above typical organic chemistry temperatures.

The presence of the expected PCl_3 and PBr_3 peaks also supports the idea that they are the precursors to the various phosphorus species, giving rise to other peaks.

Since the byproducts in the supernatant are many and in small amounts, isolating them individually was impractical and not attempted. Instead, a control experiment was performed to gather further information. In these experiments reagent PCl_3, PBr_3 and P_4 were dissolved in toluene and sealed in an evacuated pyrex ampoules by freezing the solutions in liquid N_2 (see Section 3.2.4). These ampoules were collectively added to an autoclave reactor and heated using a temperature profile which mimicked the MP_x syntheses. After heating, the ampoules were allowed to cool, were then cracked open, and the resulting solutions were prepared for NMR analysis in the same manner as the MP_x synthesis supernatants. In this way, we could compare the NMR peak shifts from reaction supernatants to the peak shifts observed in the control experiments. We also compiled a list of peak shifts for compounds that would be logical byproducts from a handbook devoted to cataloging phosphorus-containing compounds for comparison purposes.[103]

Before discussing the peak shifts, it is important to consider factors that affect the position of the peaks appearance, namely matrix (solvent) environments. All NMR samples and literature values were calibrated using H_3PO_4 in D_2O ($\delta = 0.00$ ppm) as an external reference. This standard calibration, however, can not account for shifts in peaks due to matrix affects. Many studies have been performed examining the affect of solvents on ^{31}P NMR samples by comparing similar compounds in a variety of environments. For example, elemental P_4, is listed in reference books as having a shift of -450 ppm when neat (no solvent, solid state NMR),[103] -460 in CCl_4, and -526 in hexanes.[104] It has also been observed that protic environments can affect peak positions.[105] Although the solvents we used were aprotic, we found that the supernatants in our syntheses were acidic, likely from the formation of HCl (as will be discussed below), which could also contribute to peak shifting. Matrices for samples prepared from

our reaction supernatants and those from control experiments should be similar, allowing for reasonable direct comparisons. When comparing experimental peak positions to literature values, matrix affects should be fairly negligible, since a C_7D_8 matrix does not deviate shifts to an appreciable extent from the standard H_3PO_4 reference.[104]

When examining the NMR spectra from our control experiments we found that when elemental P_4 is heated with toluene, no reaction occurred and that the P_4 peak, at -521 ppm, was the only peak observed (Table 3.5). When PCl_3 or PBr_3 was heated with toluene, the resulting NMR spectra contained several new peaks along with peaks for PCl_3 and PBr_3. This is evidence that there was chemistry occurring between the PX_3 and toluene at elevated temperatures. Although the spectra from reaction supernatants did not mirror the spectra from the control experiments exactly, they did have several peaks in common. The differences may be due to the presence of MP_x particles or steel reactor walls in the solution reaction that may have facilitated or catalyzed additional reactions.

The proposed reactions occurring between PX_3 and toluene, can be described by the following equation, where R_yH_z represents toluene:

$$PX_3 + nR_yH_z \rightarrow PX_{3-n}(R_yH_{z-n})_n + nHX \text{ (n = 1,2 or 3 and X = Cl or Br)} \qquad (3.3)$$

To summarize this possible reaction, the PX_3 reacts with toluene forming a mono, di or tri substituted alkyl or aryl phosphine and HCl or HBr as a byproduct. Experimental tests of vapor from reaction supernatants show an acidic pH consistent with HCl or HBr production. The newly formed P-C bond could potentially be formed between a carbon on the aromatic ring (3 unique sites) or on the methyl group. The literature values for related byproducts are listed in Table 3.4. Peak shifts for phenyl phosphorus halides ($P(Ph)_{3-y}X_y$ where y = 1,2 or 3 and X = Cl or Br) were collected because they should be similar to positions for phosphorus halides where the P-C bond is formed on the aromatic ring of toluene. Peak shifts for methyl phosphorus halides ($P(Me)_{3-y}X_y$ where y = 1,2 or 3 and X = Cl or Br) were collected because they should be very similar to positions for phosphorus halides where the P-C bond is formed on the methyl group of toluene. Peak

shifts for the oxidized versions of all of these compounds were also tabulated since these compounds can be oxidized by minor impurities in the reactor or upon exposure to air during isolation. Literature values for the phenyl and methyl substituted phosphorus halides (oxidized and non-oxidized) are also listed in Table 3.4. The standard peak positions are broken down into 4 shift regions so that comparisons with experimental values may be easier. It is important to remember that peak positions may fluctuate due to matrix effects (easily up to 20 ppm, especially if H^+ concentrations are high).

Table 3.4 ^{31}P NMR shifts of aryl or alkyl phosphorus halides and their analogous oxides.

Compound	<0 ppm	0-50 ppm	50-140 ppm	>140 ppm
PCl_3, PCl_3O		3.2		219
PBr_3, PBr_3O	-103			230
$PMeCl_2$, $PMeCl_2O$		43.5		192
$PMeBr_2$, $PMeBr_2O$		NA		184
$PPhCl_2$, $PPhCl_2O$		34.0		166
$PPhBr_2$, $PPhBr_2O$		1.1		150
PMe_2Cl, PMe_2ClO			96.0, 58.7	
PMe_2Br, PMe_2BrO			87.0, 72.6	
PPh_2Cl, PPh_2ClO		42.7	81.0	
PPh_2Br, PPh_2BrO		38.7	72.9	
PMe_3, PMe_3O	-62.0	36.2		
PPh_3, PPh_3O	-13.0	23.0		

The supernatant from the reaction forming CoP_3 from $CoCl_2$ showed two peaks at 179.9 and 163.3 ppm. These peaks were similar in position to peaks (179.9 and 163.1 ppm) that also appeared in the PCl_3 control experiment. These shifts are likely from phosphorus dichlorides, since literature values for methyl phosphorus dichloride and phenyl phosphorus dichloride are found at 192 and 166 ppm respectively.

The supernatant from the reaction forming CuP_2 from $CuCl_2$ showed two peaks at 179.9 and 58.0 ppm. The PCl_3 control experiment showed a peak at 179.9 ppm as well. The shift at 179.9 was again likely from phosphorus dichloride. The closest literature value to the peak at 58.0 ppm is from dimethyl phosphorus chloride oxide (58.7).

The supernatant from the reaction forming NiP_2 from $NiCl_2$ showed 3 peaks with shifts ranging from 173-180 ppm. These peaks were similar in position to two peaks (179.9 and 176.0) that also appeared in the PCl_3 control experiment. These shifts are likely from phosphorus dichlorides. The supernatant from the reaction forming NiP_2 from $NiBr_2$ showed six peaks ranging from 145-175 ppm along with three peaks at 37.09, 25.96 and -38.87 ppm. The PBr_3 control experiment also showed three peaks in the 145-175 ppm range, but did not show any peaks similar to the further upfield peaks observed in the reaction supernatant. The shifts in the 145-175 range are likely form phosphorus dibromides. Literature values for methyl phosphorus dibromide and phenyl phosphorus dibromide are 184 and 150 ppm respectively.

It should be noted that pentavalent phosphorus species, such as PCl_5, PBr_5 and PPh_5, were not observed as byproducts (-80, -101 and -89 ppm respectively). The chemistry between reaction byproducts and solvent led to a variety of phosphorus-containing byproducts, and although we did not exactly determine what those byproducts were, we rationalized some of their components by comparison to control experiments and related literature values.

The presence of PCl_3, PBr_3 and its alkyl phosphorus halide derivatives may also lend some insight into the morphology of the products seen by SEM. It is somewhat

surprising that all washed product particles were as small as they were (20-250 nm), were spherical, and had a fairly small range of particle size dispersion. These types of results are typical for solvothermal reactions where a surfactant is added to stunt particle growth. The byproducts from these reactions may well have acted as *in situ* generated alkyl phosphine surfactants. Trivalent phosphorus species, such as tri-n-octylphosphine (TOP) and triphenylphosphine (TPP), are coordinating Lewis bases that have been used as surfactants in many reported spherical nanoparticle syntheses;[30,98,106,107] since the byproducts from our reactions are trivalent and chemically similar to TOP and TPP, they could also coordinate to surface metal sites on the phosphide particle surfaces.

Table 3.5 Experimental ^{31}P NMR shifts for reaction in toluene at 275 °C.

Experiment	Observed ^{31}P NMR shifts (ppm)
P_4 Control	-521.0
PCl_3 Control	2.5, 5.2, 8.8, 23.9, 37.8, 34.5, 35.6, 44.9, 163.1, 164.6, 176.0, 179.9, 186.4, 191.6, 220.4
PBr_3 Control	152.3, 155.7, 173.4, 196.3, 230.0
CoP_3 from $CoCl_2$	163.1, 179.9
CuP_2 from $CuCl_2$	37.1, 39.5, 44.4, 58.0, 179.9
NiP_2 from $NiCl_2$	173.5, 177.9, 179.9
NiP_2 from $NiBr_2$	-38.9, 26.0, 37.1, 147.4, 152.3, 155.2, 168.1, 172.9, 229.0

3.3.5 Electron ionization mass spectrometry (EI-MS) analysis

Upon annealing washed samples, we noticed that there was material being liberated and collecting at the cool end of the ampoule. This evolved material weight was quantified by TGA analysis (detailed later) of the samples prior to and following annealing (see Table 3.2). In order to identify what was being liberated during the annealing, washed samples were analyzed by EI-MS. In this setup, a small amount of washed sample (~2 mg) was placed in an open-ended capillary, which was then introduced into the mass spectrometer via a direct insertion probe. The sample probe is then evacuated and resistively heated at roughly 150 °C/min. until it reaches 500 °C, where it is held for 17 minutes (~20 min of heating time). As material is being liberated into the gas phase upon heating, it travels out of the capillary where it is bombarded with electrons (70 eV), ionizing the material. Once ionized, the masses of the fragments are detected by a double-focusing, magnetic-sector, high-resolution mass spectrometer. For each sample, multiple spectra are collected at different times with a m/z (mass/ion charge) range of 35 to 500. Although data is constantly being collected by the detector, only spectra which correlate to spikes in material liberation are analyzed. This setup somewhat mimics our annealing process, and should be an indicator of what types of volatile materials are being liberated in our annealing process.

Three washed samples (CoP_3 from $CoCl_2$, NiP_2 from $NiCl_2$ and CuP_2 from $CuCl_2$) were analyzed and all revealed the liberation of the following compounds (m/z): HCl (36.0 and 38.0), C_7H_7 (m/z 91.1) and P_4 fragments (P_4, P_3 and P_2 at 123.9, 92.9, and 61.9 respectively). The CoP_3 and CuP_2 samples also liberated PCl_3 (135.9, 137.9 and 139.9), and the CuP_2 also liberated some Cu_xCl_y clusters which will be described in detail later. It should also be noted that the amount of volatiles fluctuated over time, giving an indication of relative volatility and release of species.

The washed NiP_2 sample revealed the liberation of HCl and P_4 (no P_2 or P_3) in the first three spectra generated at 1.17, 2.34 and 4.28 minutes into the heating ramp, which correspond to temperatures of ~180, 350 and 500 °C. In these three spectra, the HCl intensity is consistently at the upper end of the detection limits while the P_4 intensity increases in each successive spectrum. In the spectra generated at 5.65 minutes (~ 2.5 min at 500 °C) we see the HCl intensity drops, the P_4 intensity remains unchanged and a new intense signal appears, representing C_7H_7. In the next five spectra (7.98 to 18.50 minutes), we only see phosphorus fragment evolution (P_2, P_3 and P_4). The P_2 and P_3 fragments could conceivably be from P_4 fragmentation by the electron beam; if this was the case then the relative intensities of phosphorus signals (P_4:P_3:P_2) should be constant. In the early spectra, we only observe P_4 and in the later spectra the phosphorus fragments' signal ratio fluctuates. This means that the samples liberate P_4 at lower temperatures (180-500 °C), and eventually liberate P_2 and P_3 fragments along with P_4 after a time at 500 °C.

The washed CoP_3 sample, unlike the NiP_2 sample, did not liberate any material until ~3 minutes into the heating ramp (~450 °C). The first five spectra (3.90 -12.10 min.) all only contained signals for HCl, C_7H_7 and P_4. The next spectrum (13.05 min.) showed the liberation of PCl_3 along with C_7H_7 and P_4, but no HCl. The following two spectra (13.82 and 14.80 min.) also only had signals from PCl_3, C_7H_7 and P_4. The last spectrum (16.55 min) revealed only signals from P_4, P_3 and P_2, with no C_7H_7 or PCl_3.

The CuP_2 sample did not liberate material until ~4 minutes into the heating ramp (~1 min at 500 °C). The first two spectra collected (4.87 and 5.84 min.) revealed only signals from HCl. The next spectrum (8.96 min) revealed P_4, P_3, and P_2 along with HCl and traces of C_7H_7. The following spectrum at 9.74 min. revealed the liberation of PCl_3 along with HCl, P_4, P_3, and P_2. The last spectrum (10.97 min) revealed several clusters of peaks with larger m/z values along with C_7H_7, PCl_3, P_4, P_3, and P_2. The clustering of peaks indicated that they may be representative of species with multiple atoms which

have secondary isotopes of significant natural abundance. Both copper and chlorine have secondary isotopes of significant natural abundance (Relative natural abundances: ^{35}Cl-100, ^{37}Cl-32.4 and ^{63}Cu-100, ^{65}Cu-44.6), which prompted us to investigate Cu_xCl_y clusters as possible sources for the signals. By using a web-based computer program which calculates isotope patterns and relative mass intensities,[108] we were able to enter different potential clusters and compare the calculated patterns to our experimental data. For example, a Cu_2Cl_2 cluster has a calculated isotope pattern with the following m/z signals (relative abundances in parentheses): 196(65), 198(100), 200(57.2), 202(14.4) and 204(1.4). We see a cluster of signals in our spectrum that fits this pattern almost perfectly. The other clusters that had calculated patterns which matched up very well to clusters of experimental signals were Cu_2Cl, Cu_3Cl_2, Cu_3Cl_3 and Cu_4Cl_4.

If we look back to our EDS data (Table 3.2), we remember that the M:P ratios and the M:Cl ratios dropped after annealing. Our EI-MS data supports this finding, especially in the CoP_3 and NiP_2 cases where no Co or Ni containing species are liberated. The washed products M:P ratio goes down due to PCl_3 and phosphorus fragment liberation and the M:Cl ratio goes down due to HCl and PCl_3 liberation. The high amounts of chlorine found in the EDS of the washed CuP_2 products may also be rationalized by our EI-MS findings as well; the high chlorine content may be due to the presence of unreacted $CuCl_x$ which, upon annealing, are liberated as volatile Cu_xCl_y clusters.

3.3.6 Thermogravimetric-differential thermal analysis (TG-DTA)

The annealing studies and EI-MS results are complemented by bulk TG-DTA analysis. Three samples' (CoP_3 from $CoCl_2$, NiP_2 from $NiBr_2$ and CuP_2 from $CuCl_2$) thermal stabilities were analyzed by TG-DTA. In these experiments, small samples (6-10 mg) were placed in an alumina pan and heated under an argon flow at 10 °C/min to 1000 °C. The pans were placed on a platinum balance arm which is also contains a

thermocouple. The instrument utilizes an identical reference arm on which an empty alumina pan is placed. Over the course of the heating ramp, the sample weight is monitored by the balance arms (TG) and thermal events are monitored by the arms' thermocouples (DTA).

The reference arm is used so that thermal events are revealed in temperature differences between the recorded temperatures of the sample arm and the reference arm. The baseline of the DTA is horizontal when there are no thermal events occurring because the ΔT between the sample and reference arm is 0. A deviation from this horizontal baseline indicates a thermal event; a positive ΔT represents an exothermic event while a negative ΔT represents an endothermic event. Common endothermic events include melting, dehydration and decomposition as they require heat absorption by the sample. Dehydration and decomposition events are accompanied by weight loss, which can be seen in the TG. Exothermic events indicate a decrease in enthalpy as the sample is changing into a more stable structure; an example of this is when a metastable phase converts to a more thermodynamically stable form. Sometimes an endothermic event can coincide with an exothermic event making the evaluation of the DTA difficult. An example of this is when a sample decomposes to a more stable compound; this occurs in our samples when our phosphorus-rich phases decompose to a less thermodynamically favorable metal-rich phase, giving off P_4. It should also be noted that a perfectly horizontal DTA baseline is difficult to achieve due to slight asymmetries in the positions of the reference and sample arms in the tube furnace. Because of this, the DTA has a smooth arcing baseline; this is what is observed in our experiments, but thermal events can still be seen as deviations from this arcing baseline. From our TG-DTA experiments in Chapter 2, we found that liberated P_4 can react with the Pt balance arms, this reaction could be evident in the DTA. In our experiments we saw small thermal events at elevated temperatures coinciding with weight loss (P_4 liberation); these events will not be discussed, but could be evidence of P_4 reacting with the balance arms. We analyzed the

residual material, after heating to 1000 °C, by XRD to identify the decomposition product.

When the washed CoP_3 (from $CoCl_2$) was heated in the TG-DTA experiment, the sample began to lose weight at ~400 °C and continued to lose weight until 600 °C before stabilizing. The sample lost ~9% of its initial mass by this point. This weight loss region coincided with a broad endotherm (400-580 °C, Figure 3.7a) followed by a sharp exotherm at 593 °C (Figure 3.7b). By looking at the EI-MS data, we expect the washed product to release surface-bound organics (C_7H_7), HCl, PCl_3 and phosphorus fragments (P_4, P_3, and P_2) in this temperature range. We also know that the amorphous material crystallizes to CoP_3 at 600 °C from looking at our washed and annealed XRD patterns. The endotherm is consistent with the evolution of the aforementioned species and the exotherm is consistent with the crystallization of the the amorphous material. The sample weight remained fairly constant until ~780 °C, where it began to lose weight, and this loss is rapid by 850 °C. The weight stabilized by 920 °C and remained there until 1000 °C. There second weight loss was accompanied by a broad endotherm between 700 and 850 °C (Figure 3.7c) followed by a sharp endotherm at 906 °C (Figure 3.7d). We identified the decomposition product by XRD to be CoP (Figure 3.10). The following equation describes the decomposition of CoP_3 to CoP and P_4.

$$CoP_3 \rightarrow CoP + 1/2P_4 \qquad (3.4)$$

ΔH_f(kJ/mol):	-204	-126	0	ΔH_{rxn} = +78 kJ

The endotherms can be attributed to the energy required to decompose CoP_3 (ΔH_{rxn} = +78 kJ/mol) described in Equation 3.4. The sample lost 34.6 % of its weight between 600 and 1000 °C which is close to what would be expected in the reaction described in Equation 3.4, in which a 40.6 % loss is expected.

Upon heating the washed NiP_2 (from $NiBr_2$) in the TG-DTA experiment, the sample began to lose weight at ~400 °C and continued to lose weight until 456 °C before stabilizing. The sample lost 7.3 % of its initial mass by this point. This weight loss

coincided with a fairly sharp exotherm at 430 °C (Figure 3.8a). Based on EI-MS results for similar NiP_2 samples, this loss is likely due to HBr, PBr_3, C_7H_7 and phosphorus fragment evolution. The XRD pattern of our annealed sample reveals that the washed product will crystallize at 350 °C; this crystallization would be evident by an exotherm. The exotherm at 430 °C could be attributed to crystallization and would perhaps appear closer to 350 °C had we used a slower heating ramp. The absence of an endotherm in this temperature region, which we would expect because of the evolution of volatiles, could overlap with the larger exotherm. The sample weight remained stable until 500 °C, where it began to lose weight, and by 650 °C was losing significant weight. By 730 °C the weight stabilized and remained constant until 1000 °C. This second weight loss was accompanied by a broad endotherm between 475 °C and 670 °C (Figure 3.8b). To explain this event, we again have to identify the decomposition product(s), which by XRD were revealed to be Ni_2P and $Ni_{12}P_5$ (Figure 3.11). The molar ratio of Ni_2P and $Ni_{12}P_5$ were not determined, but based on XRD peak intensities estimated as ~equimolar amounts for discussion purposes. The following equation describes the decomposition of NiP_2 to Ni_2P, $Ni_{12}P_5$ and P_4, where there are equal molar amounts of Ni in each metal-rich product.

$$24NiP_2 \rightarrow 6Ni_2P + Ni_{12}P_5 + 37/4P_4 \qquad (3.5)$$

ΔH_f (kJ/mol): -129 -171 -954 0 ΔH_{rxn} = +1116 kJ

The endotherm can be attributed to the energy required to decompose NiP_2 (ΔH_{rxn}=+1116 or +46.5 kJ per mole of NiP_2) described in equation 3.5. The sample lost 32.2 % of its mass between 456 and 1000 °C which is fairly close to what would be expected in the reaction described in Equation 3.5, in which a 39.6 % loss is expected.

When the washed CuP_2 (from $CuCl_2$) was heated in the TG-DTA experiment, the sample began to lose weight at ~330 °C and continued to lose weight until 447 °C, before entering into a second, distinct weight loss region. The sample lost 15.7% of its initial mass by this point. This weight loss was accompanied by a sharp exotherm at 438 °C

(Figure 3.9a). By looking at the EI-MS data, we expect the washed product to release surface-bound organics (C_7H_7), HCl, PCl_3, phosphorus fragments and Cu_xCl_y clusters in this temperature range. The relatively large initial weight loss in this experiment, when compared to the others, can be attributed to the evolution of the Cu_xCl_y clusters. In the other EI-MS experiments we did not observe any metal-containing volatiles. The XRD pattern of our annealed sample reveals that the washed product will crystallize at 350 °C; this crystallization may be evident as an exotherm. The exotherm at 438 °C could be attributed to crystallization and would perhaps appear closer to 350 °C had we used a slower heating ramp. Weight loss continued slowly after 447 °C until 538 °C, where it began to rapidly lose weight before stabilizing at 652 °C. This weight loss region was accompanied by a broad endotherm between 450 and 640 °C (Figure 3.9b). The decomposition product(s), identified at this point by XRD, were revealed to be Cu_3P and Cu^0 (Figure 3.12). Again, the molar percentages of Cu_3P and Cu^0 in the decomposition product were not determined but are similar intensity by XRD. The following equation describes the decomposition of CuP_2 to Cu_3P, Cu^0, and P_4, where the molar amounts of Cu in the Cu_3P and Cu^0 are equal.

$$6CuP_2 \rightarrow Cu_3P + 3Cu^0 + 11/4P_4 \qquad (3.6)$$

ΔH_f (kJ/mol): -90.1 -129 0 0 ΔH_{rxn} = +416 kJ

The endotherm can be attributed to the energy required to decompose CuP_2 described in Equation 3.6 (ΔH_{rxn}= + 412or +68.7 per mole of CuP_2). The sample lost 38.3 % of its mass between 447 and 1000 °C which is fairly close to what would be expected in the reaction described in Equation 3.6, in which a 45.3 % loss is expected.

The fact that initial weight losses in all samples occurred near the temperatures at which the amorphous products crystallize, as was revealed by XRD experiments, may indicate that the washed products contained impurities that needed to be removed in order to crystallize. The higher halide content in the amorphous products, as seen by EDS, supports this idea. We also found that the thermal stabilities of the products produced by

this solvothermal route are consistent with the stabilities of the analogous products synthesized by our solvent-free method described in Chapter 2.

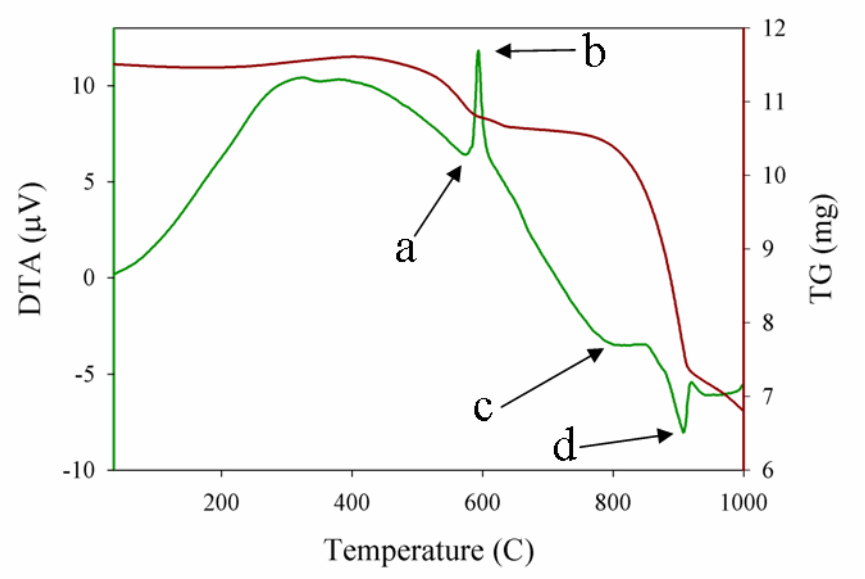

Figure 3.7 TG-DTA of washed CoP_3 synthesized from $CoCl_2$ in superheated toluene.

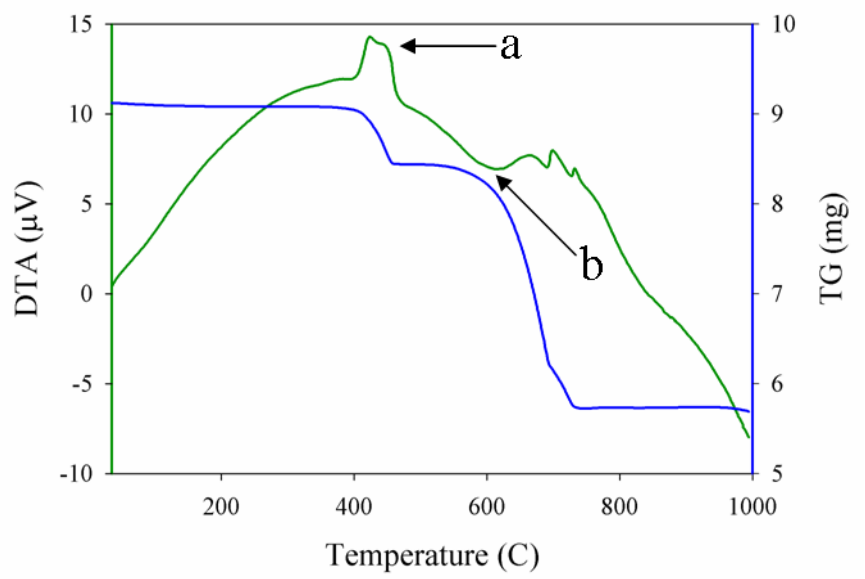

Figure 3.8 TG-DTA of washed NiP_2 synthesized from $NiBr_2$ in superheated toluene.

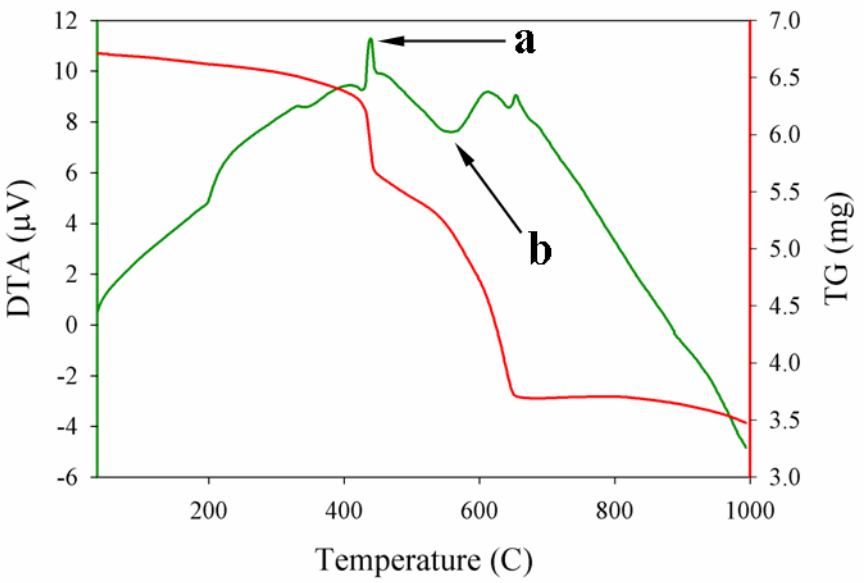

Figure 3.9 TG-DTA of washed CuP_2 synthesized from $CuCl_2$ in superheated toluene.

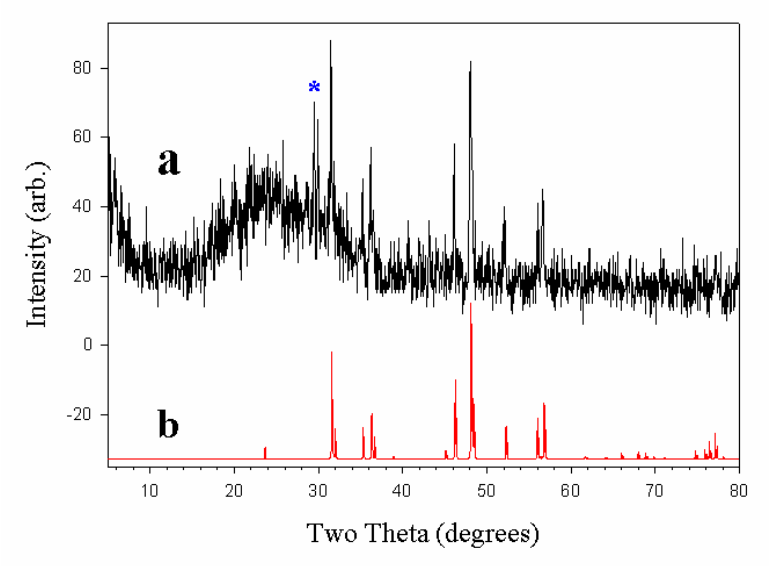

Figure 3.10 Experimental XRD pattern of residual material after TG-DTA analysis of washed CoP_3 (a) and the calculated pattern for orthorhombic CoP (b), (* - unidentified reflection).

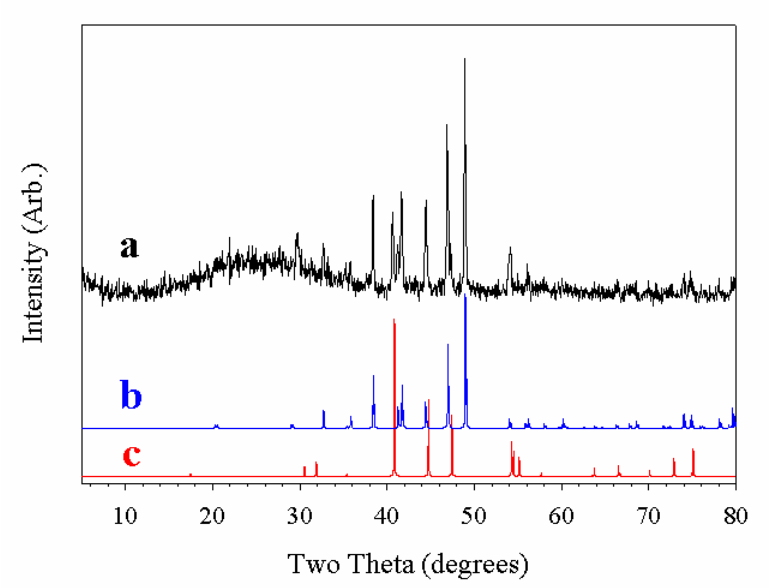

Figure 3.11 Experimental XRD pattern of residual material after TG-DTA analysis of washed NiP_2 from $NiBr_2$ (a), and the calculated patterns for tetragonal $Ni_{12}P_5$ (b) and hexagonal Ni_2P (c).

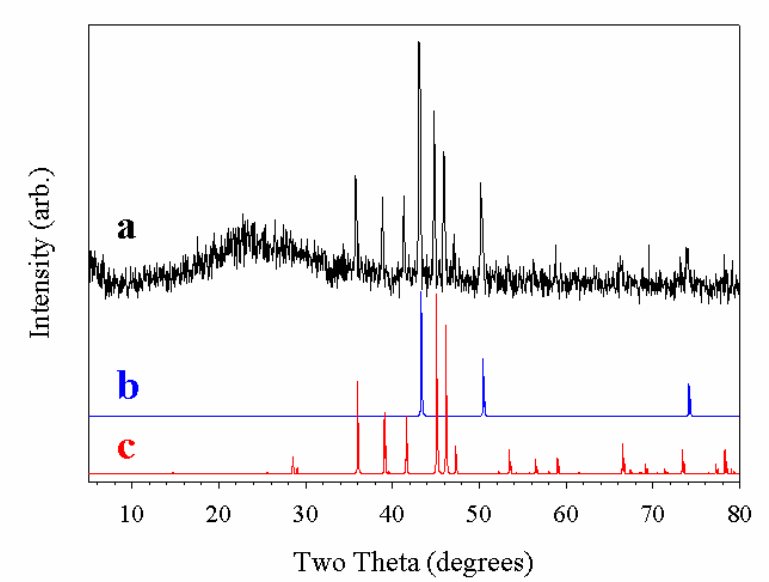

Figure 3.12 Experimental XRD pattern of residual material after TG-DTA analysis of washed CuP_2 (a), and the calculated patterns for cubic Cu^0 (b) and hexagonal Cu_3P (c).

3.3.7 Phosphorus reactions and product formation

As was previously discussed, metal phosphides have a variety of binary phases ranging from metal-rich to phosphorus-rich. Because of this, experiments were performed to see if this synthetic method could be adapted to target alternate metal phosphide phases. In these side experiments, the metal-rich phases, Co_2P, Ni_2P and Cu_3P were targeted following the stoichiometry described in Equation 3.2, and using procedures described in Section 3.2.3. The products from these reactions (as-synthesized and annealed) were analyzed by XRD to determine the resulting crystalline phases. The as-synthesized product targeting Co_2P revealed the presence of poorly crystalline CoP and upon annealing at 500 °C revealed the presence of CoP along with CoP_2 and some unidentifiable reflections (Figure 3.13). The as-synthesized product targeting Cu_3P revealed a large amorphous background along with CuCl and upon annealing at 500 °C formed a mixture of Cu_3P and CuP_2 (Figure 3.14). The as-synthesized product targeting

Ni_2P revealed the presence of Ni_2P and an unidentifiable reflection and upon annealing at 500 °C revealed a mixture of Ni_2P and Ni_5P_4 (Figure 3.15). All of these reactions targeting metal-rich phases afforded products that were more phosphorus-rich than targeted. This is a surprising result as all of these phases were synthesized from excess yellow P_4 and the appropriate metal halide hydrate in ethylenediamine at a mild 140 °C and relatively short reaction duration of 12 h.[78] The key difference between this prior synthesis and ours is that ours took place in an anhydrous environment; while in the previous synthesis yellow P_4 could have reacted with H_2O to form a phosphate with lower reactivity. This result shows that our synthetic method has wide applicability for the preferred formation of phosphorus-rich products.

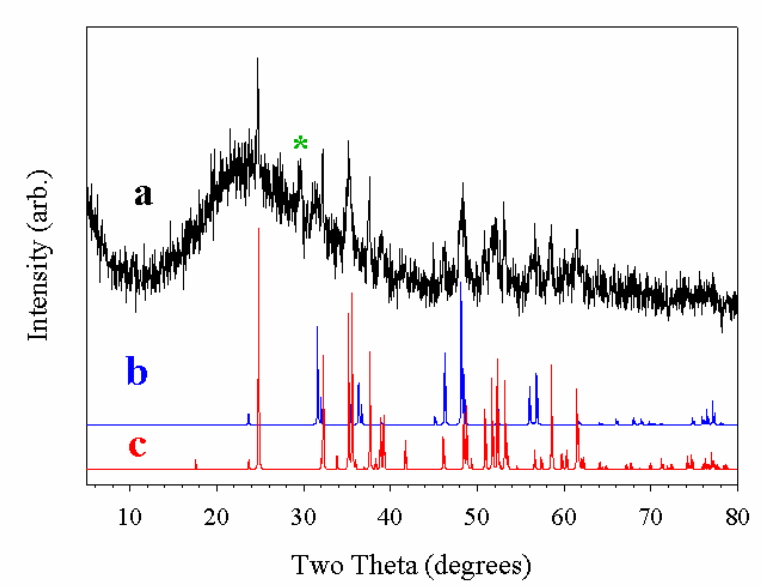

Figure 3.13 Experimental XRD pattern of the 500 °C annealed product targeting Co_2P (a), and the calculated patterns for orthorhombic CoP (b) and monoclinic CoP_2(c). (* - unidentified reflection)

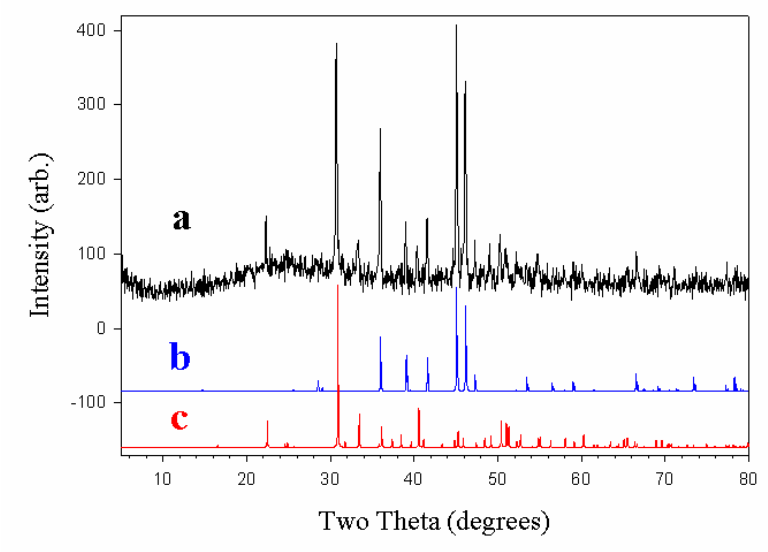

Figure 3.14 Experimental XRD pattern of the 500 °C annealed product targeting Cu_3P (a), and the calculated patterns for hexagonal Cu_3P (b) and monoclinic CuP_2(c).

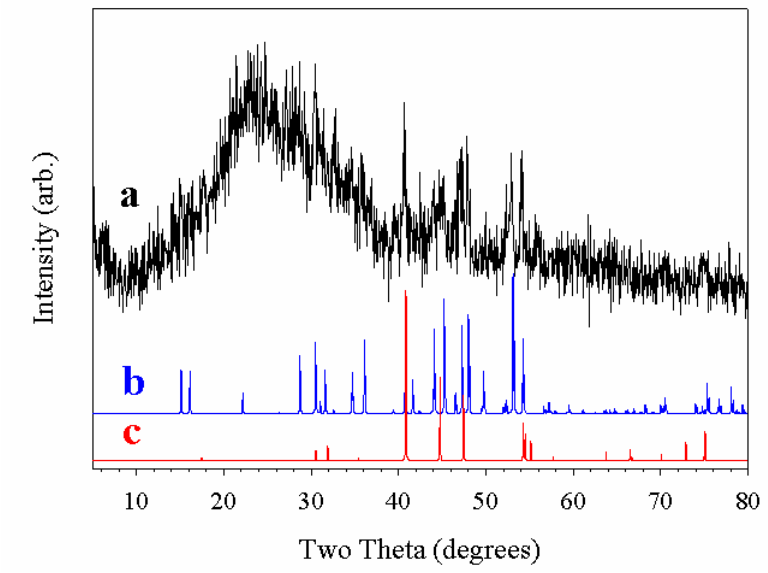

Figure 3.15 Experimental XRD pattern of the 500 °C annealed product targeting Ni_2P (a), and the calculated patterns for hexagonal Ni_5P_4 (b) and hexagonal Ni_2P (c).

In summary, this study shows that amorphous metal phosphides can be synthesized by the direct reaction of dissolved elemental P_4 with suspended metal halides in superheated toluene under rigorously anyhydrous conditions. The reaction produces PCl_3 or PBr_3 as a byproduct which subsequently reacts with toluene forming a variety of alkyl phosphorus halides. The morphologies of the products were revealed to be nano to sub-micron sized (20-250 nm) spherical particles. These morphologies may be influenced by the presence of *in situ* generated phosphine capping ligands (PCl_3, PBr_3 and alkyl phosphorus halides). These amorphous products can be crystallized into targeted phosphorus-rich phases by annealing at moderate temperatures (350-600 °C) in evacuated pyrex or silica ampoules. Upon annealing, the CoP_3 and NiP_2 products showed little change in their morphologies; however, it was evident that the particles became fused along particle boundaries. The CuP_2 products underwent significant fusion upon annealing at 350 °C, resulting in fused masses with 100-300 nm features; upon further annealing at 500 °C, growth of faceted, micron-sized plates was observed. In the next section an alternative autoclave reactor is used so that solvothermal reaction temperatures may be increased in attempts to crystallize the products directly in a solvothermal environment, hopefully avoiding particle fusion that results from annealing in the solid-state.

3.3.8 Metal phosphide (NiP_2 and CuP_2) formation in supercritical toluene

In this study we investigated the direct reaction of dissolved yellow P_4 with an anhydrous metal halide ($CuCl_2$ or $NiCl_2$) in rigorously dry, supercritical toluene at 350-400 °C. These reactions were performed using stoichiometric amounts of metal halide and P_4 according to Equation 3.2. The heating profile used in these reactions mimics those of the reactions described in section 3.3.1 (also described in 3.2.3) with the exception of the maximum temperature being 350-400 °C as opposed to 275 °C. All as-

synthesized products were washed with fresh toluene and methanol to remove any unreacted reagent and byproducts.

Since the reaction temperatures and pressures in these reactions were higher from those described in section 3.3.1, several changes had to be made. A graphite gasket was used in place a Teflon one, which would have melted at the higher reaction temperatures. The Teflon-coated stirbar was also replaced by a pyrex-coated stirbar for the same reason. A different autoclave with thicker walls also had to be used as these reactions had the potential of generating pressures above the allowed threshold for the autoclaves used in section 3.3.1. A disadvantage of the autoclave used in these experiments was that it did not have an internal thermocouple. As such, the internal temperatures could not be measured, but instead were approximated based on the external temperature of the autoclave.

In order to achieve a supercritical fluid of toluene, several considerations had to be taken into account. For example, the critical density of toluene is 0.27 g/cm^3, which means that with a reactor volume of 60 mL and the density of toluene being 0.87 g/cm^3, a minimum of 18.62 mL of toluene had to be used ([0.27/0.87]*60=18.62). The critical pressure and temperature of toluene (T_c = 319 °C, P_c = 596 psi) must also be surpassed in order to generate a supercritical fluid. Our synthetic ideal called for a minimum temperature of 350 °C, which is above T_c. Using the ideal gas law, and a temperature of 350 °C, 0.1891 mol (20 mL) of toluene and a volume of 60 mL, a predicted pressure of 2,368 psi was calculated. This pressure is above P_c and is also below the pressure maximum allowed by the reactor. The pressure is limited by the rupture disk which is calibrated to blow out at 5000 psi. Since supercritical fluids deviate from ideal gas behavior, 20 mL of toluene was slowly heated in the autoclave to confirm that the pressures generated would not be too high for our reactor.

When 20 mL of toluene was heated to an external temperature of 450 °C (350-400 °C internal temperature) in the sealed autoclave, a pressure of 900 psi was generated, well

below the predicted 2,368 psi. The reason for this is because the heating mantle used only heats roughly 75 % of the autoclave, leaving the top of the reactor, where the pressure gauge is located, at a cooler temperature. The cooler temperature near the pressure gauge results in a significantly lower pressure than what would be expected had the autoclave been heated evenly at 350-400 °C. Because of this result, a second experiment was performed using 40 mL of toluene, also heating to an external temperature of 450 °C, resulting in a generated pressure of 1520 psi. Because 40 ml of toluene allows for a larger amount of reagent, and was well below the pressure limits of the autoclave when heated, it was the volume of solvent used in the reactions. The results of these experiments show that there is a temperature and pressure gradient in the autoclave when heated. Since the reaction between the reagents will take place in the lower, heated portion of the reactor, we are confident that the local temperature will be highest in this region and solvent densities will approach critical levels.

3.3.9 Phase determination and elemental analysis (supercritical toluene)

Upon cooling, the autoclave reactor was opened, the glass lining (containing reaction solution) was removed, and the supernatant was decanted. Fresh toluene was used to wash the product powders (black) into a centrifuge tube. Successive washes and centrifugations with toluene and methanol were performed and the products were finally air-dried. The washed products were then examined by XRD to determine which if any crystalline phases were present. The washed product from the reaction targeting CuP_2 from $CuCl_2$ revealed the presence of only monoclinic CuP_2.[109] The washed product from the reaction targeting NiP_2 revealed the presence of cubic NiP_2 along with a minimal amount of FeP.[109] The XRD for both the NiP_2 and CuP_2 washed products can be seen in Figure 3.16. The presence of FeP indicated the reaction of phosphorus with the steel autoclave, a reaction that the glass liner attempted to prevent. When a (near) supercritical

fluid is achieved, the reaction environment goes from a solution with headspace to a fluid which fills the whole reactor; this limits the ability of the glass liner to prevent interaction between the reagents and the steel autoclave walls. From previous work (Chapter 2) we know that a minimum temperature of ~350 °C is required to crystallize these phases. The presence of these crystalline phases in the washed products supports our temperature estimations of 350-400 °C and confirms that supercritical temperature conditions were likely achieved.

Energy dispersive spectroscopy (EDS) analysis was performed on the washed CuP_2 and NiP_2 products to determine the M:P molar ratios and to determine the amounts of residual chloride. The EDS analysis also gave us insight into how much Fe from the autoclave ended up in the NiP_2 product. The molar ratio in the CuP_2 product was found to be 1:1.99:0.044 (Cu:P:Cl) and the molar ratio in the NiP_2 product was 1:1.913:0.034 (Ni:P:Cl). The M:P molar ratios were both within 5% of their ideal values (1:2) which is well within EDS sampling error for particulate samples. Residual chlorine amounts were found to be 1.23 % and 1.00 % by weight for CuP_2 and NiP_2 products respectively, which is near EDS detection limits (<2% wt). When looking at the EDS spectra it is clear that the chlorine signals, if any, are buried in the background noise. The Ni:Fe molar ratio was found to be 1:0.15 in the NiP_2 sample, which is consistent with low intensities of the FeP reflections seen in the XRD pattern.

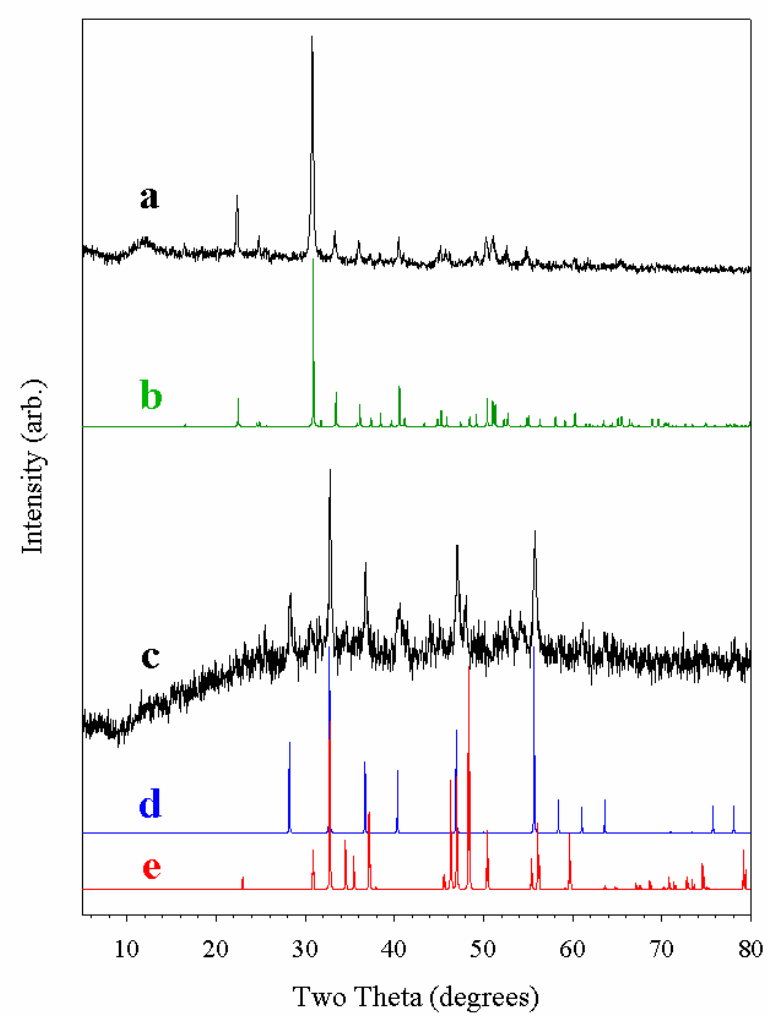

Figure 3.16 Experimental XRD pattern of washed CuP_2 (a), calculated pattern for monoclinic CuP_2 (b), experiment pattern of washed NiP_2 (c), calculated pattern for cubic NiP_2 (d) and of orthorhombic FeP (e).

3.3.10 Product morphologies (supercritical toluene)

Scanning electron microscopy (SEM) revealed that the washed products of CuP_2 were rods of various lengths with diameters of 100 -200 nm and rough surfaces (Figure 3.17). The SEM of washed NiP_2 revealed that the product consisted of discrete, spherical nanoparticles (20-70nm) with no evidence of fusion between particles (Figure 3.18). The appearance of CuP_2 rods was a surprise as they are not at all like the products from CuP_2 formed in superheated toluene (washed or annealed). The nature of the rough surfaces on

the rods suggests that a collection of initially-formed particles may have organized and grown into the irregular rods. The rod formation is certainly a result of the supercritical toluene environment (350-400 °C) as the solid-state annealed products (350 °C) from superheated toluene showed no evidence of rod formation. Both NiP_2 products from $NiCl_2$ in superheated or supercritical toluene were morphologically similar with the exception of their particle size ranges. The spherical NiP_2 particles formed in supercritical toluene had a slightly smaller range (20-70 nm) than those formed in superheated toluene (50-100 nm).

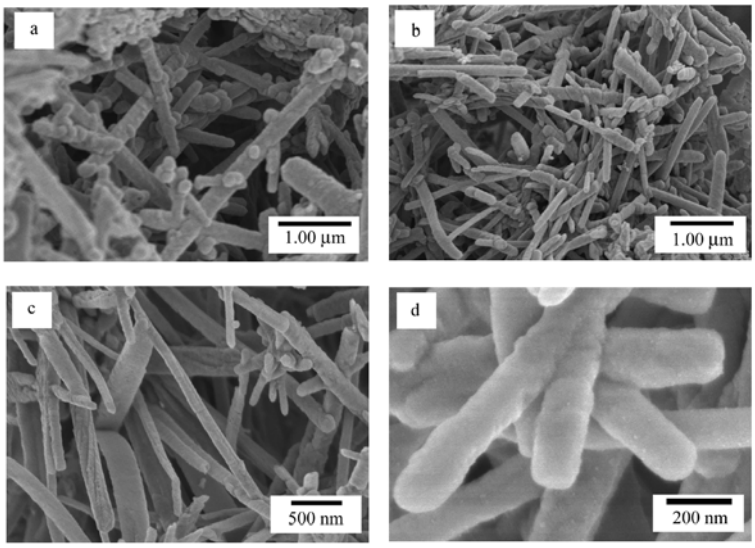

Figure 3.17 Various SEM images of washed CuP_2 synthesized in supercritical toluene.

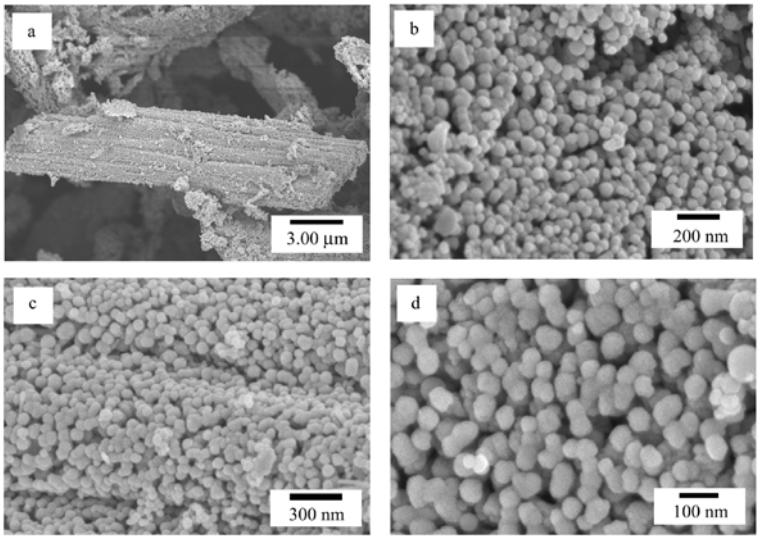

Figure 3.18 Various SEM images of washed NiP_2 synthesized in supercritical toluene.

3.4 Conclusions

The stoichiometric reaction of dissolved yellow P_4 with a suspended metal halide ($CoCl_2$, $NiCl_2$, $NiBr_2$ or $CuCl_2$) in either superheated or supercritical toluene led to the formation of the phase-pure polyphosphides cubic CoP_3, cubic NiP_2 and monoclinic CuP_2. Reactions in superheated toluene required post-reaction annealing (350-600 °C) in order to achieve crystallinity, while the reactions in supercritical toluene were crystalline as-synthesized. This phosphorus-rich phosphide formation reaction is facilitated by thermochemically favorable processes that include the elimination of a PCl_3 or PBr_3 byproduct which subsequently reacts with the toluene forming a variety of alkyl phosphorus halides. These byproducts likely acted as surfactants, stunting the growth of the phosphide particles, resulting in small spherical particles (20-250 nm) or, in the case of CuP_2 in supercritical toluene, rods with sub-micron (100-200 nm) diameters.

CHAPTER 4

BENCHTOP SOLVOTHERMAL SYNTHESIS OF MP_X FROM MCl_2 AND YELLOW OR RED PHOSPHORUS IN NON-COORDINATING, HIGH BOILING-POINT SOLVENTS (M= Co, Ni AND Cu, X= 2 OR 3)

4.1 Introduction and Background

The previous chapter described the synthesis of metal phosphides in superheated or supercritical toluene in high-pressure reactors. These autoclave reactors are inconvenient as they require regular maintenance, replacement of parts, pre-reaction pressure testing and are very expensive. These reactors are also steel and do not allow for any visual observations over the course of the heating ramp. Having the ability to perform similar chemistry on the benchtop would have many advantages, particularly the ease in setup, use of far less expensive glass reaction flasks and the ability to visualize reaction solutions. Benchtop reactions are, however, limited in their maximum temperature potential by the boiling point of the solvent at ambient pressures.

When reactions similar to those in Chapter 3, between a metal halide and yellow P_4, were attempted in refluxing toluene on the benchtop, metal phosphide formation did not occur. In these attempts, the stirred reaction slurry took on the color of the anhydrous metal halide, and after refluxing multiple days, the color persisted. If the reaction had occurred, we would have observed a change in color to black from the presence of metal phosphide particles. The boiling point of toluene is 110 °C, a temperature that was found to be below the temperature threshold for the reaction of metal halides with dissolved P_4. As such, alternative solvents with higher boiling points were explored.

Many types of high boiling point solvents have been used in solvothermal benchtop chemistry such as polycyclic aromatics, long-chain hydrocarbons, long-chain ethers and long chain amines and phosphines. Some of these solvents, like the amines and phosphines, are coordinating Lewis bases; whereas others, such as the hydrocarbons,

are non-coordinating. Although amines and phosphines may be used as solvents, they are typically added as surfactants in conjunction with a non-coordinating solvent. In this chapter, we will focus on the non-coordinating solvents, saving discussion of the coordinating solvents and additives for the next chapter. It should also be noted that there are very few examples in literature of solvothermal, materials syntheses using a non-coordinating, high boiling point solvent without the addition of a surfactant.

One such example is a synthesis using mesitylene, which has a moderately high boiling point of 165 °C. In this synthesis, $TaCl_5$ was refluxed with either solid $LiNH_2$ or Mg_3N_2 for 72 h and upon post-reaction annealing at 600 °C, led to either Ta_3N_5 or TaN.[110] The next two examples use hexadecane as the solvent, which has a boiling point of 287 °C. In one experiment, TiO_2 was synthesized from an exothermic metathesis reaction between $TiBr_4$ and Na_2O_2 in refluxing hexadecane, which acted not only as a solvent but as a heat sink for the heat given off by NaBr formation.[111] In another experiment, $InCl_3$ or $GaCl_3$ was reacted with NaN_3 to form a metal azide which, upon refluxing in hexadecane, decomposed to the corresponding mononitride.[112] In the last example, germanium nanocrystals were synthesized by decomposing organogermane precursors (e.g. tetrabutylgermane) in the exotic, very high boiling point solvents, octacosane ($C_{28}H_{58}$, saturated 28-carbon alkane) and squalene ($C_{30}H_{50}$, 2,6,10,15,19,23-hexamethyl-2,6,10,14,18,22-tetracosahexaene), which reportedly boil between 380 and 429 °C.[113]

In this chapter, we will show how the chemistry introduced in Chapter 3 can be translated to the benchtop by implementing high boiling point solvents. We will also introduce the use of red phosphorus as a phosphorus source, replacing the more toxic yellow P_4. These benchtop reactions will also allow for the visualization of the onset temperature for metal phosphide formation.

4.2 Experimental Section

4.2.1 Reagents used

Metal halides used were anhydrous $CoCl_2$, $NiCl_2$, $NiBr_2$ and $CuCl_2$ (Alfa-Aesar, 99.7%, 98.0%, 98.0% and 98.0% respectively). All metal halides were dried under dynamic vacuum at 250 ºC for a minimum of four hours to remove any adsorbed water and stored in an argon-filled glovebox prior to use. Other reagents and solvents used were elemental white/yellow P_4 (Aldrich, yellow phosphorus 99+% stored in water), red phosphorus (Aldrich, powder, 99%), 1-octadecene (ODE, Aldrich, technical grade, 90%), hexadecane (Aldrich, anhydrous, 99+%), hexanes (Fisher Scientific, 99.9%), and methanol (Fisher Scientific, 99.9%). Low level impurities in white P_4 frequently give it a light yellow appearance. These impurities have been ascribed to traces of polymeric red phosphorus that form on exposure to UV light.[65] All solvents were used as-received without further purification or drying.

4.2.2 Metal phosphide (CoP_3, NiP_2 and CuP_2) synthesis using yellow P_4

In a typical experiment 2.60 mmol of ground metal halide, stoichiometric amounts of P_4 to form the desired MP_x phase and PCl_3 (e.g., 215 mg or 1.73 mmol of P_4 for MP_2, and 295 mg or 2.38 mmol of P_4 for MP_3) and a stirbar were loaded into a 100 ml Schlenk flask in an inert atmosphere argon-filled glovebox. The P_4 was cut from a monolith that was stored under water and dried under vacuum prior to use. Any visible surface oxidized material was shaved from the P_4 block in the glovebox using a razor blade. The resulting yellow/white P_4 was shiny yellow. The Schlenk flask was then sealed with a rubber septum and removed from the glovebox. On the benchtop, 50 mL of N_2 degassed solvent (hexadecane or ODE) was then added to the reaction flask via cannula transfer. The reaction flask was then fit with a condenser under an N_2 blanket and placed in a heating mantle. Reactions were then heated with constant stirring to an

internal temperature of 120 °C over 2 h and held overnight (~15 h), and then heated to reflux (287 °C-hexadecane, 330 °C-ODE) over 2 h and held for two days (~40 h) before being cooled to room temperature (heating scheme A). A second heating profile was used in which reactions were heated with constant stirring to an internal temperature of 120 °C over 2 h and held overnight (~15 h), and then heated to 185 °C over 5 h and held overnight, followed by heating to reflux (287 °C-hexadecane, 330 °C-ODE) over 2 h and held for two days (~40 h) before being cooled to room temperature (heating scheme B). The lower 185 °C temperature step in this scheme was added to ensure the volatile P_4 did not sublime out of the solution prior to reacting with the metal chloride.

Black powder products from hexadecane reactions were then allowed to settle out of the resulting suspension, followed by supernatant removal via cannula transfer. Fifty mL of N_2 degassed hexanes were then added to the reaction flask via cannula transfer and the resulting suspension was stirred for 5 min. after which the stirring was stopped and the products were again allowed to settle out. The resulting supernatant was removed via cannula transfer and the process was repeated with two more 50 ml portions of hexanes and one 50 ml portion of N_2 degassed methanol. The products were then dried under vacuum at room temperature resulting in a dry, fine black powder. The repeated addition of the hexanes served not only to wash the products, but also to thin the hexadecane which cannot easily be removed via vacuum. Methanol addition was solely for the purpose of washing any unreacted metal halide.

Reactions ran in ODE resulted in a very viscous, almost solid suspension from which the particles could not settle out. To remove the supernatant in these reactions, the resulting suspension was heated to 80 °C and the supernatant was removed via filter cannula. The heating was necessary to increase the viscosity of the supernatant allowing for easier removal. The cannula was also heated with a heatgun during filtration so that the supernatant would not cool and resolidify in the cannula. The post-reaction viscosity of the ODE was likely due to polymerization of the ODE across the sight of unsaturation,

possibly catalyzed by the metal phosphide particles. The polymerization of the ODE was also demonstrated as the reactions reached internal temperatures of 330 °C, which is well above its reported boiling point of 319 °C. After removal of the ODE supernatant, the product was washed in the same manner as the products from hexadecane reactions. Selected washed samples were sealed in evacuated pyrex (for annealing ≤500 °C) or silica (for annealing >500 °C) ampoules and heated for 15 h in a horizontal tube furnace for annealing and crystallization studies.

4.2.3 Metal phosphide (CoP_3, NiP_2 and CuP_2) synthesis using red phosphorus

In a typical experiment ~1.80 mmol of ground metal halide, stoichiometric amounts of ground red phosphorus (e.g., 149 mg or 1.20 mmol of red phosphorus for MP_2, and 204 mg or 6.60 mmol of red phosphorus for MP_3) and a stirbar were loaded into a 100 ml Schlenk flask in an inert atmosphere argon-filled glovebox. The Schlenk flask was then sealed with a rubber septum and removed from the glovebox. On the benchtop, 50 mL of N_2 degassed hexadecane was then added to the reaction flask via cannula transfer. The reaction flask was then fit with a condenser under an N_2 blanket and placed in a heating mantle. Reactions were then heated with constant stirring using a similar heating ramp to the reactions described in Section 4.2.2. Although red phosphorus will not sublime out of solution as yellow P_4 does (~140 °C), the initial, lower-temperature heating was used as to mimic the heating used in P_4 reactions. The washing and isolation of as-synthesized black powder products was performed identically to the reactions ran in hexadecane with yellow P_4, with the exception that MeOH washes were not performed. Post-reaction annealings were also performed in the same manner as previously described in section 4.2.2.

4.2.4 Product characterization

SEM analyses were performed on a Hitachi S-4800 or a Hitachi S-3400N microscope with EDS analysis capabilites. XRD data was obtained from a Siemens D5000 XRD system (CuK_{α}, 0.04 step size and 4 sec/step acquisition times).

4.3 Results and Discussion

4.3.1 Metal phosphide (CoP_3, NiP_2 and CuP_2) formation from reactions with yellow P_4

In this study, we investigated the direct reaction of a suspended metal halide ($CoCl_2$, $NiBr_2$, $NiCl_2$ or $CuCl_2$) with dissolved yellow P_4 in refluxing hexadecane or ODE. Reactions were *stoichiometrically balanced* such that all halide was ideally removed as PX_3 and the remaining P_4 formed the metal phosphide product.

$$3\ MX_2 + [(3y + 2)/4]\ P_4 \rightarrow 3\ MP_y + 2\ PX_3 \qquad (4.1)$$

Initial opaque reaction slurries took on the color of the suspended metal halide ($CuCl_2$-brown, $NiCl_2$ and $NiBr_2$-yellow, $CoCl_2$-blue). As was discussed in Chapter 3, initial low-temperature heating for 15 h at 120 °C was necessary to ensure that volatile P_4 would not sublime out of solution, which would perturb the stoichiometry described by Equation 4.1. When yellow P_4 was dissolved by itself in hexadecane and heated at 140 °C, P_4 could clearly be seen condensing at the cooler, upper half of the Schlenk flask. Alternatvely, when 140 °C was reached in all reactions, with a metal halide present, no P_4 condensation was observed. This result was somewhat surprising since in all reactions, except for the reaction with $CuCl_2$, the color of the reaction slurry had not yet changed. Even though there was no clear visual evidence of metal phosphide formation by this point, the lack of P_4 sublimation indicated some P_4-metal halide interaction. Metal phosphide formation could be visualized in these reactions by a color change in the reaction slurry to black. The onset temperatures for metal phosphide formation from the reaction of yellow P_4 with a given metal halide can be seen in Table 4.1.

Table 4.1 Summary of reactions from yellow P_4.

MX_2	Target Phase	Rxn Onset Temp.(°C)	Solvent[1]	Heating Scheme[2]	XRD[3]	
					Crude	Annealed
$CuCl_2$	CuP_2	~ 100	HD	A	amorph. + Cu_3P	CuP_2 + Cu_3P
$CuCl_2$	CuP_2	~ 100	HD	B	CuP_2 + Cu_3P	CuP_2
$CuCl_2$	CuP_2	~ 100	ODE	B	amorph. + CuP_2	CuP_2
$NiBr_2$	NiP_2	~ 200	HD	A	amorph. + Ni_2P	NiP_2 + Ni_5P_4
$NiBr_2$	NiP_2	~ 200	HD	B	amorph. + Ni_2P	NiP_2
$NiCl_2$	NiP_2	~ 240	HD	B	amorph. + Ni_2P	NiP_2
$NiCl_2$	NiP_2	~ 240	ODE	B	NiP_2 + Ni_5P_4 + Ni_2P	NiP_2 + Ni_5P_4
$CoCl_2$	CoP_3	~ 220	HD	B	amorph.	CoP_3

1) HD = hexadecane ODE = 1-octadecene
2) Heating schemes are described in section 4.2.2.
3) Annealing temperatures are either 350 °C (CuP_2 and NiP_2) or 600 °C (CoP_3).
amorph. = broad amorphous humps.

4.3.2 Product phase determination from reactions with yellow P_4

Washed and annealed products were analyzed by XRD to determine which crystalline phases were present in the powders. Initial reactions with $CuCl_2$ and $NiBr_2$ were performed in hexadecane using heating scheme A, which parallels the scheme used for reactions in superheated toluene described in Chapter 3. The XRD pattern of washed product from $CuCl_2$ targeting CuP_2 revealed broad amorphous humps along with low intensity reflections consistent with Cu_3P and upon annealing this sample at 350 °C, the XRD pattern revealed CuP_2 as the major product along with Cu_3P as the minor product (significantly less intense reflections, see Figure 4.1). The XRD pattern of washed product from $NiBr_2$ targeting NiP_2 revealed broad amorphous humps along with reflections consistent with Ni_2P and upon annealing this sample at 350 °C, the XRD pattern revealed NiP_2 as the major product along with Ni_5P_4 as the minor product (Figure 4.2).

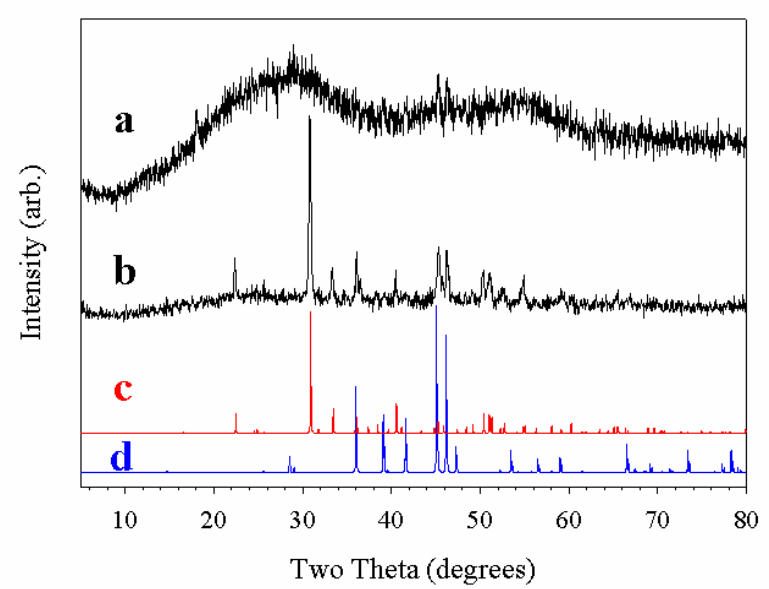

Figure 4.1 Experimental XRD of the washed (a) and annealed (b) products from the reaction targeting CuP_2 from yellow P_4 using heating scheme A in hexadecane. Calculated patterns for CuP_2 (c) and Cu_3P (d).

Both of these experiments resulted in products which contained metal-rich phosphide phases along with the targeted phosphorus-rich phase, indicating that the samples were phosphorus deficient. Even though P_4 could not be visualized subliming out of solution upon fast heating from 120 to 287 °C (2h), it is possible that unnoticeable small amounts were during this stage, which could account for phosphorus deficiencies. To test this notion, a second heating profile was used in which after heating to 120 °C overnight, reactions were slowly (over 5 h) heated to 185 °C, and held there overnight before finally being heated to reflux, where they were again held for 2 days (heating scheme B).

Using heating scheme B, reactions of yellow P_4 with $CoCl_2$, $NiCl_2$, $NiBr_2$ and $CuCl_2$ were performed in hexadecane. The XRD pattern of the washed product from $CoCl_2$ targeting CoP_3 revealed only broad amorphous humps, but upon annealing at 600 °C, the XRD pattern revealed only the targeted CoP_3 (Figure 4.3). The XRD patterns

from the washed products targeting NiP_2 from $NiCl_2$ and $NiBr_2$ both revealed broad amorphous humps along with Ni_2P and upon annealing at 350 °C, both XRD patterns showed only the targeted NiP_2 (Figure 4.4). The XRD pattern of the washed product from $CuCl_2$ targeting CuP_2 revealed the presence of CuP_2 as a major product and Cu_3P as a minor product and upon annealing at 350 °C, the XRD pattern revealed only the presence of the targeted CuP_2 (Figure 4.5). All of these products, upon annealing, showed the presence of only the targeted phosphorus-rich metal phosphide, supporting the necessity of the extra heating step in heating scheme B.

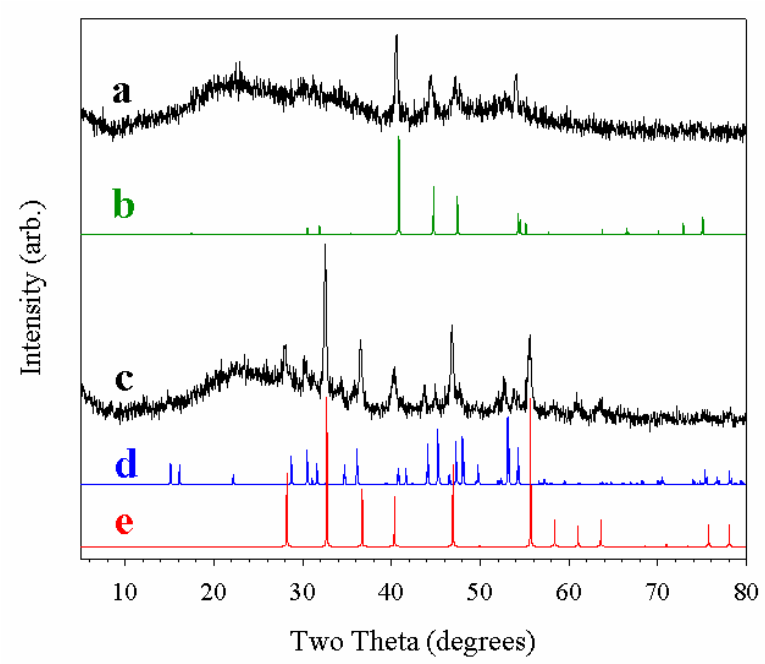

Figure 4.2 Experimental XRD of the washed (a) and annealed (c) products from the reaction targeting NiP_2 from yellow P_4 using heating scheme A in hexadecane. Calculated patterns for Ni_2P (b), Ni_5P_4 (d) and NiP_2 (e).

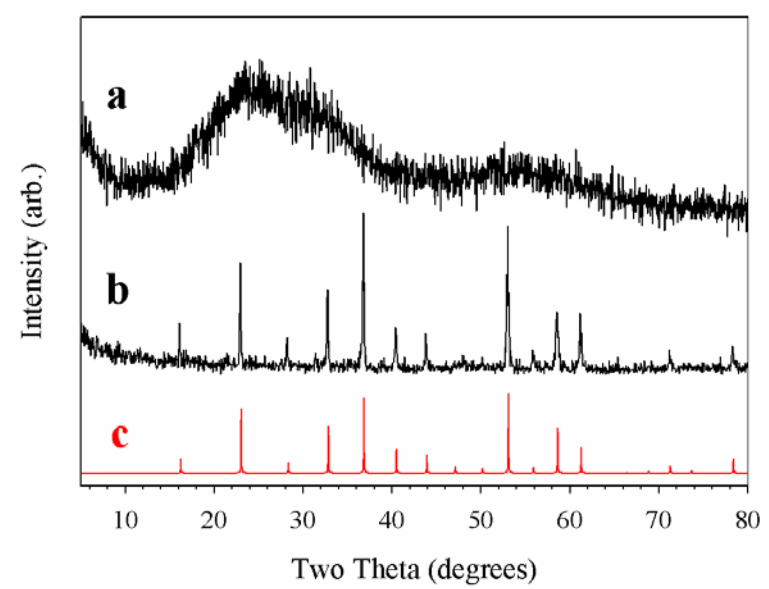

Figure 4.3 Experimental XRD of the washed (a) and annealed (b) products from the reaction targeting CoP_3 from yellow P_4 using heating scheme B in hexadecane and the calculated pattern for CoP_3 (c).

From looking at these results, we can see that crystallizing NiP_2 can be achieved at 350 °C, while CuP_2 was shown to crystallize, albeit along with Cu_3P, at 287 °C, (boiling point of hexadecane) and after annealing at 350 °C, was phase-pure CuP_2 (Figure 4.5). The minor increase in temperature moving from the solvent reaction to solid state annealing begs the question as to whether phase-pure, crystalline products could be synthesized in solution if hexadecane was replaced with a higher boiling-point solvent. To test this, ODE (boiling point 319 °C) was used in place of hexadecane in reactions of yellow P_4 with $CuCl_2$ or $NiCl_2$ using heating scheme B. In these reactions, the internal temperature was able to reach 330 °C, as discussed in Section 4.2.2, bringing the reaction temperature closer to the 350 °C annealing temperature used for products from hexadecane reactions.

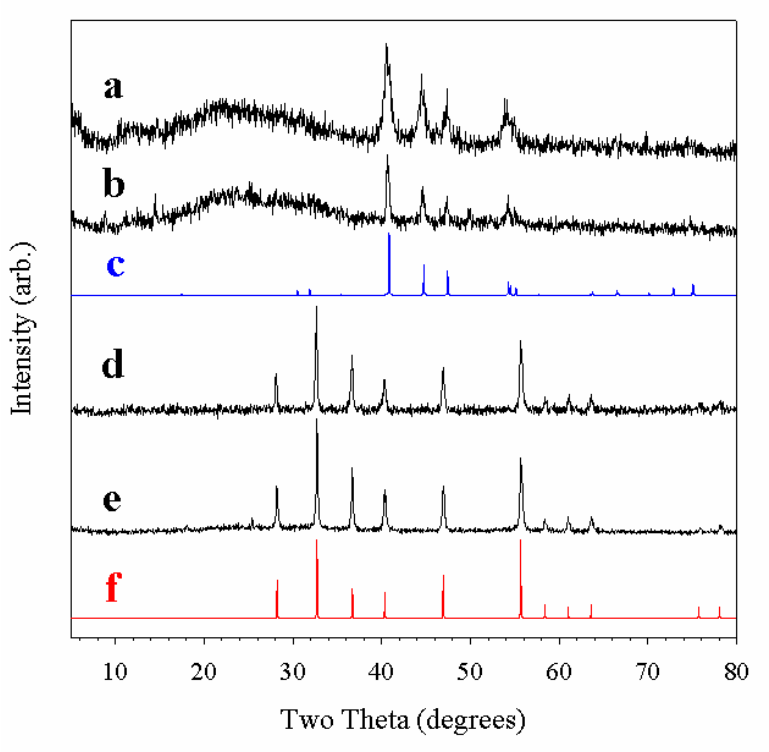

Figure 4.4 Experimental XRD of washed products from either $NiBr_2$ (a) or $NiCl_2$ (b) and yellow P_4 using heating scheme B in hexadecane. Experimental XRD of 350 °C annealed samples from $NiBr_2$ (d) and $NiCl_2$ (e). Calculated patterns for Ni_2P (c) and NiP_2 (d).

The XRD of washed product from $CuCl_2$ targeting CuP_2 in ODE revealed broad amorphous humps along with low-intensity reflections from CuP_2 and upon annealing at 350 °C showed only the targeted CuP_2 (Figure 4.6). The analogous washed product from reaction in hexadecane showed less amorphous diffraction and far more crystalline CuP_2 and Cu_3P. Upon annealing to 350 °C, this product transformed, revealing only CuP_2. The washed product from the reaction in ODE, which peaked at 330 °C (between 287 and 350 °C), revealed an XRD pattern that may be representative of a transition in which Cu_3P is being consumed and CuP_2 is beginning to recrystallize.

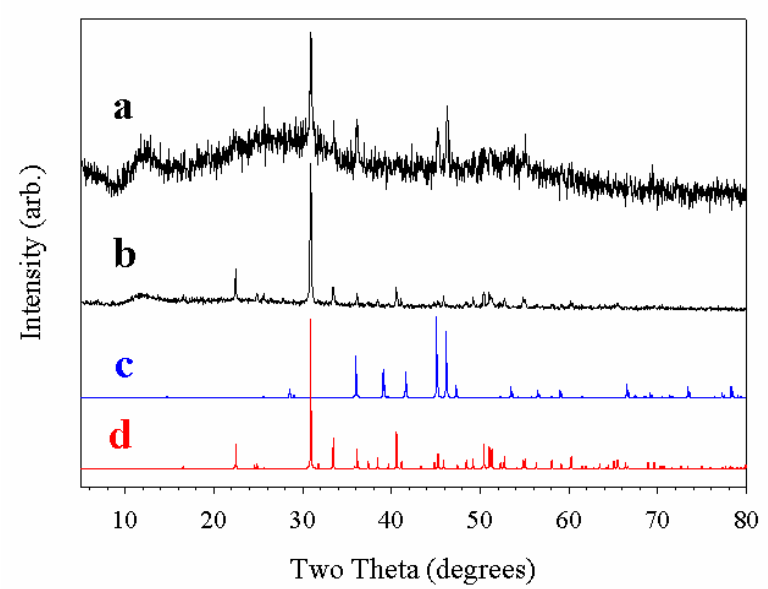

Figure 4.5 Experimental XRD of the washed (a) and annealed (b) products from the reaction targeting CuP_2 from yellow P_4 using heating scheme B in hexadecane. Calculated patterns for Cu_3P (c) and CuP_2 (d).

The XRD of washed product from $NiCl_2$ targeting NiP_2 in ODE revealed the presence of crystalline Ni_2P along with evidence of poorly crystalline Ni_5P_4 and NiP_2 and upon annealing at 350 °C revealed NiP_2 and Ni_5P_4 (Figure 4.7). The result of the washed XRD shows an improvement from the reaction in hexadecane in that the targeted NiP_2 is present without annealing. However, the persistence of crystalline Ni_5P_4 through the annealing process is a shortcoming when compared to the hexadecane reaction. In my experience, once Ni_5P_4 forms it is not consumed upon annealing as occurs with Cu_3P and Ni_2P. This observation indicates that Ni_5P_4 may be a thermodynamic trap, which once formed, prevents the production of the phase-pure, targeted phosphorus-rich NiP_2. A summary of all experimental XRD results from reactions with yellow P_4 can be seen in Table 4.1.

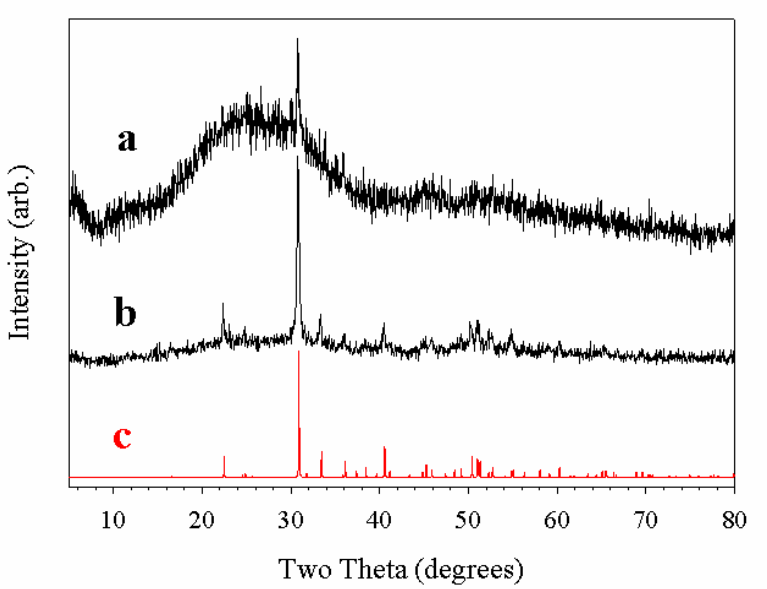

Figure 4.6 Experimental XRD of the washed (a) and annealed (b) products from the reaction targeting CuP_2 from yellow P_4 using heating scheme B in ODE. Calculated pattern for CuP_2 (c).

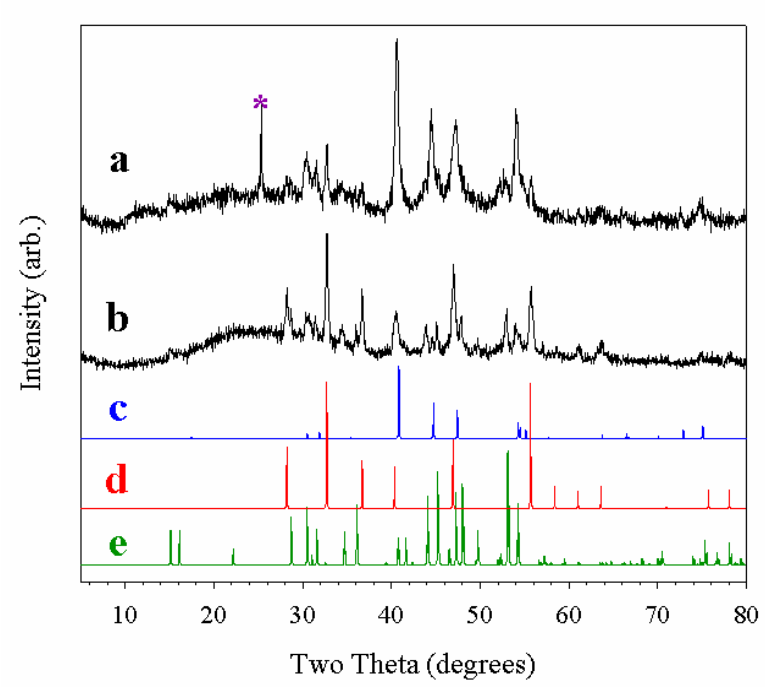

Figure 4.7 Experimental XRD of the washed (a) and annealed (b) products from the reaction targeting NiP_2 from yellow P_4 using heating scheme B in ODE. Calculated patterns for Ni_2P (c), NiP_2 (d) and Ni_5P_4 (e).

4.3.3 Product morphologies from reactions with yellow P_4

Scanning electron microscopy (SEM) images were taken on the washed and annealed samples that were synthesized from yellow P_4 in hexadecane using heating scheme B. The images of the washed product from the reaction targeting CoP_3 revealed spherical particles ranging from 10-30 nm in size and upon annealing the particles fused, forming irreregular aggregates with 50-300 nm sized features (Figure 4.8). The images of the washed product from the reaction targeting CuP_2 revealed fused ellipsoidal aggregates with features ranging from 50-200 nm in size and upon annealing these aggregates grew into large, irregular, micron-sized, faceted plates (Figure 4.9). The

growth of similar plates was seen in annealed CuP_2 products from superheated toluene (Chapter 3) as well. The images of washed product from the reaction targeting NiP_2 revealed irregular ellipsoidal particles 10-100 nm ellipsoidal particles which upon annealing showed no significant change in shape (Figure 4.10).

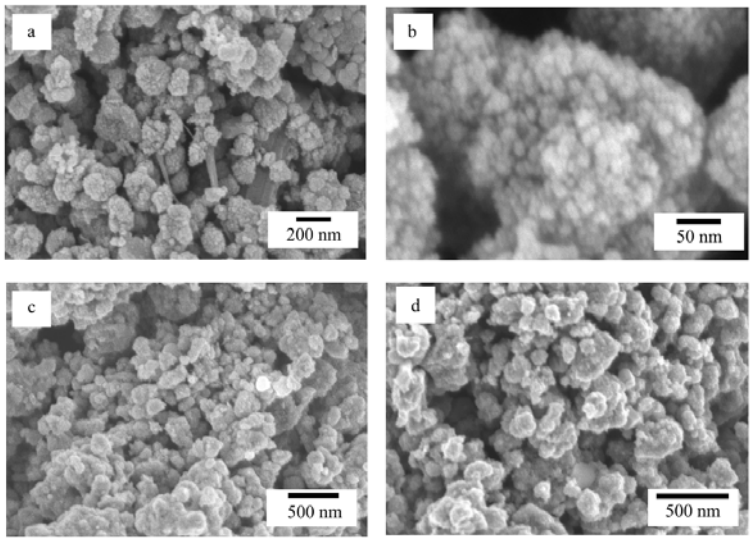

Figure 4.8 SEM images of washed (a and b) and annealed (c and d) samples from reactions targeting CoP_3 from yellow P_4 using heating scheme B in hexadecane.

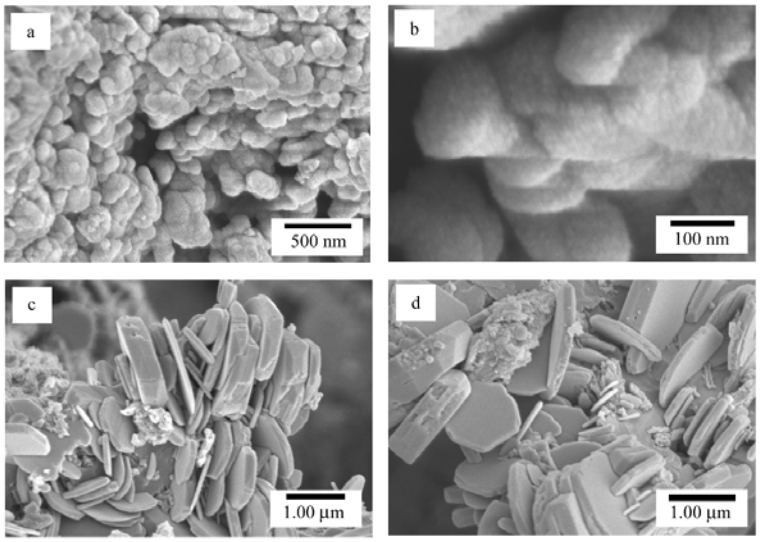

Figure 4.9 SEM images of washed (a and b) and annealed (c and d) samples from reactions targeting CuP_2 from yellow P_4 using heating scheme B in hexadecane.

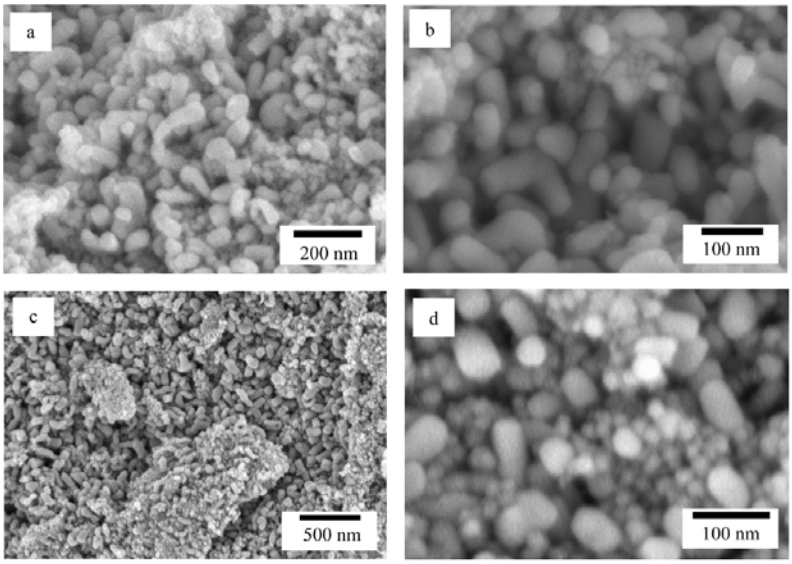

Figure 4.10 SEM images of washed (a and b) and annealed (c and d) samples from reactions targeting NiP_2 from yellow P_4 and $NiCl_2$ using heating scheme B in hexadecane.

4.3.4 Metal phosphide (CoP_3, NiP_2 and CuP_2) formation
from reactions with red phosphorus

In these reactions, conducted with the assistance of an undergraduate Miller Li, a suspension of a metal halide ($CoCl_2$, $NiBr_2$ and $CuCl_2$) and red phosphorus were reacted together directly in hexadecane. Reactions were *stoichiometrically balanced* such that all halide was ideally removed as PX_3 and the remaining red phosporus formed the metal phosphide product.

$$3\ MX_2 + (3y+2)\ P_{red} \rightarrow 3\ MP_y + 2PX_3 \qquad (4.2)$$

Red phosphorus is a polymeric form of phosphorus that is air-stable and far-less reactive and toxic than yellow P_4. Unlike yellow P_4, red phosphorus is commercially available, and can be purchased as a fine powder. The reactions in this section are intended to mimic the reactions from Section 4.2.3, with the only change being that reactive, commercially unavailable yellow P_4 is replaced with less toxic, commercially available red phosphorus.

Red phosphorus, being polymeric as opposed to molecular like P_4, will not sublime out of solution. This is advantageous when compared to reactions with yellow P_4, as P_4 can transport out of the reaction flask and condense in the condenser, disrupting the reaction stoichiometry. One disadvantage, when compared to yellow P_4, is that it is insoluble and less reactive. The insolubility of the red phosphorus and the metal halide in hexadecane only allow for reactions to occur between reagent particle surfaces. Because of this, reactions may rely on slow solid-solid diffusion for reaction completion.

Initial reaction slurries are opaque and brick red from the presence of red phosphorus and change to black as metal phosphide formation occurs. The onset temperatures for metal phosphide formation are 225, 230, and 270 °C for $CuCl_2$, $NiBr_2$ and $CoCl_2$, respectively. These temperatures are all higher than in their yellow P_4 reaction counterparts, especially for $CuCl_2$ which reacts at ~100 °C with yellow P_4. This result is not surprising as red phosphorus is more stable than yellow P_4, which is highly

reactive due to its ring strain and lone pairs on each P atom in the P_4 tetrahedron. The complete color change of reaction slurries to black also occurs more slowly (hours verus minutes) than analogous P_4 reactions, an observation that may be directly related to red phosphorus' insolubility and low reactivity.

4.3.5 Product phase determination from reactions with red phosphorus

Washed and annealed products were analyzed by XRD to determine which crystalline phases were present in the powders. All reactions were performed using heating scheme B. The XRD pattern of washed product from $CuCl_2$ targeting CuP_2 revealed broad amorphous humps along with a low intensity reflection consistent with the most intense reflection for CuCl and upon annealing this sample at 350 °C, the XRD pattern revealed only the targeted CuP_2. The XRD pattern of washed product from $NiBr_2$ targeting NiP_2 revealed broad amorphous humps along with reflections consistent with $NiBr_2$ and upon annealing this sample at 350 °C, the XRD pattern revealed only the targeted NiP_2. The XRD pattern of washed product from $CoCl_2$ targeting CoP_3 revealed an amorphous product that upon annealing at 500 °C revealed the presence of crystalline CoP_3. Experimental XRD patterns for annealed samples can be seen in Figure 4.11.

The presence of $NiBr_2$ and CuCl in washed products indicates incomplete reactions occurred. Methanol washes were not performed because we desired to see if reactions could proceed to completion via Equation 4.2. However, upon annealing these halides were no longer detected and only the targeted NiP_2 and CuP_2 were observed. This indicates that the halides underwent further reaction with the as-synthesized MP_x products during annealing. Annealing temperatures (350 °C) for the NiP_2 and CuP_2 products were below reduced pressure sublimation temperatures for $NiBr_2$ and CuCl, which rules out halide sublimation as a means for the elimination of the halides during the annealing process. Any significant transport of metal halide would have been

visually evident as well. A fraction of the as-synthesized NiP_2 was washed with methanol to remove any unreacted $NiBr_2$ and then put through the same annealing process to see if NiP_2 was still afforded. The removal of $NiBr_2$ was confirmed by XRD prior to annealing, and the post-annealing product was found to be NiP_2. This result indicates that the residual $NiBr_2$ must have been minimal and that the stoichiometry in equation 4.2 was not perturbed to a large extent. Experimental XRD patterns of annealed products synthesized from red phosphorus can be seen in Figure 4.11.

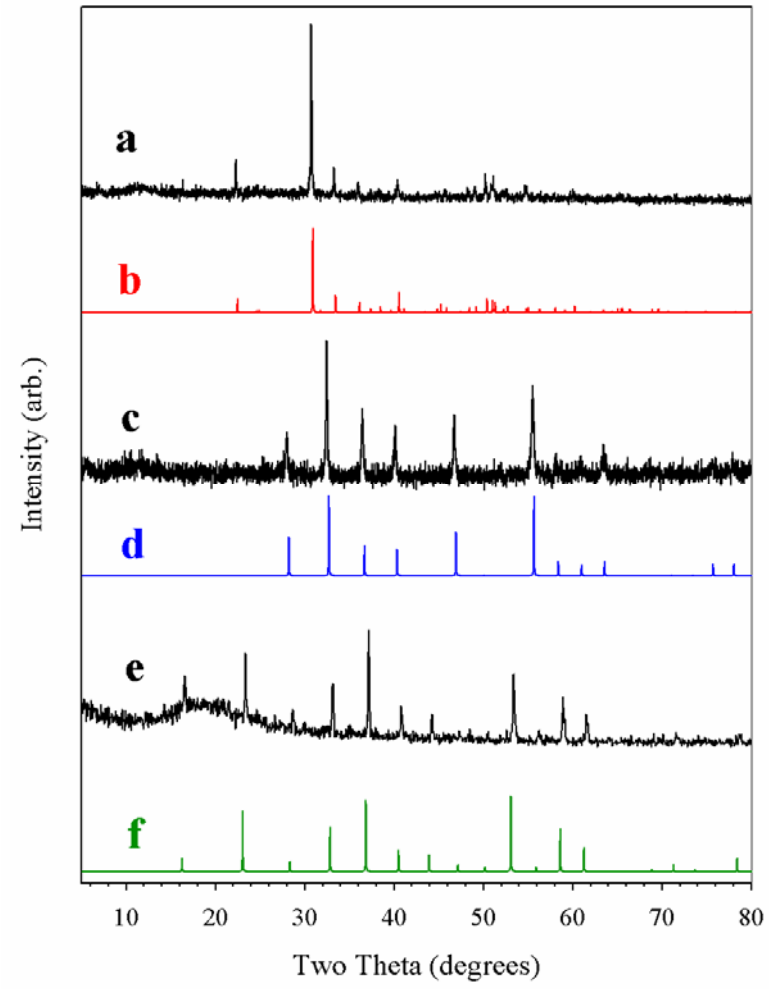

Figure 4.11 Experimental XRD of annealed products from reactions targeting CuP_2 (a), NiP_2 (c) and CoP_3 (e) from red phosphorus and the calculated patterns for CuP_2 (b), NiP_2 (d) and CoP_3 (f).

4.3.6 Product morphologies from reactions with red phosphorus

Scanning electron microscopy (SEM) images were taken on the crude and annealed samples that were synthesized from red phosphorus in hexadecane using

heating scheme B (Figure 4.12). The morphologies of all of these products were micron-sized, highly irregular particles. This is likely due to the reaction occurring between two highly insoluble, solid, particulate reagents.

The crude and annealed products from the reaction targeting CoP_3 showed very similar morphologies consisting of large particles (~2-20 μm) with smaller surface features (50-200 nm). The crude product and annealed products from the reaction targeting NiP_2 also showed similar morphologies consisting of large particles (~sub-micron to 20 μm) with smaller surface features (~30-300 nm). The crude product from the reaction targeting CuP_2 revealed large particles (~1-10 μm) with smaller surface features (~100-600 nm). The annealed samples of CuP_2 revealed a mixture of particles similar to the crude along with smoother, more faceted surface features (~100-1000 nm). SEM images of these products can be seen in Figure 4.12.

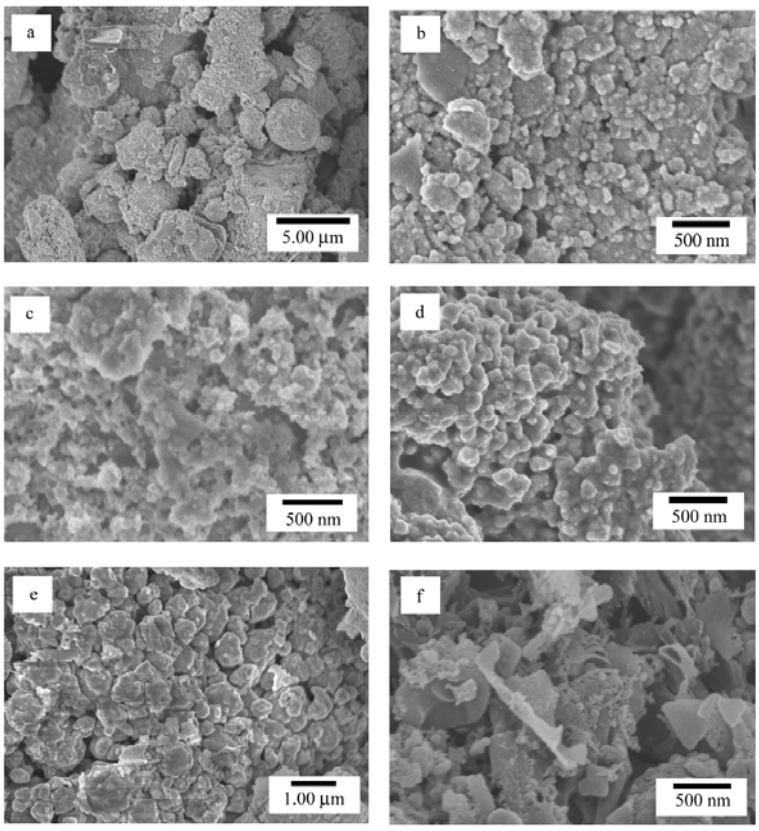

Figure 4.12 SEM images of crude products from the reaction targeting CoP_3 from red phosphorus (a and b). SEM images of crude (c) and annealed (d) products from the reaction targeting NiP_2 from red phosphorus. SEM images of crude (e) and annealed (f) products from the reaction targeting CuP_2 from red phosphorus.

4.4 Conclusions

The stoichiometric reaction of a suspended metal halide ($CoCl_2$, $NiCl_2$, $NiBr_2$ or $CuCl_2$) with either dissolved yellow P_4 or suspended red phosphorus in a high-boiling point solvent (hexadecane or ODE) led to the formation of the phase-pure polyphosphides cubic CoP_3, cubic NiP_2 and monoclinic CuP_2 when heating scheme B was used. The reactions with yellow P_4 using the shorter heating scheme B resulted in

products with mixtures of the targeted phosphorus-rich phase along with a metal-rich phosphide phase. In all reactions, post-reaction annealing (350-600 °C) was necessary to produce the phase-pure, targeted phase.

These experiments demonstrated how the chemistry from Chapter 3 can be adapted to a more convenient, benchtop reflux route in high boiling point solvents, avoiding the use of high-pressure reactors. We also demonstrated how commercially unavailable, pyrophoric, and toxic yellow P_4 can be replaced with the more benign allotrope, red phosphorus, and still produce the targeted phosphorus-rich phosphides.

CHAPTER 5

SURFACTANT-AIDED SOLVOTHERMAL SYNTHESIS OF MP_X (M = Ni OR Cu)

5.1 Introduction and Background

The previous chapter presented successful syntheses of phase-pure, phosphorus-rich transition-metal phosphides from the reaction of a metal halide with an elemental phosphorus source in either superheated toluene or in a refluxing, high boiling point solvent or without solvent. In this chapter, we will modify these syntheses by introducing a molecular, Lewis base surfactant in attempts to stunt and control solution particle growth and potentially improve solution crystallization.

In recent years, the development of nanomaterials has been at the forefront of materials research.[114] This is due to many advantageous properties associated with nanoparticles that are not seen in their bulk counterparts. Nanoparticles have an inherently higher surface area which has shown to increase their catalytic abilities.[115,116] The optical and electronic properties of semiconducting nanoparticles are size dependent in the nano-regime (> 20 nm),[4] making them attractive, tunable materials for electronics and photovoltaics.[5,117] Nanoparticles can also exist as water soluble colloids which can be used for medical imaging.[13]

The synthesis of inorganic nanostructures can be achieved by either "top-down," templated routes or by "bottom-up" self-assembly routes. There are several "top-down" approaches including vapor phase growth, the vapor-liquid-solid approach and physical template routes to name a few. The vapor phase growth method is used to form nanometer thick films by depositing gaseous molecular precursors on substrates at high temperatures (chemical vapor deposition) or by using high energy sources (i.e., laser ablation) to vaporize non-volatile precursors and deposit them on substrates (molecular beam epitaxy).[118] The vapor-liquid-solid approach involves the dissolution of gaseous

reactants into nanosized liquid droplets of a metal catalyst which, upon saturation, direct the growth of nanowires.[119] In physical template routes, an easily removable, non-reactive template such as polystyrene or silica nanospheres, are coated with precursors and are removed post-reaction, leaving materials with morphologies reminiscent of the template.[120]

The "bottom-up" routes are primarily low-temperature, solvothermal routes in which reactive molecular precursors react to form nuclei which grow in a snowball like manner. This growth is stunted, and the nanoparticles are stabilized by the presence of surfactants; this method is also referred to as arrested precipitation.[6] One of the most common surfactants is tri-n-octylphosphine oxide (TOPO), which is often used as a surfactant and also as a high boiling point solvent (bp = 370 °C).[121,122] In these reactions, dissolved molecular precursors are injected into hot TOPO resulting in a short burst of homogeneous nucleation. Upon injection, reagents are depleted during the rapid nucleation and the temperature of the reaction solution drops from the injection of room temperature solvent; these two occurrences prevent the nuclei from further growth. Upon reheating the solution, the nuclei react with each other, growing in size, a process called "Ostwald ripening." The extent of ripening, particle size and particle size distribution can often be controlled by varying surfactant amounts, temperature and ripening durations.[123]

Surfactants stabilize nanoparticles by coordinating to surface metal sites and in doing so, passivate the particles' surface, disallowing further growth. By passivating the surface, the surface energies are lowered, stabilizing the otherwise labile and reactive nanoparticles.[124] Coordination to metal sites is achieved by surfactants which are Lewis bases that can form dative (when neutral) or polar covalent (when anionic) bonds with the metal through their lone pairs. There are many types of surfactants which are commonly used such as thiols,[125,126] amines,[107,127] phosphines,[98,106] carboxylates,[128,129] and phosphonic acids.[130,131] These functional groups make up the "head groups" of the

surfactant and typically have greasy, long-chain alkyl "tail groups." The long chain of the tail groups is used to sterically stabilize the particles and also forms a monolayer on the particles which is miscible with commonly-used, non-polar, organic solvents; both of these attributes help prevent particle aggregation.[132]

The interaction of the surfactant with the particle is referred to as the organic-inorganic interface. At this interface, the interaction is dynamic, meaning that the surfactants are constantly changing between being bound and unbound (ligand exchange). This ligand exchange process is thermodynamically driven, where at high temperatures the equilibrium is shifted in favor of unbound surfactant. Because the syntheses are typically performed in hot solvents (~150-350 °C), excess surfactant is necessary to ensure that particles are passivated, and therefore stabilized at elevated temperatures, stunting particle growth. The addition of excess surfactant to stabilize nanoparticles is an example of Le Chatlier's Principle where by increasing the surfactant concentration shifts the equilibrium in favor of the ligand being in the bound state. This process is depicted in Figure 5.1. The discussion in this paragraph was adapted from a 2005 review by Yin and Alivisatos published in *Nature*.[133]

Surfactant-aided nanoparticle syntheses of monophosphides and metal-rich phosphides from molecular precursors have been performed successfully in several ways.[134] In one synthesis, $Mn_2(CO)_{10}$ or $Fe(CO)_5$ was injected into a hot (350 °C) surfactant mixture of tri-n-octylphosphine (TOP) and TOPO in ODE (1-octadecene) affording MnP and Fe_2P nanocrystals.[98,135] In another synthesis, metal halide hydrates were reacted with excess yellow P_4 in ethylenediamine, which acted as a solvent and surfactant, affording Ni_2P, Co_2P and Cu_3P nanoparticles.[78]

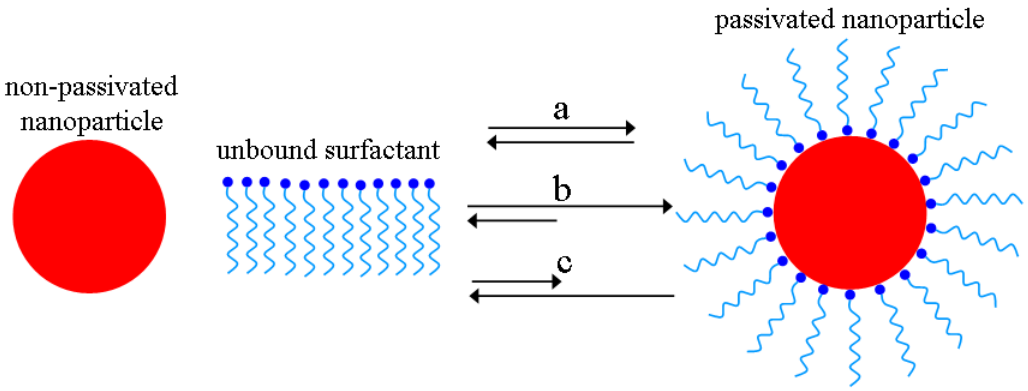

Figure 5.1 Cartoon schematic illustrating the dynamic process at the organic-inorganic interface. Arbitrary equilibrium state (a), the shift in equilibrium towards passivated nanoparticles achieved by the addition of excess surfactant (b) and the shift in equilibrium towards unbound surfactant and non-passivated nanoparticles achieved by increasing the temperature (c).

Solvothermal routes to phosphorus-rich metal phosphides are far less reported. To our knowledge, there are only three solvent-aided syntheses that produce phosphorus-rich metal phosphides; one converted metal nanoparticles into metal phosphides using trioctylphosphine as the solvent and the phosphorus source at 360 -370 °C (Au_2P_3, PdP_2, and PtP_2)[100,101] and another used phosphorus-containing organometallic complexes that were incorporated into silica xerogels and subsequently decomposed at elevated temperatures of 700 °C (PtP_2).[102] The third example is our recent report describing reactions between dissolved molecular yellow/white molecular P_4 and metal chlorides in superheated toluene that produce amorphous products at 275 °C, which crystallize to CoP_3, NiP_2, and CuP_2 upon annealing at 350-500 °C.[136]

None of these reports can be considered a surfactant-aided, arrested precipitation route. The TOP report utilized a surfactant, however this route is still a template route as metal nanoparticles were converted to the phosphide, not grown from nuclei. The

organometallic complex report was also a templated route and did not use surfactants. Our recent report was a mixed solid suspension/molecular route, and we did not utilize surfactants to stunt particle growth. In this chapter, we will present various syntheses targeting NiP_2 and CuP_2 using various surfactant-aided, solvothermal systems.

5.2 Experimental Section

5.2.1 Reagents used

Metal halides used were anhydrous $NiCl_2$, $NiBr_2$ and $CuCl_2$ (Alfa-Aesar, all 98%), which were all dried in vacuo for a minimum of 4 hours at 250 °C and 100 mTorr to remove any adsorbed water and stored in an argon-filled glovebox prior to use. Acetylacetonates (acac) used were $Cu(acac)_2$ (Strem 98 +%) and $Ni(acac)_2$ (Alfa-Aesar 95%) which were stored in an argon-filled glovebox and used as-received. Elemental phosphorus used was white/yellow P_4 (Aldrich, yellow phosphorus 99+% stored in water). Surfactants used were oleylamine (OA, Aldrich, 70 % technical grade, >98 % primary amine), tri-n-octylamine (TOA, Alfa-Aesar, 98%), tri-n-octylphosphine (TOP, Strem, 97%) and tri-n-octylphosphine oxide (TOPO, Aldrich, 90% technical grade) all used without further purification. Solvents used were 1-octadecene (ODE, Aldrich, technical grade, 90%), hexadecane (Aldrich, anhydrous, 99+%), toluene (Fisher Scientific, 99.9%), mesitylene (Alfa-Aesar 98+%), hexanes (Fisher Scientific, 99.9%), and methanol (Fisher Scientific, 99.9%). Toluene and mesitylene were distilled from sodium prior to use, all other solvents were used as-received.

5.2.2 Metal phosphide synthesis from metal halides and yellow P_4 in refluxing toluene

In a typical synthesis, ~3.00 mmol of ground metal halide ($CuCl_2$, ~403 mg or $NiBr_2$, ~655 mg) was loaded into a 100 mL round-bottom Schlenk flask along with a stirbar. Stoichiometric amounts of yellow P_4 to form MP_2 and PCl_3 or PBr_3 (~2.00 mmol,

248 mg), and a stir bar were loaded into a separate, 100 mL round-bottom Schlenk flask. The P_4 was cut from a monolith that was stored under water and dried under vacuum prior to use. Any visible surface oxidized material was shaved from the P_4 block in the glovebox using a razor blade. The resulting yellow/white P_4 was shiny yellow. These flasks were fit with rubber septa and brought out of the glovebox.

On the benchtop, 25 mL of N_2 degassed toluene was transferred into each of the two Schlenk flasks via cannula transfer. Oleylamine was added via N_2 flushed syringe to the halide-containing flask such that the metal:OA molar ratio was 1:4 (12 mmol, ~4 mL). The added OA acted to complex the metal halide, resulting in a completely toluene-soluble molecular metal halide, amine complex. Complete complexation of the $CuCl_2$ was achieved in less than five minutes when the solution is heated to 75 °C with vigorous stirring under an N_2 blanket, resulting in a deep royal blue, translucent solution. The complexation of the $NiBr_2$ was a far more timely process requiring heating at 75 °C for 3 days under an N_2 blanket, resulting in a green, translucent solution. Metal halide complex solutions were then allowed to cool to room temperature.

The yellow P_4 was dissolved in the 25 mL of toluene at room temperature by vigorously stirring for ~15 minutes. Once completely dissolved, the metal halide complex solution was transferred to the yellow P_4 containing Schlenk flask via cannula transfer. The resulting reaction solution was then fit with a condenser under an N_2 blanket and placed in a heating mantle. While stirring, the reaction was kept at room temperature for 30 minutes before slowly heating to reflux (30 °C/ hour), where it was kept for 1-4 days, before cooling back down to room temperature.

The resulting MP_x particles were then isolated by inducing flocculation with an anti-solvent. In this process, ~10 mL increments of reaction solution were placed in a centrifuge tube and diluted to 25 mL with hexanes. Then 25 mL of the anti-solvent, methanol, was added to the tube. The resulting solution was centrifuged at 3000 RPM for 10 minutes resulting in the aggregation of the particles in the end of the tube. This

process was repeated by adding an additional 10 mL of reaction solution to the same centrifuge tube until all of the reaction solution had been added. This resulted in all of the MP_x particles being isolated at the bottom of one centrifuge tube. The resulting waxy, black solid was then dried *in vacuo* at 75 °C for 2 hours.

Selected washed samples were subjected to a variety of post reaction heat treatments. Solid-state annealing was performed by placing some washed sample in a pyrex ampoule, which was then sealed by a CH_4/O_2 torch under vacuum. The resulting evacuated ampoule was then heated to 350 °C in a tube furnace overnight. Solvent-mediated annealings were performed by placing washed product in a Schlenk flask with a stirbar and resuspending it in a solvent or solvent mixture (OA, ODE, TOPO or a TOP/TOPO mixture). The flasks were then fit with a condenser under an N_2 blanket and placed in a heating mantle where they were heated (~100 °C/ h) to between 320-360 °C, depending on the solvent, overnight. The resulting MP_x particles were isolated by the same flocculation-inducing process described above, although in some cases anti-solvent was not necessary to induce particle aggregation.

5.2.3 Metal phosphide synthesis from metal halides and yellow P_4 in high boiling point solvents

This section describes syntheses that, while similar, have multiple variables that were adjusted from reaction to reaction. These variables include solvent, surfactant, surfactant to metal ratio, phosphorus amount and heating profile. A tabular summary of these reactions is presented later in Table 5.1.

In a typical synthesis, ~2.00 mmol of ground metal halide ($CuCl_2$, $NiCl_2$ or $NiBr_2$) and a varying amount of yellow P_4 were loaded together with a stirbar in a 100 mL round bottom Schlenk flask in an argon-filled glovebox. Amounts of yellow P_4 were either stoichiometric (~1.33 mmol) or 50% greater than stoichiometric (~2.00 mmol). This Schlenk flask was fit with a rubber septum and brought out of the glovebox. On the

benchtop, solvent was added to the reaction flask via cannula transfer. When the solvent used was non-coordinating ODE or HD, 50 mL was used. When the solvent used was coordinating TOA or TOP, ~20 mL was used, as these solvents more effeiciently dissolve MX_2. Reactions in HD or ODE had surfactant (TOA or TOP) added via N_2 flushed syringe in varying amounts. The metal to surfactant molar ratio can vary from 1:2 to 1:4 in reactions in HD or ODE. The metal to surfactant ratio increases significantly (1:22-25) in reactions ran in TOA or TOP as the TOA and TOP act as both the solvent and the surfactant. In all of these systems, the addition of surfactant resulted in the partial dissolution of the metal halide as evident by the appearance of a colored solution (metal halide complexation) and uncomplexed metal halide powder settled at the bottom of the reaction flask.

Once solvent and surfactant were added to the flask containing the metal halide and yellow P_4, the flask was fit with a condenser under an N_2 blanket and placed in a heating mantle. Reactions were heated over 3 h to ~120 °C, where they were held overnight (~15 h), and are then heated over 2h to between 287 and 330 °C, depending on the solvent, and were held at this temperature for 1-2 days before being cooled to room temperature.

The resulting cooled reaction suspension was transferred to a centrifuge tube and centrifuged at 3000 RPM for 5 minutes. The black powder product collects at the tip of the tube and the supernatant was decanted. Fifty mL of hexanes was then added to the tube and the product was resuspended by shaking the tube. This hexane suspension was then centrifuged again and the supernatant was decanted. This washing process was repeated with another 50 mL of hexanes and two 50 mL portions of methanol. The resulting product was then dried *in vacuo* at ~80 °C and 100 mTorr for 1 h. Selected washed samples were annealed in evacuated pyrex ampoules at 350°C overnight. Ampoules are prepared as described in Section 5.2.2.

5.2.4 Metal phosphide synthesis from metal acetylacetonates and yellow P_4

This phosphide section will describe similar syntheses with multiple variables that are adjusted from reaction to reaction. The variables include solvent and surfactant choice, phosphorus amount and reaction durations. These reactions are also summarized later in Table 5.1.

In a typical synthesis, 2.00 mmol of metal acetylacetonate ($Cu(acac)_2$ or $Ni(acac)_2$ acac = $[CH_3COCHCOCH_3]^{1-}$) and a varying amount of yellow P_4 were loaded into a 100 mL Schlenk flask along with a stirbar in an argon filled glovebox. Phosphorus amounts used were stoichiometric (1.33 mmol), 50% greater than stoichiometric (2.00 mmol) or 100% greater than stoichiometric (2.66 mmol). This flask was fit with a rubber septum and brought out of the box.

On the benchtop, 40 mL of degassed solvent (mesitylene or ODE) was transferred to the Schlenk flask via cannula transfer. After solvent addition, surfactant was added to the flask via N_2 flushed syringe. Surfactants used were either OA or TOA and were added in a 1:3 metal to surfactant molar ratio (~6.00 mmol). The flask containing the resulting reaction slurry was then fit with a condenser under an N_2 blanket and placed in a heating mantle. Reactions in ODE were then heated with stirring to 120 °C over the course of 3 h and held there overnight (~15 h) before being heated over the course of 3 h to ~320 °C (refluxing) and held there for an additional night (~15 h) before cooling to room temperature. Reactions in mesitylene were heated to 165 °C (refluxing) over the course of 3 h and were held there overnight (~15 h) before being cooled to room temperature. Reaction products (black powder) were then isolated in the same manner as products from reactions described in Section 5.2.3. Selected washed samples were subjected to post-reaction, solid-state annealings at 350 °C in evacuated pyrex ampoules. Ampoules were prepared in the same manner as previously described in Section 5.2.2.

5.2.5 Product characterization

Experimental XRD data was obtained from a Siemens D5000 XRD system (CuK_{α}, 0.04 step size and 4 sec/step acquisition times). Simulated XRD patterns were generated using Powder Cell 2.3 computer program (http://www.ccp14.ac.uk/). SEM analyses were performed on a Hitachi S-4800 or a Hitachi S-3400N microscope with EDS analysis capabilites. XPS measurements were performed on samples fixed to indium foil using a Kratos Axis Ultra XPS instrument (monochromic Al Kα radiation).

5.3 Results and Discussion

5.3.1 Metal phosphide (NiP_2 and CuP_2) formation in surfactant-aided syntheses

In this study, we investigated the reaction of a metal halide or acetylacetonate complex with yellow P_4 in various solvothermal systems. Metal complexes were formed by the addition of a coordinating, Lewis base, alkyl pnictogen (amine or phosphine) surfactant. Reaction stoichiometries were primarily the same as in previous chapters, however in some reactions excess phosphorus was added and the reasons for doing this will be noted later. The amount of excess phosphorus used is described relative to the balanced, stoichiometric reactions shown in Equations 5.1and 5.2.

$$3\ MX_2 + 2\ P_4 \rightarrow 3\ MP_2 + 2\ PX_3 \quad (X= Cl \text{ or } Br \text{ and } M= Cu \text{ or } Ni) \qquad (5.1)$$

$$3\ M(acac)_2 + 2\ P_4 \rightarrow 3\ MP_2 + 2\ P(acac)_3 \quad (M= Cu \text{ or } Ni) \qquad (5.2)$$

Surfactants are not present in the balanced reactions as they are thought to remain unchanged during the reaction; they are, however, highly involved in the dissolution and activation of the metal precursor. It should be noted that the formation of the phosphite byproduct $P(acac)_3$ was not confirmed, although unsuccessful attempts were made to identify the clear liquid byproduct.

Metal halides have minimal solubility in non-polar, organic solvents, but when complexed with long-chain amines or phosphines, their solubilties are significantly

improved. Metal acetylacetonates have better solubility in non-polar organics than their halide counterparts, but also have significantly improved solubilities when complexed. The introduction of metal acetylacetonates in this chapter was largely motivated by the thought that the organic acetylacetonate ligands would allow for greater metal precursor solubility in non-polar organics.

For surfactant-aided reactions conducted in toluene, complete metal precursor dissolution was achieved resulting in colored, translucent solutions. Since yellow P_4 is also toluene soluble, having two completely soluble precursors provides some significant advantages over similar, previously described solvothermal reactions that do not utilize surfactants (Chapters 3 and 4). Solubilized molecular precursors can allow homogenous nucleation and growth, and when the growth is controlled by the addition of surfactants, monodisperse nanoparticles can potentially be obtained. When reactions occur between irregular, suspended, solid particulates they typically result in very heterogeneous morphologies, especially if no surfactant is present.

The higher boiling point solvents, ODE and HD, are far more viscous and less capable at solubilizing metal precursors than toluene. Because of this, reactions that were run in HD and ODE did not achieve complete dissolution of the metal precursors. Complexation of the metal precursors was evident by the color change of the solution, however some solid material could still be seen settled at the bottom of the flask, resulting in a mixture of complexed and uncomplexed metal precursor. Even though complete dissolution was not achieved, once the dissolved precursors react forming MP_x particles, the solvent and surfactant are free to dissolve remaining undissolved solid; in this way, a homogeneous reaction pathway is still possible.

In all solvent systems, reactions between the $Cu(acac)_2$ and $CuCl_2$ complexes with yellow P_4 occured immediately (<1 min.) upon mixing at room temperature, which was evident by the reaction solution turning black and opaque, indicating MP_x formation. Reactions between $Ni(acac)_2$ and $NiCl_2$ complexes with yellow P_4 did not react at room

temperature, but they did all occur upon mild heating to temperatures of ~40-50 °C. These reaction onset temperatures are significantly reduced from reactions without coordinating surfactants. The reason for these lower reaction temperatures may be due to the activation of the M-Cl or M-acac bonds by the surfactant. These M-halide or M-acac bonds then become more labile allowing for phosphorus to insert into these bonds at lower temperatures. Copper and nickel nuclei can only handle so much electron density and when the lone pairs of the surfactants form dative bonds with the metal they are increasing electron density on the metal. To counteract this addition, the metals may weaken their bonds with the halides or acetylacetonates. When these bonds are weakened they become more reactive or activated. A cartoon schematic of metal halide bond activation by surfactant addition can be seen in Figure 5.2.

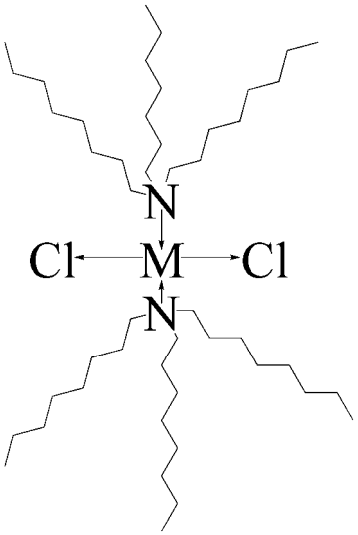

Figure 5.2 Illustration of a MCl_2-TOA complex emphasizing the activation or weakening of M-Cl bonds by the addition of a coordinating surfactant.

The onset temperatures of reactions without surfactant addition are ~100 °C for reactions with $CuCl_2$ and are between ~200-240 °C for reactions with $NiCl_2$ or $NiBr_2$ (see

Chapter 4). These temperatures are significantly lowered by the addition of surfactant and this has several advantages. Reactions between $NiCl_2$ or $NiBr_2$ and yellow P_4 are not possible in refluxing toluene (~110 °C) without surfactant addition as the temperature of reflux is too low. Also when reaction temperatures are lowered, the ability of the surfactant to be bound to particle surfaces is increased (see Figure 5.1), which should help stunt particle growth.

Dissolved molecular reagents are also more reactive then their undissolved, solid counterparts. Reactions between polymeric, red phosphorus and dissolved metal halide-TOA complexes supported this notion. In these side experiments (ran in HD), reaction onset temperatures (~170-200 °C) were similar to reactions between dissolved yellow P_4 and uncomplexed metal halides, which also had one dissolved and one suspended reagent. Reactions between two suspended reagents, as performed between uncomplexed metal halides and red phosphorus in Chapter 4, require even higher temperatures for MP_x formation (~225-230 °C for reactions with $CuCl_2$ and $NiBr_2$).

In reactions between metal halide complexes (OA or TOA) in HD or ODE, a white solid material could be seen transporting into the condenser at refluxing temperatures. This material was analyzed by XRD and was revealed to be NH_4Cl (or NH_4Br when $NiBr_2$ was used). This material was not produced in the lower temperature toluene reactions or in reactions when $M(acac)_2$ was used. The chemistry of ammonium halide formation in these systems is certainly complex and a balanced reaction forming this byproduct is difficult to envisage. We have seen in previous syntheses (Chapter 3) that the PCl_3 byproduct is very reactive and is likely involved, along with OA or TOA, in the formation of the ammonium halide. The formation of the ammonium halide is an unwanted process as it degrades the amine surfactant.

In reactions where TOP was used as solvent, low boiling point volatile species were evolved at high temperatures. The boiling point of TOP (370 °C) was never reached due to the production of lower boiling point species, and as more was produced,

the temperature of the solution slowly dropped without altering the set temperature of the heating mantle. After one night at elevated heating mantle temperatures (400 °C external temperature), the volatile species were removed via distillation and the reaction solution was then reheated to see if temperatures near 370 °C could be reached. In this attempt, upon reheating, the temperature was able to surpass the temperature at which the solution was found to be prior to distillation (~230 °C), but the production of more low boiling point species persisted. The continual production of volatile byproduct hints at TOP degradation; if the volatiles were due to PBr_3 or PCl_3 or PBr_3 or PCl_3 reaction products, then the evolution of volatiles would cease at some point since halides are present in a limited amount. It should be noted that TOP has been previously used as a "P" source in MP_x synthesis. In this report, TOP was decomposed catalytically by metal nanoparticles, but the identity of the decompostition byproduct(s) were not reported.[100,101]

In the next section, we will present the results of various analyses of the products synthesized in a variety of reaction conditions. The reaction observations that were previously described in this section will, in many cases, help to rationalize and explain the results.

Table 5.1 Reaction summary of surfactant-aided solvothermal MP_x syntheses (M = Ni or Cu)

ID	M Source	P amount[1]	Solvent	Surf.(Ratio)[2]	Heating[3]	XRD[4]	
						Crude	Annealed
1	$CuCl_2$	stoich	toluene	OA (1:4)	1 d (110)	amorph.	$CuP_2 + Cu_3P$
2	$CuCl_2$	stoich	toluene	OA (1:4)	4 d (110)	amorph.	CuP_2
3	$CuCl_2$	stoich	ODE	TOA (1:2)	1 d (330)	**CuP_2** + Cu_3P	**CuP_2** + Cu_3P
4	$CuCl_2$	stoich	ODE	TOA (1:4)	2 d (335)	CuP_2 + **Cu_3P**	CuP_2 + **Cu_3P**
5	$CuCl_2$	50% xs	ODE	TOA (1:4)	2 d (335)	CuP_2	---
6	$CuCl_2$	stoich	TOA	TOA (1:25)	1 d (345)	Cu_3P	**CuP_2** + Cu_3P
7	$CuCl_2$	stoich	TOP	TOP (1:22)	1 d (330)	amorph.	CuP_2
8	$Cu(acac)_2$	stoich	mesitylene	OA (1:3)	1 d (165)	amorph.	CuP_2
9	$Cu(acac)_2$	stoich	ODE	TOA (1:3)	1 d (330)	Cu_3P	amorph.
10	$Cu(acac)_2$	50% xs	ODE	TOA (1:3)	1 d (330)	**CuP_2** + Cu_3P	**CuP_2** + Cu_3P
11	$Cu(acac)_2$	100 % xs	ODE	TOA (1:3)	1 d (330)	amorph.	CuP_2
12	$NiBr_2$	stoich	toluene	OA (1:4)	1 d (110)	amorph.	Ni_2P
13	$NiBr_2$	stoich	toluene	OA (1:4)	4 d (110)	amorph.	$NiP_2 + Ni_5P_4$
14	$NiBr_2$	stoich	HD	TOA (1:3)	1 d (287)	amorph.	**NiP_2** + Ni_5P_4
15	$NiBr_2$	stoich	ODE	TOA (1:3)	1 d (330)	Ni_2P	**NiP_2** + Ni_5P_4
16	$NiCl_2$	stoich	ODE	TOA (1:3)	1 d (330)	**NiP_2** + Ni_5P_4	**NiP_2** + Ni_5P_4
17	$NiCl_2$	50% xs	ODE	TOA (1:3)	1 d (330)	amorph.	NiP_2
18	$NiBr_2$	stoich	TOP	TOP (1:30)	1 d (330)	NiP	NiP_2
19	$Ni(acac)_2$	stoich	mesitylene	OA (1:3)	1 d (165)	amorph.	**NiP_2** + Ni_5P_4
20	$Ni(acac)_2$	stoich	ODE	TOA (1:3)	1 d (330)	Ni_2P	amorph.
21	$Ni(acac)_2$	50% xs	ODE	TOA (1:3)	1 d (330)	amorph.	**NiP_2** + Ni_5P_4
22	$Ni(acac)_2$	100 % xs	ODE	TOA (1:3)	1 d (330)	amorph.	NiP_2

1) stoich = stoichiometric amounts according to Equations 5.1 and 5.2. xs amounts of P used are in relation to stoichiometric amounts.
2) Surf. = surfactant. Ratios indicate the M:surfactant molar ratios used.
3) Heating durations listed indicate the time reactions are held at maximum reaction temperatures (measured internal temp.) in degrees C.
4) amorph. = amorphous XRD patterns. Annealed results listed are all from solid-state annealings performed at 350 °C. Major phases are represented in **bold**.

5.3.2 Product phase determination of MP_x products from metal halides

All washed and annealed products were analyzed by XRD to determine which crystalline phases were present in the product powders, a summary of XRD results for all reactions can be seen in Table 5.1. In this section, descriptions of samples are accompanied with bolded numbers, which correspond to the reaction ID's found in Table 5.1. Products were often found to be a mixture of the targeted phosphorus-rich phase and a metal-rich phase. The relative amounts of each phase were not quantified, however they will often be described as being the major or minor component of products. The assignment of major and minor component is substantiated by the differences in relative intensities of their XRD diffraction peaks, which is often significant. All solid state annealings were performed at 350 °C overnight in sealed pyrex ampoules.

Reactions between dissolved $NiBr_2$-OA and $CuCl_2$-OA complexes (1:4 metal:oleylamine molar ratio) with stoichiometric amounts (see Equation 5.1) of dissolved yellow P_4 in toluene were performed by maintaining refluxing temperatures (110 °C) for either 1 or 4 days (**1,2,12 and 13**). Washed products from these four reactions all resulted in essentially amorphous products (Figures 5.3a and 5.4a). Upon annealing the amorphous CuP_x products in the solid state, the 1 d reaction product resulted in a mixture of CuP_2 and Cu_3P (~1:1 molar ratio). The annealed amorphous CuP_x product from the 4 d reaction resulted in only the targeted CuP_2 (Figure 5.3b). This result tells us that the longer 4 d duration is required to completely incorporate the sought after amount of phosphorus into the product.

The amorphous CuP_x product from the 4 d reaction was resuspended in various high boiling point solvents (ODE, OA or TOPO) and heated with constant stirring under an N_2 blanket to elevated temperatures (330, 327 and 325 and °C respectively) where they were held overnight. These "solution annealings" were performed in attempts to

achieve crystallinity while avoiding particle aggregation and fusion which occurs in solid-state annealings. Solution annealed CuP_x products resulted in Cu_3P when ODE or OA (Figure 5.3 c and d) was used as a solvent and a CuP_2/Cu_3P mixture when TOPO (CuP_2 major, Cu_3P minor, Figure 5.3e) was used.

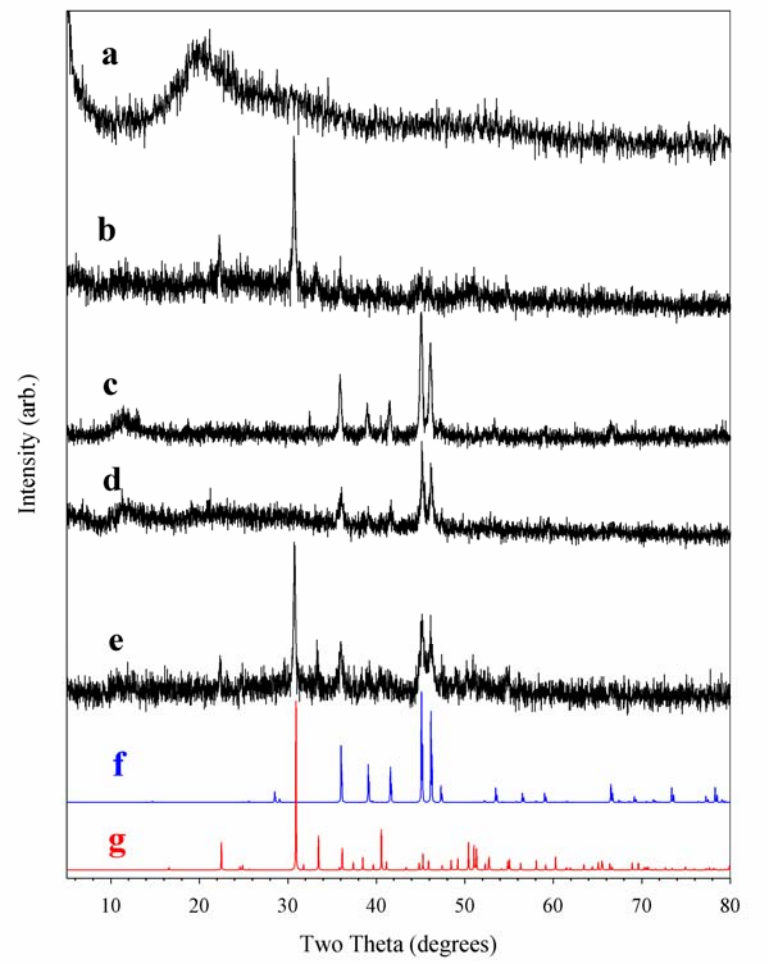

Figure 5.3 Experimental XRD patterns for washed (a), solid-state annealed (b), and ODE, OA and TOPO solution annealed (c,d and e, respectively) products from reaction **2**. Calculated XRD patterns for Cu_3P (f) and CuP_2 (g).

All of these products showed a loss of phosphorus content during the solution annealing process as indicated by the appearance of only CuP_2 when the washed amorphous

product was annealed in the solid state. The solvents in these annealings are all capable of dissolving yellow P_4 and may have extracted phosphorus from the amorphous CuP_x products. If this occurred, then extracted molecular P_4 may sublime out of the heated solutions resulting in the crystallization of CuP_x products with phosphorus deficiencies. Alternatively, reactive P in the CuP_x product may have reacted with solvent.

Upon annealing the amorphous NiP_x products in the solid state, the 1 d reaction product resulted in only Ni_2P. The annealed amorphous NiP_x product from the 4 d reaction resulted in a pattern with all poorly crystalline reflections consistent with NiP_2 and Ni_5P_4 (Figure 5.4a). This result is, again, an indication of elevated phosphorus incorporation when the longer 4 d reaction duration is used. Since the annealed 4 d reaction product still resulted in a metal-rich byproduct, it indicates that phosphorus incorporation into NiP_x products may require higher temperatures to obtain the targeted NiP_2. The poor crystallinty in the annealed 4 d reaction product is somewhat surprising; the phases may struggle to crystallize due to off-stoichiometric amounts of phosphorus.

Similar reactions were performed between partially surfactant dissolved (room temperature) metal halide complexes (where MX_2 = $CuCl_2$, $NiCl_2$ or $NiBr_2$ and surfactant = TOA or TOP) and dissolved yellow P_4 in high boiling point solvents (HD, ODE, TOA or TOP). The metal to surfactant molar ratios ranged from 1:2 to 1:4 when HD or ODE was used as solvent and increased significantly (1:22-1:45) when TOP or TOA was used as a solvent as they acted as both the solvent and surfactant. In all of these reactions, the solutions were heated to 120 °C, and held at this temperature overnight, before heating to various elevated, solvent-dependent temperatures (287-340 °C) where they were held overnight and then cooled to room temperature. All annealed samples were prepared by annealing in pyrex ampoules at 350 °C overnight in the solid-state. It should also be noted that indicated reaction temperatures for reactions using TOP as the solvent are for maximum reaction temperatures. As previously described (Section 5.3.1), these reactions produced volatile species that gradually lowered the solution temperature.

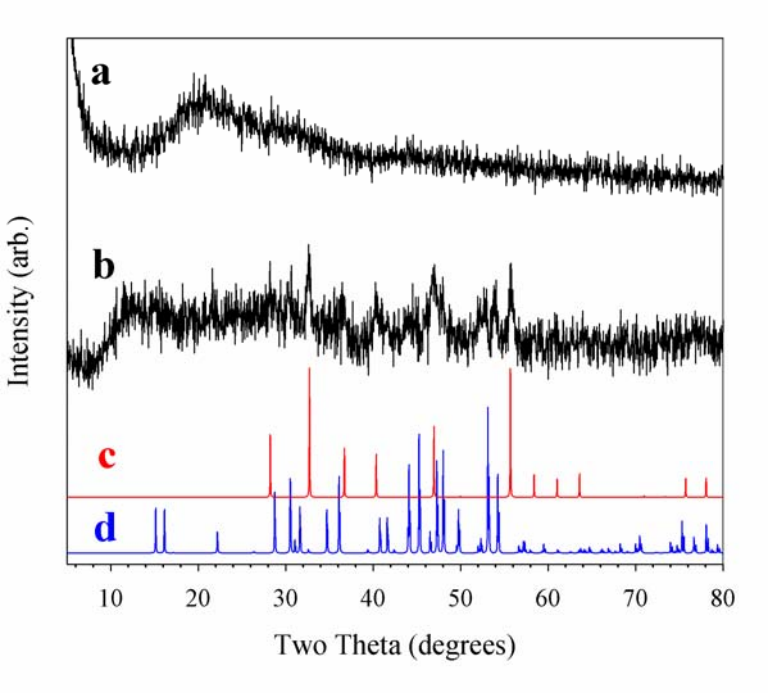

Figure 5.4 Experimental XRD patterns for washed (a) and annealed (b) products from reaction **13**. Calculated XRD patterns for NiP_2 (c) and Ni_5P_4 (d).

Reactions between $NiBr_2$-TOA complexes (1:3 metal to TOA molar ratio) and stoichiometric amounts of yellow P_4 were performed in both ODE (330 °C) and HD (287 °C) (**14 and 15**). Washed samples of both of these products were revealed to be amorphous by XRD and upon annealing, both revealed primarily a NiP_2 diffraction pattern along with very minor Ni_5P_4 peaks (Figure 5.5). Reactions with $NiCl_2$-TOA complexes (1:3 metal to TOA molar ratio) were performed with stoichiometric or a 50% stoichiometric excess of yellow P_4 in ODE (330 °C) (**16 and 17**). Washed and solid-state annealed products from reactions using stoichiometric amounts of yellow P_4 both revealed poorly crystalline peaks consistent with NiP_2 as the major component along with Ni_5P_4 as the minor component (Figure 5.6a). Reactions in ODE with stoichiometric amounts of yellow P_4 and uncomplexed $NiCl_2$ (no surfactant, see Chapter 4) resulted in only NiP_2 when annealed.

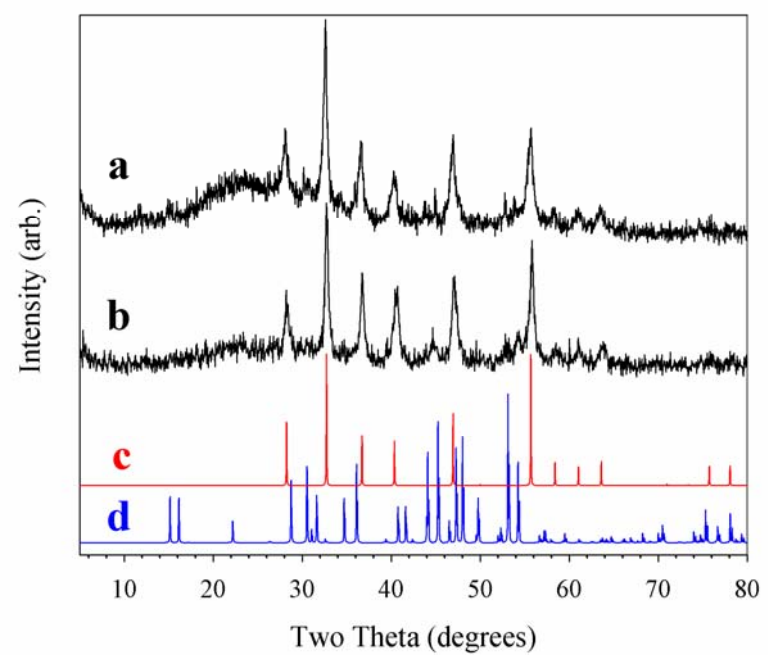

Figure 5.5 Experimental XRD patterns for annealed samples from reactions **14** (a) and **15** (b). Calculated XRD patterns for NiP_2 (c) and Ni_5P_4 (d).

This comparison shows that the addition of the TOA surfactant lowers the amount of phosphorus incorporation into NiP_x products and affects annealed particle crystallinity. When a 50 % stoichiometric excess of yellow P_4 was used, the washed product was amorphous and upon annealing, formed only NiP_2 (Figure 5.6b). The absence of Ni_5P_4 reflections in this reaction indicates that the excess phosphorus is necessary to avoid the formation of the metal-rich byproduct when TOA is used. Reactions between $NiBr_2$-TOP complexes (1:30 metal:TOP molar ratio) and stoichiometric amounts of yellow P_4 using TOP as the solvent (**18**) revealed only NiP in the washed product and upon annealing resulted in only NiP_2 (Figure 5.7). This result is surprising as previously described amorphous CuP_x products lost phosphorus content when heated at elevated temperatures in TOP. This may indicate that the NiP_x formed in TOP may not be as susceptible to phosphorus loss when heated in TOP as its CuP_x counterpart.

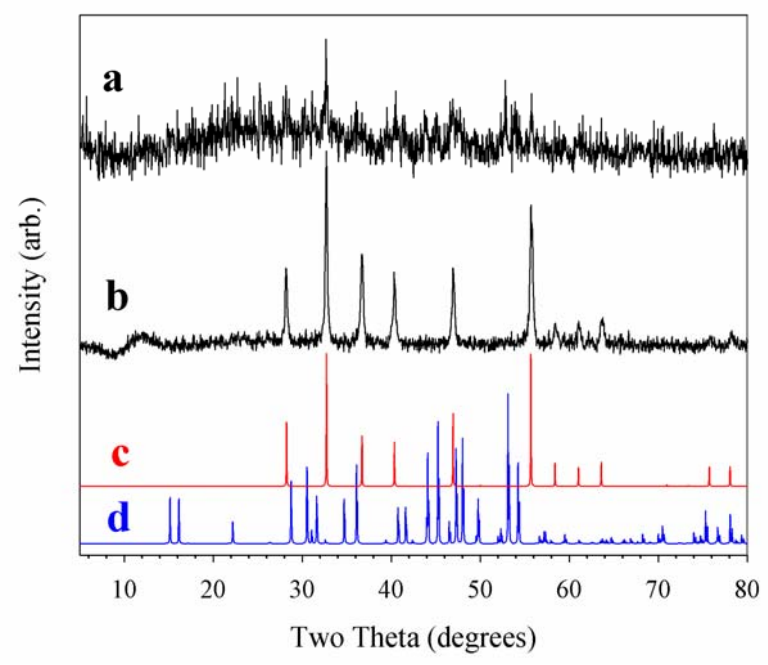

Figure 5.6 Experimental XRD patterns for annealed samples from reactions **16** (a) and **17** (b). Calculated XRD patterns for NiP_2 (c) and Ni_5P_4 (d).

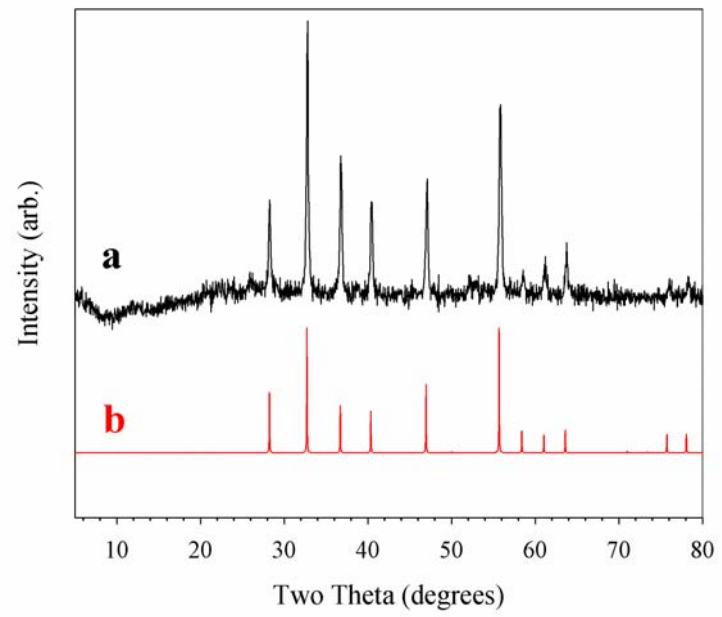

Figure 5.7 Experimental XRD pattern for the annealed product from reaction **18** (a) and the calculated XRD pattern for NiP_2.

Reactions between $CuCl_2$-TOA complexes and yellow P_4 were performed in ODE (330 °C) with either a 1:2 or 1:4 Cu:TOA molar ratio (**3 and 4**). The washed product using a 1:2 ratio revealed a mixture of phases with CuP_2 as the major component and Cu_3P as the minor component. Upon annealing this sample the CuP_2/Cu_3P mixture persisted, however the relative amount of Cu_3P decreased as indicated by a drop in relative CuP_2 to Cu_3P reflection intensity (Figure 5.8a). The washed and annealed products from the reaction using a 1:4 ratio both revealed a mixture of phases with Cu_3P being the major component and CuP_2 as the minor component (Figure 5.8b). The increase of Cu_3P in the reactions using a larger 1:4 ratio further supports the idea that phosphorus may be removed from CuP_x products formed at low temperatures by the TOA. A similar reaction was performed between the $CuCl_2$-TOA complex and a 50% stoichiometric excess of yellow P_4 in ODE (**5**). The washed product revealed only the presence of the targeted CuP_2, as such no post-reaction annealing was required (Figure 5.8c). The addition of excess phosphorus counteracts the phosphorus-removing ability of the TOA, allowing for the targeted CuP_2 to form. This is an exciting result as it is the only benchtop reaction at this point where crystalline, single-phase MP_2 is afforded directly from solution, avoiding particle fusion that would occur by solid-state annealing.

Reactions between $CuCl_2$ complexed to TOA or TOP and stoichiometric amounts of yellow P_4 were performed using either TOA (340 °C) or TOP (330 °C) as the solvent and surfactant (**6 and 7**). Metal to surfactant molar ratios were 1:25 and 1:22 for TOA and TOP, respectively. The washed product from the reaction using TOA as the solvent revealed only crystalline Cu_3P by XRD and upon annealing, revealed only the targeted CuP_2 along with Cu_3P (Figure 5.9a). The washed product from the reaction using TOP as the solvent was amorphous, but upon annealing it crystallized to only the targeted CuP_2 (Figure 5.9b).

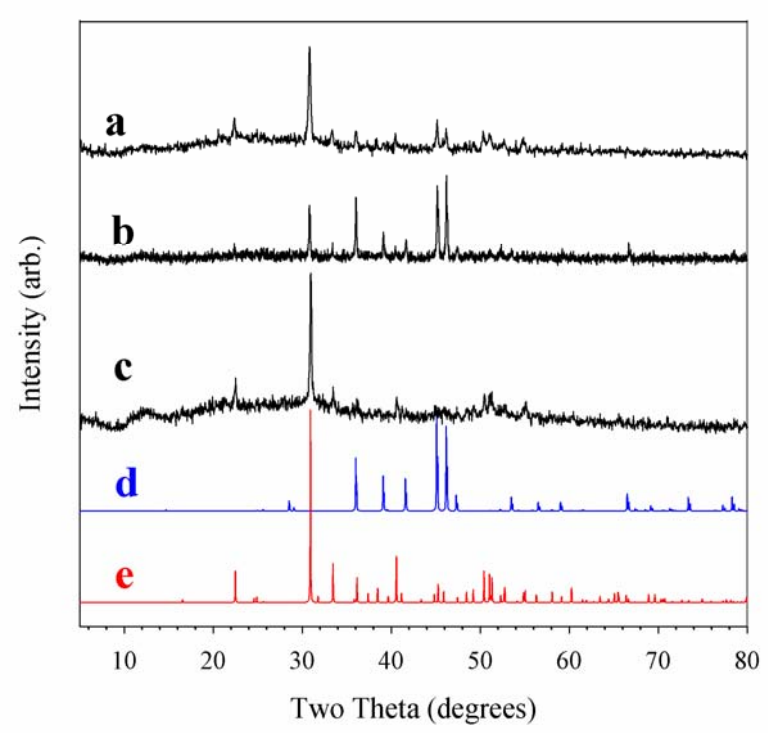

Figure 5.8 Experimental XRD patterns for annealed products from reactions **3** (a), and **4** (b) and for washed product from reaction **5** (c). Calculated XRD patterns for Cu_3P (d) and CuP_2 (e).

The result from the TOP reaction is surprising as the amorphous CuP_x products formed in similar reactions using toluene, lost phosphorus when heated at elevated temperatures in solution. The only synthetic difference between the solution-annealed CuP_x products from toluene and this product is that initial, low temperature CuP_x formation occurred in different solvent/surfactant environments. In the toluene reactions, CuP_x formation occurred in a toluene-diluted, 1:4 metal to surfactant molar ratio environment, while the reaction in TOP occurred in environments with a single coordinating solvent and with higher (1: 22) metal to surfactant molar ratio. This may indicate that the initial CuP_x products formed in TOP are more stable and less susceptible to phosphorus loss by the TOP at elevated temperatures.

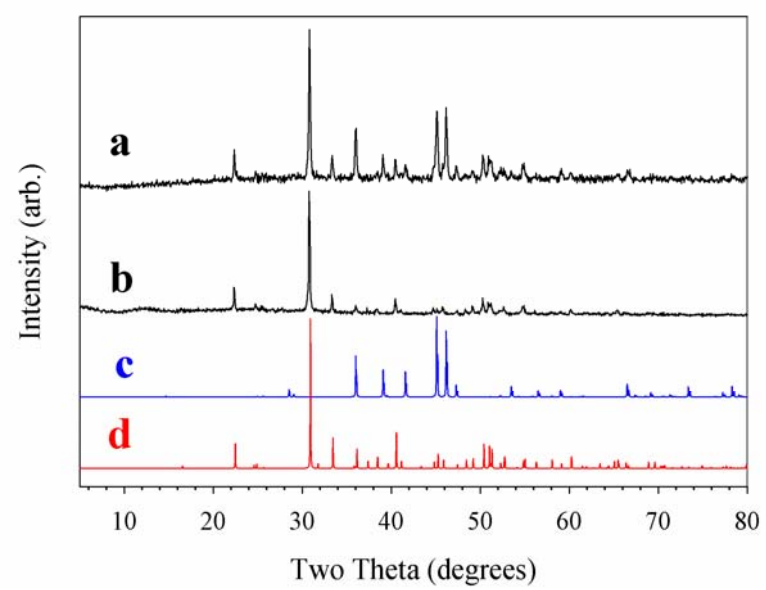

Figure 5.9 Experimental XRD patterns for annealed products from reactions **6** (a) and **7** (b). Calculated XRD patterns for Cu_3P (c) and CuP_2 (d).

5.3.3 Product phase determination of MP_x products from metal acetylacetonates

Reactions between $Ni(acac)_2$ complexed to OA or TOA with a 1:3 metal to surfactant ratio and reacted with various amounts of yellow P_4 using either mesitylene (165 °C) or ODE as a solvent The amount of phosphorus used was either stoichiometric, a 50% stoichiometric excess or a 100% stiochiometric excess according to Equation 5.2. Reactions performed in mesitylene were heated over 3 h to 165 °C where they were held overnight before cooling to room temperature. Reactions performed in ODE were heated over 3 h to ~120 °C and held there overnight before being heated to reflux (~330 °C) and held there overnight before being cooled to room temperature. All annealings, unless otherwise stated, were conducted in the solid-state in evacuated pyrex ampoules.

The washed product from the reaction between the $Ni(acac)_2$-OA complex and stoichiometric amounts of yellow P_4 performed in mesitylene (**19**) resulted in an amorphous product that upon annealing resulted in a mixture of NiP_2 as the major

component along with Ni_5P_4 as the minor component. Three similar reactions between the $Ni(acac)_2$-TOA complex and various amounts of yellow P_4 in ODE were performed. The washed product from the reaction using stoichiometric amounts of yellow P_4 (**20**) revealed only Ni_2P and upon annealing yielded an amorphous product (Figure 5.10a). The washed product from the reaction using a 50% stoichiometric excess of yellow P_4 (**21**) yielded an amorphous product that upon annealing crystallized to a mixture of NiP_2 as the major product along with Ni_5P_4 as the minor product (Figure 5.10b). The washed product from the reaction using a 100% stoichiometric excess of yellow P_4 (**22**) resulted in an amorphous product that upon annealing crystallized to only the targeted NiP_2 (Figure 5.10c). The washed product from this reaction was also annealed overnight in solution using TOA and resulted in an amorphous product. These results indicate that a stoichiometric excess of yellow P_4 is necessary to yield a product containing only the targeted NiP_2 and no metal-rich phases. The result of the TOA solution annealing is consistent with previous solution annealings using products formed with a metal halide in that phosphorus was lost during the solution annealing process. The peak widths from the annealed products from reaction **22** are very broad (Figure 5.10c), indicative of small crystallite sizes. The average crystallite size can be calculated from the Warren-Scherrer equation[1] and was found to be ~12 nm for the annealed product from reaction **22**. For comparison purposes, the average crystallite size was calculated for the annealed product from reaction **15**, which had slightly less broad peaks; the average crystallite size for this sample was found to be ~23 nm.

Reactions between $Cu(acac)_2$ complexed with OA or TOA and various amounts of yellow P_4 were performed using either mesitylene (165 °C) or ODE as a solvent with a 1:3 metal to surfactant ratio. The amount of phosphorus used was either stoichiometric, a 50% stoichiometric excess or a 100% stiochiometric excess according to Equation 5.2. Reactions performed in mesitylene were heated over 3 h to 165 °C where they were held overnight before cooling to room temperature. Reactions performed in ODE were heated

over 3 h to ~120 °C and held there overnight before being heated to reflux and held there overnight before being cooled to room temperature. All annealings, unless otherwise stated, were solid-state annealings performed in evacuated pyrex ampoules.

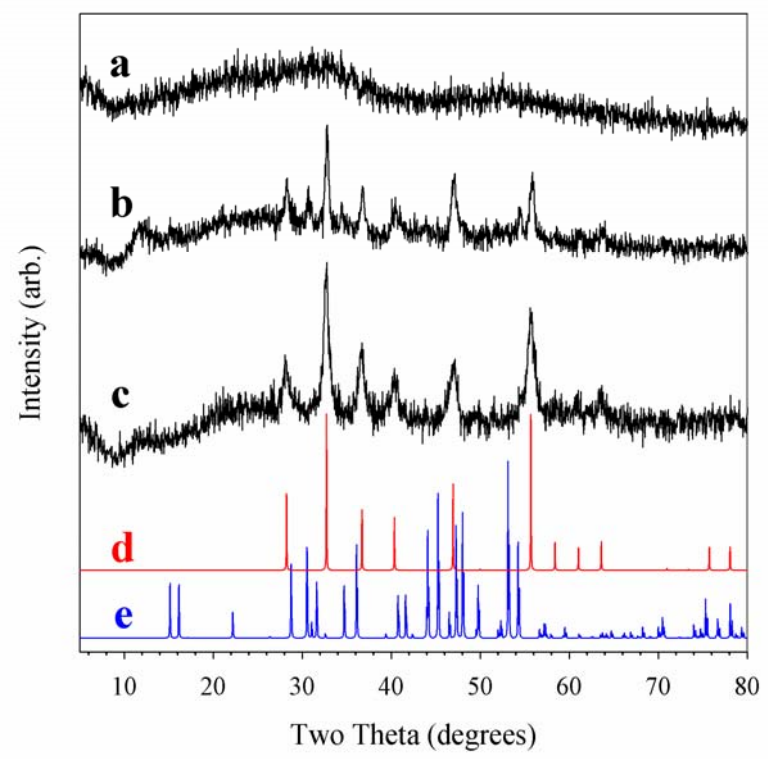

Figure 5.10 Experimental XRD patterns for annealed products from reactions **20** (a), **21** (b) and **22** (c). Calculated XRD patterns for NiP_2 (d) and Ni_5P_4 (e).

The washed product from the reaction between the $Cu(acac)_2$-OA complex and stoichiometric amounts of yellow P_4 performed in mesitylene resulted in an amorphous product that upon annealing resulted in only the targeted CuP_2 (**8**). Three similar reactions between the $Cu(acac)_2$-TOA complex and various amounts of yellow P_4 in ODE were performed. The washed product from the reaction using stoichiometric amounts of yellow P_4 (**9**) revealed only Cu_3P and, upon annealing, revealed an amorphous product (Figure 5.11a). The washed product from the reaction using a 50% stoichiometric excess

of yellow P_4 (**10**) revealed a mixture of CuP_2 and Cu_3P that, upon annealing, revealed a mixture of CuP_2 as the major product along with Cu_3P as the minor product (Figure 5.11b). The relative CuP_2 to Cu_3P XRD peak intensity ratio was reduced upon annealing. The washed product from the reaction using a 100% stoichiometric excess of yellow P_4 (**11**) resulted in an amorphous product that upon annealing resulted in only the targeted CuP_2 (Figure 5.11c). The washed product from this reaction was also annealed overnight in solution using TOA and resulted in only Cu_3P. These results showed that the annealed product from the reaction in mesitylene produced only the targeted CuP_2 where similar reactions using ODE required a 100% excess of yellow P_4 to obtain only the targeted CuP_2. This result indicates that phosphorus is lost in the presence of surfactant when reactions are performed at elevated temperatures, a result consistent with previously described experiments forming MP_x from metal halides in toluene at low temperatures.

The reactions described in this section were essentially modifications of the reactions performed in Chapters 3 and 4, which were successful at producing phase pure CuP_2, NiP_2 and CoP_3. These reactions were modified by the addition of surfactant and were aimed at producing CuP_2 and NiP_2 nanoparticles. Ideally, the addition of surfactants should not hinder the chemistry of MP_x formation and only acts to control morphology. The XRD results revealed that the synthesis of phase pure CuP_2 could be achieved with surfactant addition with the same metal to yellow P_4 molar ratios used in Chapter 3 and 4 when MP_x formation was performed with relatively low temperatures in either mesitylene or toluene. Similar, stoichiometric toluene and mesitylene reactions targeting NiP_2 resulted in mixtures of NiP_2 and Ni_5P_4, indicating that the temperatures used to form NiP_x particles were too low to incorporate the appropriate amount of phosphorus. High temperature reactions using both metal halides and acetylacetonates in ODE revealed that an excess of phosphorus was needed in order to achieve phase pure CuP_2 and NiP_2. The common occurrence of products with multiple crystalline phases in these syntheses is a problem that has been previously reported in literature.[40,62,100]

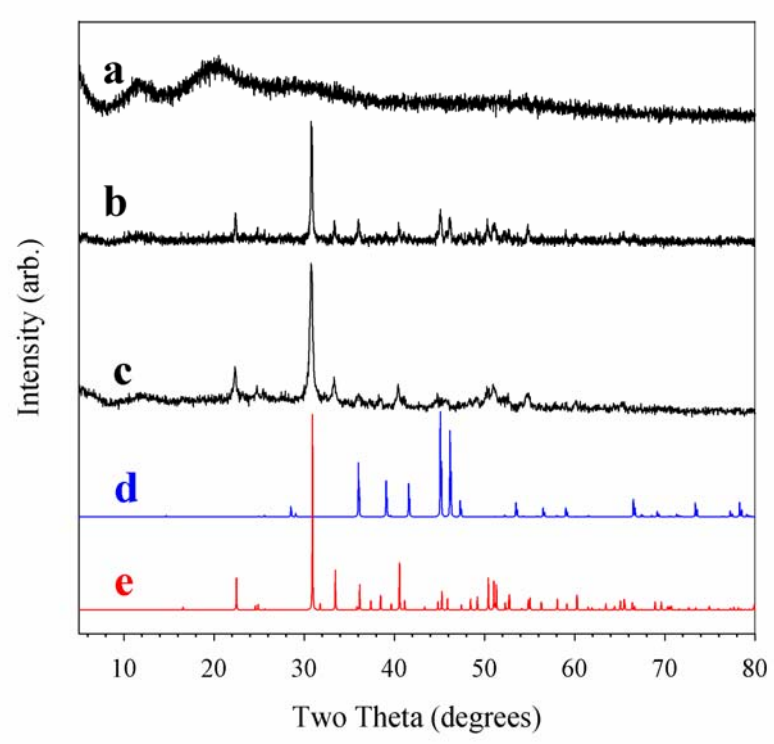

Figure 5.11 Experimental XRD patterns for annealed products from reactions **9** (a), **10** (b) and **11** (c). Calculated XRD patterns for Cu_3P (d) and CuP_2 (e).

5.3.3 Elemental analysis of selected MP_x products

Energy dispersive spectroscopy (EDS) analysis was performed on all CuP_x and NiP_x products (**9**, **10**, **11**, **20**, **21** and **21**) from the reactions of $M(acac)_2$-TOA complexes with various amounts of yellow P_4 in ODE. Various other MP_x products (**2**, **5** and **15**) were analyzed by EDS as well and will be presented. As previously described, these reactions used either stiochiometric amounts, a 50% stoichiometric excess or a 100% stoichiometric excess of yellow P_4. EDS analysis does not yield bulk compositional analysis but does give relative elemental composition ~1 μm deep into the solid. This section will present the M:P molar ratios obtained from the selected samples. A summary of EDS results for products from acetylacetonate reactions is shown in Table 5.2.

The CuP_x products from the reaction using stoichiometric amounts of yellow P_4 revealed a 1:1.04 and 1:0.89 Cu:P molar ratio for the washed and annealed products respectively. These amounts are well below the 1:2 ratio expected in the targeted CuP_2 and are consistent with the absence of CuP_2 and presence of metal-rich phases in XRD patterns of these products. The CuP_x products from the reaction using a 50% stoichiometric excess of yellow P_4 resulted in a 1:1.81 and 1:1.69 Cu:P molar ratio for the washed and annealed products respectively. These amounts are closer, but are still lower, to the 1:2 ratio of CuP_2. The XRD of these products revealed a mixture of CuP_2 (major) and Cu_3P (minor), a result from which a molar ratio slightly below 1:2 would be expected. The CuP_x products from the reactions using a 100% stoichiometric excess of yellow P_4 resulted in a 1:3.07 and 1:2.32 molar ratio for the washed and annealed product respectively. The XRD of the annealed product from this reaction showed only the targeted CuP_2. The EDS results show that the phosphorus content exceeds the 1:2 ratio of CuP_2, indicating that the annealed products likely contain amorphous regions with greater than 1:2 Cu:P molar ratios along with the crystalline CuP_2. The Cu:P molar ratios increased as expected as more yellow P_4 was used, and in all products, phosphorus was lost upon annealing, consistent with results from EDS analysis of products from Chapter 3. These results also suggest that a stoichiometric excess of phosphorus between 50 and 100% may result in a crystalline CuP_2 product with a Cu:P molar ratio close to 1:2.

The NiP_x products from the reaction using stoichiometric amounts of yellow P_4 revealed a 1:1.30 and 1:1.00 M:P molar ratio for the washed and annealed products respectively. These amounts are well below the 1:2 ratio expected in the targeted NiP_2 and are consistent with the absence of NiP_2 and presence of metal-rich phases in XRD patterns of these products. The NiP_x products from the reaction using a 50% stoichiometric excess of yellow P_4 resulted in a 1:1.82 and 1:1.60 Ni:P molar ratio for the washed and annealed products respectively. These amounts are, again, closer to the 1:2 ratio of NiP_2, but are still low. The XRD of these products revealed a mixture of NiP_2

(major) and Ni_5P_4 (minor), a result in which a molar ratio slightly below 1:2 would be expected, consistent with our results. The NiP_x products from the reactions using a 100% stoichiometric excess of yellow P_4 resulted in a 1:3.31 and 1:2.64 molar ratio for the washed and annealed product respectively. The XRD of the annealed product from this reaction showed only the targeted NiP_2. The EDS results indicate that the phosphorus content exceeds the 1:2 ratio of NiP_2, indicating that, again, that the annealed product must contain amorphous regions with greater than 1:2 Ni:P molar ratios along with the crystalline NiP_2. As in the CuP_x products, the Ni:P molar ratios also increased as expected as more yellow P_4 was used, and in all products, phosphorus was lost upon annealing. These results also suggest that a stoichiometric excess of phosphorus between 50 and 100% may result in a crystalline NiP_2 product with a Ni:P molar ratio closer to 1:2. The product from reaction using a 100% excess of phosphorus (**22**) was also annealed in solution using TOA and was analyzed by EDS as well. This product was found to be amorphous by XRD and the Ni:P molar ratio from this product was found to be 1:1.72. The molar ratio of the washed product from this synthesis was 1:3.31, and when annealed in the solid-state was 1:2.64, which means that more phosphorus was lost when annealed in TOA.

The washed product from the reaction of the $NiBr_2$-TOA complex in ODE (**15**) showed the presence of Ni_2P only by XRD, but upon annealing (solid-state) revealed a mixture NiP_2 as the major component along with Ni_5P_4 as the minor product. The EDS results from these products showed a Ni:P molar ratio of 1:2.02 and 1:1.88 for the washed and annealed products, respectively. We have previously seen the presence of only Ni_2P even when the Ni:P ratio was adequate to form only the targeted NiP_2 upon annealing (see Chapter 2). As such, it was not a surprise to see a molar ratio of 1:2.02 by EDS and only Ni_2P by XRD. The molar ratio of the annealed product (1:1.88) was also consistent with the XRD in that the ratio was slightly below the targeted ratio of 1:2 for NiP_2 and as a result, a minimal amount of metal-rich Ni_5P_4 was detected along with NiP_2.

The annealed product from the 4 d reaction of the $CuCl_2$-OA complex in toluene (**2**), which showed only the targeted CuP_2 by XRD, had a Cu:P molar ratio of 1:2.04, which is very close to the ideal 1:2 ratio. The washed product from this reaction was also annealed in solution resulting in products which showed only Cu_3P or a mixture of Cu_3P and CuP_2 by XRD, consistent with phosphorus loss. The TOPO solution annealed product showed a mixture of CuP_2 and Cu_3P by XRD and was revealed by EDS to have a Cu:P molar ratio of 1:1.76. The OA solution annealed product showed only Cu_3P by XRD and was revealed by EDS to have a Cu:P molar ratio of 1:1.22. These EDS and XRD results show a clear correlation between the XRD phases detected and the phosphorus content in the products.

Table 5.2 Summary of EDS results from $M(acac)_2$ reactions.

CuP_x[2]		Phosphorus Amount[1]	NiP_x[2]	
Crude	Annealed (350)		Crude	Annealed (350)
1 : 1.04 (Cu_3P)	1 : 0.89 (amorph.)	Stoichiometric	1 : 1.30 (Ni_2P)	1 : 1.00 (amorph.)
1 : 1.81 (**CuP_2** + Cu_3P)	1 : 1.69 (**CuP_2** + Cu_3P)	50% excess	1 : 1.82 (amorph.)	1 : 1.60 (**NiP_2** + Ni_5P_4)
1 : 3.07 (amorph.)	1 : 2.32 (CuP_2)	100% excess	1 : 3.31 (amorph.)	1 : 2.64 (NiP_2)

1) Phosphorus amounts are relative to amounts described in Equation 5.2.
2) Corresponding XRD results are listed in parentheses under the molar ratios. Major phases are bolded.

The results from these EDS analysis show how MP_x products with various amounts of phosphorus can be synthesized by varying the amount of phosphorus used and how the phosphorus content in the washed MP_x products will influence which crystalline phases are obtained upon annealing. These results also confirm the loss of phosphorus upon solution annealings. In the $M(acac)_2$ syntheses, the metal to surfactant

ratios and the heating profiles were held constant, and only the phosphorus amounts were varied. A change in these variables would likely alter the amount of phosphorus incorporations as well. Further fine-tuning of these reactions could lead to products where only the targeted MP_2 phase is seen by XRD along with a M:P ratio closer to the expected 1:2.

5.3.4 Product morphologies

Selected washed and annealed samples were analyzed by scanning electron microscopy (SEM) to acquire product morphologies. SEM analysis will focus on the samples that produced phase-pure CuP_2 or NiP_2.

The annealed product from the reaction of the $NiCl_2$-TOA complex with a 50% excess of yellow P_4 in ODE (**17**) showed fused, spherical particles ranging in size from 10-50 nm. The annealed product from the reaction of the $NiBr_2$-TOP complex with stoichiometric amounts of yellow P_4 using TOP as the solvent as well (**18**), revealed fused, spherical particles ranging in size from 10-30 nm. SEM images of these two products can be seen in Figure 5.12. The morphologies of the washed and annealed samples of the reaction from the $Ni(acac)_2$-TOA complex with a 100% excess of yellow P_4 in ODE (**22**) were revealed to be spherical particles 10-20 nm in size (see Figure 5.13). This size range of particles is consistent with average crystallite size calculations, which was found to be ~12 nm for this annealed product (see Section 5.3.3). The particle sizes produced from all analyzed NiP_2 samples in this section show a reduction in size and a more uniform size distribution as compared to the products produced without surfactant in previous chapters. The sizes ranges of NiP_2 products from previous chapters were 50-100 nm, 20-70 nm and 10-100 nm particles for superheated toluene products (Chapter 3), supercritical toluene products (Chapter 3) and for benchtop HD reactions with yellow P_4, (Chapter 4) respectively.

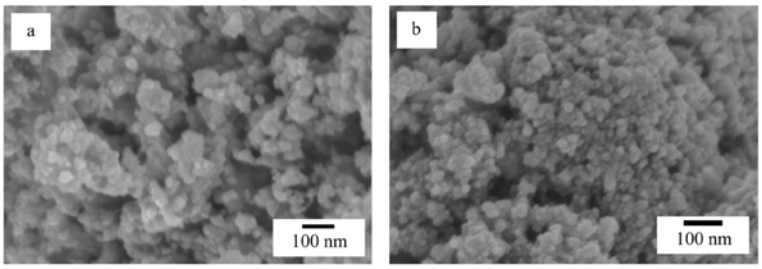

Figure 5.12 SEM images of annealed products from reactions **17** (a) and **18** (b).

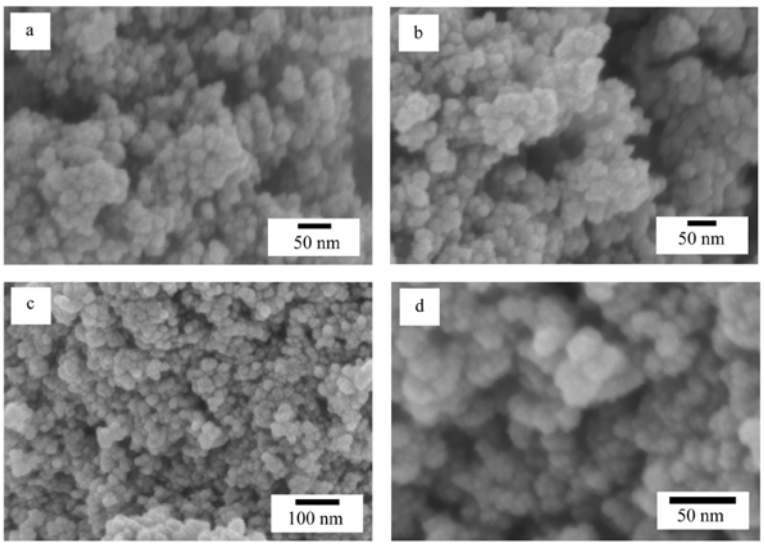

Figure 5.13 SEM images of washed (a and b) and annealed (c and d) products from reaction **22**.

The morphology of the washed product from the reaction of the $CuCl_2$-TOA complex with a 50% excess of yellow P_4 in ODE (**5**) showed irregular, fused particles (500 nm-10 μm) along with large microspheres ranging in size from 1-6 μm (Figure 5.14a). These microspheres and irregular particles have smooth, ellipsoidal surface features ranging from 50-250 nm (Figure 5.14b). This product was the only one in this chapter where the targeted MP_2 phase was found to be crystalline without post-reaction

annealing and with no metal-rich phases present. Unfortunately, in this synthesis it appears that the surfactant was not able to prevent particle fusion and growth.

The morphology of the washed product from the reaction of the $CuCl_2$-TOP complex with stoichiometric amounts of yellow P_4 using TOP as the solvent (**7**), produced large spherical aggregates (1-3 μm) made from collections of ellipsoidal particles ranging in size from 10-20 nm (Figure 5.15 a and b). Upon annealing, the micron-sized spherical aggregates became porous but retained their overall shape (Figure 5.15c). These voids may have been produced as bound surfactants were desorbed or pyrolyzed away during the annealing process. The resulting morphology of these porous spheres consists of fused particles ranging in size from 5-20 nm (Figure 5.15d).

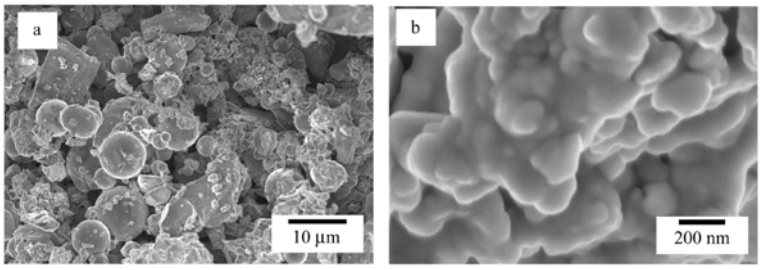

Figure 5.14 SEM images of washed product from reaction **5** (a and b).

The morphologies of the washed and annealed samples of the reaction from the $Cu(acac)_2$-TOA complex with a 100% excess of yellow P_4 in ODE (**11**) were revealed to be spherical particles 10-20 nm in size (see Figure 5.16). The particle sizes produced from these CuP_2 samples show a reduction in size and size distribution from the products produced without surfactant in previous chapters. The size ranges of annealed, crystalline CuP_2 products from previous chapters revealed fused, faceted particles ranging in size from 100-300 nm, rods with diameters from 100-200 nm, and large, micon-sized, faceted plates for superheated toluene products (Chapter 3), supercritical

toluene products (Chapter 3) and for benchtop HD reactions with yellow P_4 (Chapter 4) respectively.

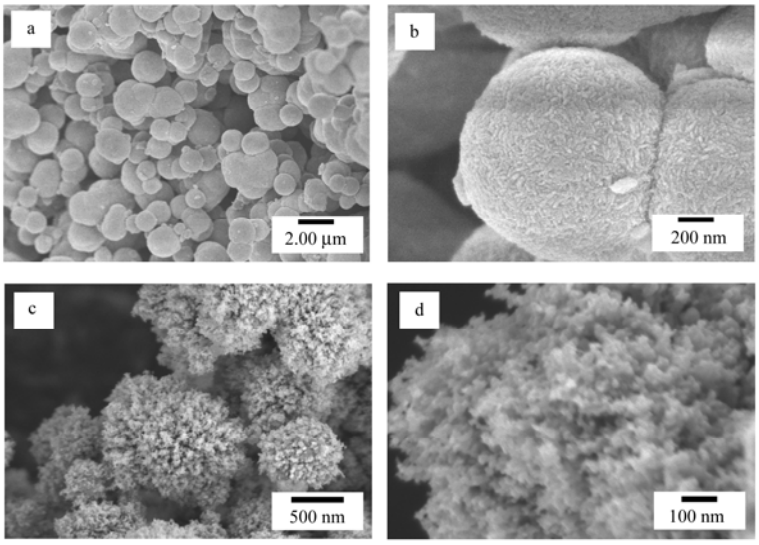

Figure 5.15 SEM images of washed (a and b) and annealed (c and d) products from reaction **7**.

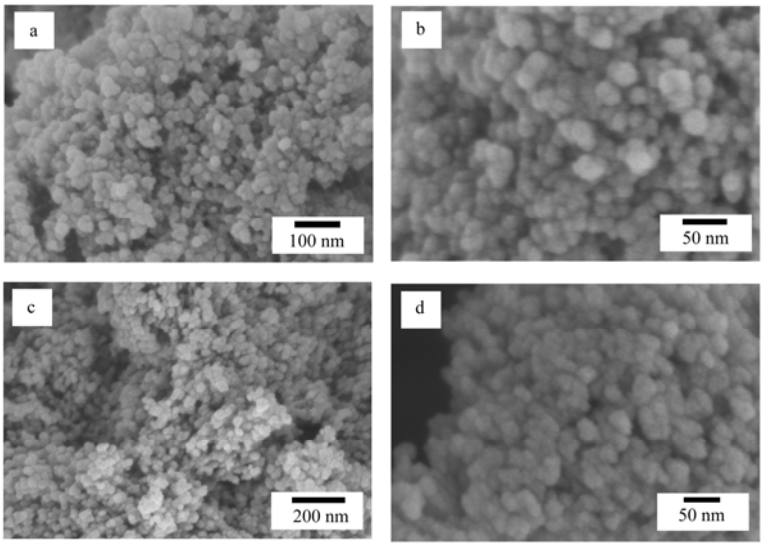

Figure 5.16 SEM images from washed (a and b) and annealed CuP_2 products from reaction **11**.

5.3.5 X-ray photoelectron spectroscopy (XPS) analysis

In this section, the XPS results from various CuP_x and NiP_x samples will be presented. The MP_x products analyzed are from reactions in various chapters, but will be presented here in a comparative manner. There are two sets of samples that will be presented, one for CuP_x and another for NiP_x. Each of these sets has an amorphous washed product from a solvothermal synthesis, a crystalline phase-pure (NiP_2 or CuP_2) annealed product from a solvothermal synthesis and a crystalline phase pure (NiP_2 or CuP_2) product from a solvent-free, solid-state synthesis. The solid-state samples are the most crystalline (largest crystalline domains) and are meant to act as standards for NiP_2 and CuP_2. The solvothermal samples are analyzed to see if there are significant differences between the amorphous (washed) and crystalline (annealed) samples and also to see if there are any significant differences when compared to the solid-state samples.

Since XPS is a surface sensitive tool (~0-5 nm sampling depth) the elemental specific information from XPS is strongly biased towards a sample's surface composition (including surfactant coatings).

The specific samples analyzed by XPS are solvothermal NiP_x from the reaction of a $Ni(acac)_2$-OA complex with yellow P_4 in ODE (washed and annealed, reaction **22**) and a solid-state NiP_2 sample from the reaction of $NiCl_2$ with yellow P_4. The solvothermal CuP_x products are from the autoclave reaction of $CuCl_2$ with yellow P_4 in toluene (washed and annealed), and the solid-state sample is from the reaction of $CuCl_2$ with yellow P_4. Experimental data was also collected for amorphous red phosphorus. MP_x samples described here will be referred to as "washed", "annealed" or "solid-state" samples in the remainder of this section.

In these XPS experiments, the binding energy of the samples' metal and phosphorus 2p 3/2 electrons was investigated. In the best case scenario, the binding energy of these electrons will give us an indication of relative oxidation states and chemical environment. An increase in relative binding energy indicates an increase in oxidation state (more cationic) and a decrease in relative binding energy indicates an increase in anionic charge (more anionic). XPS is a surface sensitive (0-5 nm) technique and will often show surface oxidation, as is the case for the phosphorus spectra we obtained. Experimental binding energies will be compared between samples and between binding energies of compounds of interest from literature.[137]

Metal binding energies for MP_2 phases are expected to fall between elemental values (Cu^0 or Ni^0) and oxidized values (CuF_2 or NiF_2). Phosphorus binding energies for MP_2 phases are expected to fall between elemental values (P) and reduced values (GaP); as was previously mentioned, oxidized phosphorus species are present due to surface oxidation and are similar to values for phosphates and phosphites. Before making oxidation state comparisons it is useful to revisit the structures of monoclinic CuP_2 and cubic NiP_2.

As was described in Chapter 1, NiP_2 and CuP_2 are complex polyphosphides containing polyatomic phosphorus anions with covalent P-P bonds. To rationalize the bonding in these anions, Zintl-Klemm rules are used to count electrons.[138] This method assumes that the metals are discrete M^{n+} cations (where n is an integer) and then applies the octet rule to count electrons in the polyphosphide anion; the structure of which is determined crystallographically. By this method, cubic NiP_2 is found to have discrete P_2^{4-} (-2 per P) polyanions, implying a Ni^{4+} oxidation state. Monoclinic CuP_2 is found to have infinite, fused P_{10}^{5-} (-0.5 per P) rings, implying a Cu^{1+} oxidation state. The oxidation states found by this method assume complete compartmentalization of the M and P electrons, consistent with ionic compounds. These substances are not ionic and contain partially covalent bonding between the M and P atoms. Because of this, binding energies found in XPS should show a reduction in metal ($Ni^{<4+}$ or $Cu^{<1+}$) and phosphorus (<-2 per P for NiP_2 or <-0.5 per P for CuP_2) oxidation states relative to those found by the Zintl-Klemm rule.

Experimental Ni 2p 3/2 binding energies were found to be 855.5, 854.8 and 853.9 eV for annealed, solid-state and washed samples of NiP_x respectively. Ni 2p 3/2 binding energy spectra from NiP_x samples can be seen in Figure 5.17. All of these values show an increase in oxidation state relative to elemental Ni^0 (852.0-853.0 eV), but are below values found in NiF_2 (858.20 eV), which has an oxidation state of ~2+. The crystalline NiP_2 samples (annealed and solid-state) samples also show an increase in oxidation relative to the amorpous (washed) NiP_x sample. The change in eV between Ni^0 and NiF_2 is ~ +6, and the Δ in eV between $Ni^0$and our NiP_x samples is ~ +1.5-3.0 eV, suggesting that the oxidation state of Ni surface atoms in our samples is closer to +1. The peak in the washed sample is also markedly broader than those from the crystalline samples, perhaps a consequence of being amorphous and structurally disordered.

Experimental P 2p 3/2 binding energies were found to be 129.8, 129.7 and 129.1 eV for annealed, washed and solid-state NiP_x samples respectively and was found to be

130.4 eV for red phosphorus. P 2p 3/2 binding energy spectra from NiP_x samples can be seen in Figure 5.17. Literature values for elemental red phosphorus are found between 129.90-130.45 eV, consistent with our results. The binding energies of the NiP_x samples are consistently lower than elemental red phosphorus consistent with an increase of anionic charge when compared to elemental P. Literature values for GaP, which contains a highly anionic P (~3-), fall between 128.5-129.4. This range of values includes one of our NiP_x values, but is generally lower than our experimental results. It is clear that shifts in binding energies are minimal for P reductions, which can make evidence of relative reduction difficult. The oxidation of phosphorus species, on the other hand, shows more dramatic shifts. In most of our samples surface oxidation is revealed by the appearance of a second P 2p 3/2 peak at ~134.0-135.0 eV, consistent with literature values for oxidized phosphorus species (e.g. $NaPO_3$ 134.2-134.5 eV).

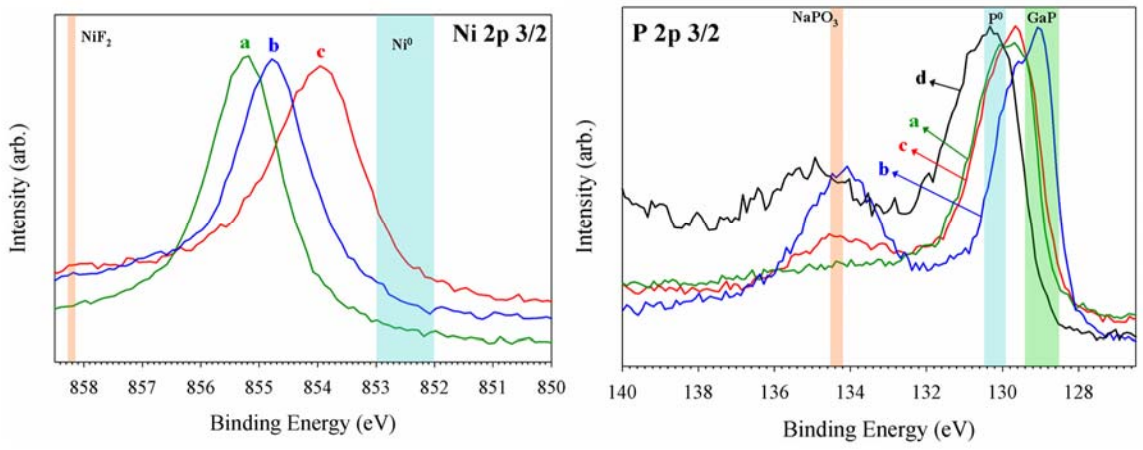

Figure 5.17 XPS spectra for products from the NiP_x sample set. Washed and annealed product from the surfactant-aided, solvothermal synthesis using $Ni(acac)_2$ can be seen in spectra (c) and (a) respectively. Product from the solvent-free, solid-state synthesis (Chapter 2) can be seen in spectrum (b). The spectrum of red phosphorus can be seen in spectrum (d).

Experimental Cu 2p 3/2 binding energies were found to be 933.2, 933.2 and 932.8 eV for solid-state, annealed and washed CuP_x samples respectively. Cu 2p 3/2 binding energy spectra from CuP_x samples can be seen in Figure 5.18. These values are similar, but consistently greater than literature values found for Cu^0 (932.2-932.7 eV) but are well below literature values for highly oxidized (~2+) CuF_2 (936.0-937.0). The change in eV between Cu^0 and CuF_2 is ~ +4 eV, and the Δ in eV between Cu^0 and our samples is ~ +0.3-0.7, suggesting that the oxidation state in our samples is only slightly positive (< +1). Our experimental values are slightly higher than reported in literature (932.2-932.4 eV).[139]

Experimental P 2p 3/2 binding energies were found to be 130.4, 130.3 and 130.0 eV for annealed, washed and solid-state CuP_x samples, respectively. P 2p 3/2 binding energy spectra from CuP_x samples can be seen in Figure 5.18 with amorphous red phosphorus added for comparison. These samples show little to no shift in binding energy relative to elemental phosphorus, indicative of an oxidation state very similar to elemental P. These samples, as the NiP_x samples, also showed secondary P 2p 3/2 binding energies consistent with oxidized P species.

These XPS results show consistent trends and complementary data within MP_x sets. For example, NiP_x samples show greater positive shifts in Ni 2p 3/2 binding energy relative to elemental Ni than does CuP_x samples' Cu 2p 3/2 shifts relative to elemental Cu. This trend is consistent with the Zintl-Klemm descriptions which describe Ni as +4 and Cu as +1 cation. To neutralize the positive charge on the metals, the phosphorus' atoms must be anionic. Since the Ni in NiP_x samples are more oxidized than the Cu in CuP_x samples, we expect the P in NiP_x to also be more reduced (lower binding energy) than the P in CuP_x samples, which they are. Our XRD data from the annealed and solid-state samples confirmed the presence of crystalline NiP_2 and CuP_2 and so the presence of Cu, Ni and P 2p 3/2 binding energies consistent with these phases was expected and was confirmed. The absence of unexpected Cu or Ni 2p 3/2 binding energy shifts in

amorphous versus crystalline products also suggests that amorphous products may consist of disordered but intimately bonded M-P regions that are related to the eventual oxidation states and chemical environments of crystalline products.

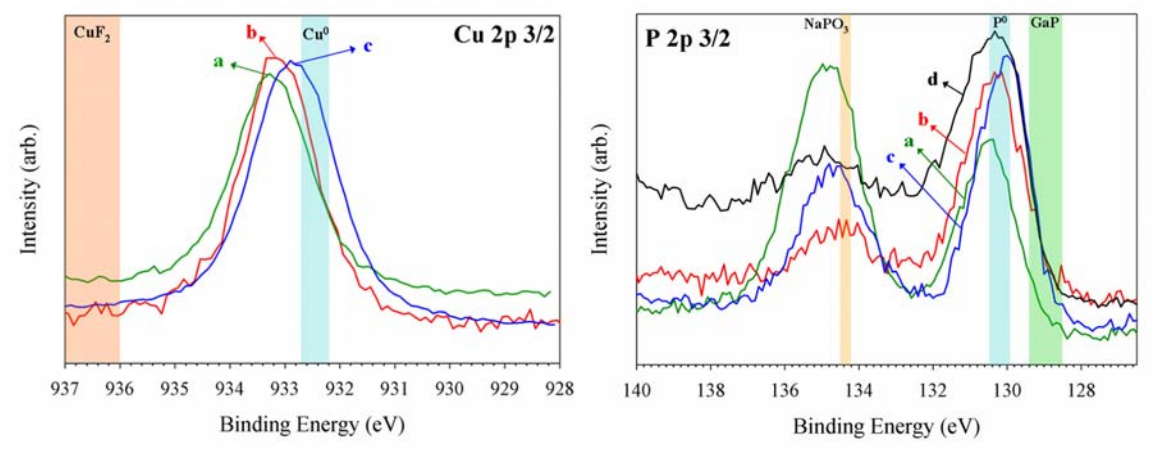

Figure 5.18 XPS spectra for products from the CuP_x sample set. Washed and annealed product from the superheated toluene reaction (Chapter 3) can be seen in spectra (c) and (b) respectively. Product from the solvent-free, solid-state synthesis (Chapter 2) can be seen in spectrum (a). The spectrum of red phosphorus can be seen in spectrum (d).

5.4 Conclusions

Reactions between copper or nickel complexes and yellow P_4 in several solvents, and with varying amounts of phosphorus and surfactant were performed resulting in a variety of metal phosphides or metal phosphide mixtures. Surfactant addition was found to significantly lower the reaction onset temperatures for MP_x formation relative to similar reactions without surfactant (Chapters 3 and 4). Surfactant complexation of metal reagents also increased their solubility in non-polar organics which is critical for "bottom-up" arrested precipitation routes to nanoparticles. Several samples afforded small nanoparticles (10-20 nm) or particles with nanofeatures as small as 5-20 nm. This targeted decrease in particle size is an improvement from the surfactant free syntheses

from similar reactions in Chapters 3 and 4. The resulting nanoparticles, particularly those from $M(acac)_2$, resulted in nanospheres with a more narrow size distribution as well, another improvement over metal phosphide syntheses described in previous chapters.

While the introduction of surfactants has shown to improve many aspects of the solvothermal syntheses, they are also detrimental in other areas. The surfactants have shown the ability to degrade phosphorus-rich MP_x particles and result in MP_x products with a loss in phosphorus content when used at high temperatures. This process is especially evident when surfactants are used as solvents in solution annealings, producing products with less phosphorus content than their solid-state annealing product counterparts. Phosphorus loss in this process can be counteracted by the addition of stoichiometric excesses of phosphorus in certain systems, but this makes dialing in phosphorus content in the MP_x products more difficult as balanced stoichiometry can not be used to target M:P molar ratios in the products.

Surfactant-aided, solvothermal syntheses from molecular sources of crystalline nanoparticulate metal/non-metal phases by arrested precipitation has been shown to work for a variety of phases. These syntheses benefit when precursors are highly soluble and reactive, when crystallization temperatures are low and reaction durations are short. They also benefit when the surfactant can passivate the particle surface by coordinating to metal surface sites and at the same time remain uninvolved in the chemical reaction. Many of these prerequisites for facile, crystalline nanoparticle growth work against targeting CuP_2 and NiP_2. Crystallization temperatures for these phases have shown to be consistently around 350 °C and require maintaining these elevated temperatures for several hours (>15 h). These relatively high temperatures and long durations required for crystallization are reflective of the crystal structures of polyphosphides which, in many instances, consist of complex, covalently bonded polyatomic phosphorus networks. Maintaining high temperatures for long durations favors particle growth and also allows for particle degradation by corrosive surfactants. It is for these reasons that targeting

crystalline nanoparticles of NiP_2 and CuP_2 is a challenging task, as was evident from our results. This chapter, however, did present several syntheses that were successful in producing crystalline CuP_2 and NiP_2 nanoparticles, and overcome several of the synthetic obstacles noted above.

CHAPTER 6

CONCLUSIONS AND FUTURE OUTLOOK

6.1 Summary and Conclusions

Several transition-metal polyphosphides were synthesized by various low-temperature reactions. Solvent-free, solid state syntheses from metal chlorides and either elemental yellow P_4 or red phosphorus yielded phase-pure orthorhombic FeP_2, cubic CoP_3, cubic-NiP_2, monoclinic PdP_2 and monoclinic CuP_2. High-pressure autoclave reactions from metal halides and yellow P_4 in superheated toluene afforded CoP_x, NiP_x and CuP_x products which, upon moderate post-reaction annealings, crystallized to phase-pure CoP_3, NiP_2 and CuP_2. Similar reactions in supercritical toluene afforded phase-pure crystalline NiP_2 and CuP_2 without the need for post-reaction annealing. Benchtop reactions in high boiling point solvents (HD or ODE) between metal halides and either yellow P_4 or red phosphorus afforded CoP_x, NiP_x and CuP_x products which, upon moderate post-reaction annealings, crystallized to phase-pure CoP_3, NiP_2 and CuP_2. Several benchtop reactions between metal halide or metal acetylacetonate complexes with yellow P_4 in several solvents (toluene, mesitylene, HD or ODE) in the presence of surfactants (OA, TOA or TOP) yielded CuP_x and NiP_x products.

Solvent-free, solid-state reactions were performed in evacuated ampoules at temperatures ranging from 500-700 °C. These reactions were stoichiometrically balanced such that all chloride was ideally removed as PCl_3 and the remaining P was used to form the targeted MP_x phase (M = Fe, Co, Ni, Pd or Cu and x = 2 or 3). When yellow P_4 was used, the reaction took place between either ground (loose powder) or pelletized metal chlorides and P_4 vapors. When red phosphorus was used, the reaction took place between the metal chloride and phosphorus which were intimately mixed and co-pelletized. In pellet reactions (both yellow P_4 and red phosphorus), the overall macroscopic shape of the pellet was retained through the conversion from metal halide to

metal phosphide. Product pellet morphologies from yellow P_4 and red phosphorus reactions were drastically different as pellet weight loss going from reagent to product was greater when red phosphorus was used as it was co-pelletized with the metal halide, contributing to the pellets' initial mass. Because of this, the products from reactions using red phosphorus contained a greater amount of void space; in turn these pellets appeared black and matted whereas the pellets from yellow P_4 reactions appeared silver with a metallic luster.

Autoclave reactions between metal halide ($CoCl_2$, $NiCl_2$, $NiBr_2$ and $CuCl_2$) suspensions and dissolved yellow P_4 in superheated toluene were also stoichiometrically balanced such that all halide was ideally removed as PCl_3 or PBr_3 and the remaining P was used to form the targeted MP_x phase (M = Co, Ni or Cu and x = 2 or 3). All washed (as-synthesized) products from these reactions consisted of spherical products with sizes ranging from 150-250 nm, 50-100 nm, 75-150 nm and 20-60 nm for CoP_3, NiP_2 (from $NiCl_2$), NiP_2 (from $NiBr_2$) and CuP_2, respectively. Upon annealing washed products, the NiP_2 products generally retained their shapes but showed signs of particle fusion between particle surfaces. The washed CoP_3 product retained spherical morphologies through the annealing process, but the particle size increased to 200-350 nm and also showed signs of particle fusion between particle surfaces. The washed CuP_2 products became highly fused when annealed at 350 °C, resulting in micron-sized particles with 100-300 nm surface features. When CuP_2 products were annealed at 500 °C, the growth of faceted, micron-sized plates resulted. The PCl_3 and PBr_3 byproducts were shown by ^{31}P NMR to have reacted with toluene during the reactions forming alkyl phosphorus halides, which may have acted like *in situ* generated surfactants, contributing to the spherical morphologies seen in these products.

Similarly balanced autoclave reactions between $NiCl_2$ or $CuCl_2$ suspensions and dissolved yellow P_4 were performed in supercritical toluene (350-400 °C). To achieve supercritical conditions in these reactions, a thicker-walled autoclave had to be used and

Teflon components (gasket and stirbar) used in superheated toluene reactions were replaced with a graphite gasket and pyrex-coated stirbar in order to handle the higher temperatures. In these reactions, washed (as-synthesized) products were crystalline and required no post-reaction thermal treatment. By avoiding post-reaction annealings, particle fusion could be avoided. Washed NiP_2 products consisted of spherical nanoparticles ranging from 20-70 nm in size while CuP_2 products consisted of rods several microns in length with diameters ranging from 100-200 nm in size.

Benchtop reactions between metal halide ($CoCl_2$, $NiCl_2$, $NiBr_2$ and $CuCl_2$) suspensions and either dissolved yellow P_4 or suspended red phosphorus were performed in either HD or ODE. Again, these reactions were stoichiometrically balanced such that all halide was ideally removed as PCl_3 or PBr_3 and the remaining P was used to form the targeted MP_x phase (M = Co, Ni or Cu and x = 2 or 3). Washed CoP_3 product morphologies from yellow P_4 reactions consisted of spherical nanoparticles ranging in size from 10-30 nm, but upon annealing resulted in irregular, fused aggregates with features ranging from 50-300 nm in size. Washed CuP_2 product morphologies consisted of fused, ellipsoidal aggregates which upon annealing grew into micron-sized, faceted plates. Washed and annealed NiP_2 product morphologies consisted of ellipsoidal particles ranging from 10-100 nm in size. By replacing toluene with a high-boiling point solvent, inconvenient autoclave reactors, necessary to attain high temperatures with toluene, were no longer needed. Also, these reactions showed that toxic, reactive yellow P_4 could be replaced with non-toxic, air stable red phosphorus and still afford targeted MP_x products, albeit with different morphologies.

Benchtop reactions described in the previous paragraph were modified by the addition of surfactants and by the introduction of metal acetylacetonates as a metal source. In these reactions, a completely or partially dissolved MX_2 surfactant complex (where M = Ni or Cu, X = Cl, Br or acac and surfactant = OA, TOA or TOP) was reacted with various amounts of dissolved yellow P_4 in a variety of solvents (toluene, mesitylene,

TOA, TOP, HD or ODE). The addition of surfactant significantly increased the solubility of the metal reagent and also significantly lowered the reaction onset temperature for MP_x formation by activating the M-X bond (X = Cl, Br or acac). The addition of surfactant was not only motivated by their ability to increase solublilty, but also by their ability to passivate particle surfaces, stunting their growth. By having completely soluble reactants in the presence of surfactants, a homogeneous reaction between discrete, dissolved reactants could take place and particle size and particle size distribution may both be reduced. In most of these reactions when surfactants were used at elevated temperatures in conjunction with high boiling point solvents, the surfactants were found to be corrosive, degrading MP_x products and yielding products with phosphorus deficiencies. Because phosphorus loss was detected, excess amounts of yellow P_4 was added to achieve targeted NiP_2 or CuP_2 formation. Surfactant addition was successful in reducing particle size and in several syntheses affording spherical nanoparticles with sizes ranging from 10-30 nm.

Overall, we were successful in improving upon the synthesis of several MP_x polyphosphides by significantly reducing reaction temperatures and by synthesizing products with nanoscale morphologies. Much of the success in these syntheses was accomplished by the formation of the PCl_3 or PBr_3 byproduct which allowed us to use stoichiometric amounts of phosphorus. By using a stoichiometric amount of phosphorus in rigorously anhydrous reaction environments we were able to discretely target specific MP_x polyphosphide phases, avoiding products with multiple binary MP_x phases.

The majority of previously reported syntheses of transition-metal polyphosphides have been elemental reactions. These reactions were performed by either heating a mixture of the elements at high-temperatures in ampoules, or by heating a mixture of the elements in a Sn flux.[40,66-68] To our knowledge, there are only two reports where transition-metal polyphosphides introduced in this work have been synthesized using at least one non-elemental source, and in both of these reports the polyphosphides were

present in a mixture of MP_x phases. In one report, Na_3P and $FeCl_3$ were reacted together resulting in a FeP/FeP_2 mixture.[140] In the other report, metal nanoparticles are reacted with TOP yielding Cu_3P/CuP_2 and Pd_5P_2/PdP_2 mixtures.[100]

Our syntheses are not only the first to provide non-elemental (at least one source), low-temperature reaction routes to several phase-pure, transition-metal polyphosphides, they also represent the first reports of phase-pure CuP_2 and NiP_2 nanoparticles. These are exciting results as polyphosphides are promising materials for use as anode materials in Li^+ ion batteries, and are currently being investigated by many groups.[11,43-45,47-50,52,53,70,141] The use of Li^+ technology in batteries has already shown to significantly improve the usability of modern electronics such as laptop computers and cell phones, and will certainly play a larger role in the auto industry as alternatives to combustion engines are currently under intense scrutiny. The ability to produce these polyphosphides as nanoparticles could also improve battery performances as they are inherently high-surface area materials.

6.2 Future Work

This section will briefly describe some syntheses that have already been performed but were not included in any of the previous chapters, and will also discuss ideas for potential future research related to work in this thesis, but not yet performed. Although some preliminary results were promising for certain syntheses, a more detailed analysis of these reactions were not performed due to time constraints.

6.2.1 Preliminary results: solid-state synthesis of nickel diphosphide from acetylacetonates and stearates

As was mentioned in Chapter 2, the morphology of MP_x pellets was altered by changing the phosphorus source from yellow P_4 to red phosphorus, as this changed the amount of pellet weight loss in the transformation from metal halide to metal phosphide. The pellet weight loss can also be increased by substituting the metal halides with a metal

acetyacetonate or stearate ($[CH_3(CH_2)_{16}CO_2]^{1-}$). The use of red phosphorus instead of yellow P_4 in conjuction with an acetylacetonate or stearate (St) will further increase pellet weight loss.

In these reactions, $Ni(acac)_2$ or $Ni(St)_2$ was pelletized and reacted with P_4 vapors or co-pelletized and reacted directly with red phosphours in evacuated sealed ampoules (2 d, 500 °C). These reactions used the same stoichiometry as previously described in Equation 5.2, and can be seen here in Equations 6.2 and 6.3.

$$3\ Ni(X)_2 + 2\ P_4 \rightarrow 3NiP_2 + 2\ P(X)_3\ (X = acac\ or\ St) \quad (6.1)$$

$$3\ Ni(X)_2 + 8\ P_{red} \rightarrow 3\ NiP_2 + 2\ P(X)_3\ (X = acac\ or\ St) \quad (6.2)$$

The formation and identification of the phosphite $P(X)_3$ was envisioned for stoichiometry purposes but, as in Chapter 5, was not confirmed. Substituting organometallic compounds for metal halides in these reactions brings about some synthetic differences, primarily pellet shape retention.

The melting point for $NiCl_2$ is 1001 °C whereas the melting points for $Ni(St)_2$ and $Ni(acac)_2$ are 80 and 229 °C respectively. Upon heating, the pellets from these reactions form black liquid melts, suggesting that even with initial MP_x formation, as indicated by the color change to black, the pellets can not retain their shape due to the low-melting points of the nickel precursors. The integrity of the pellets may also be hard to sustain given the large change in weight they undergo when forming the metal phosphide. When $NiCl_2$ is used, the percentage of original pellet mass remaining in the product pellet is 93 and 57 % for reactions with yellow P_4 and red phosphorus respectively. When $Ni(acac)_2$ is used these values drop to 47 and 35 % and when $Ni(St)_2$ is used, drop even further to 19 and 17 % for yellow P_4 and red phosphorus respectively.

The XRD patterns for these experiments show that NiP_2 is formed for all reactions except in the reaction between $Ni(acac)_2$ and red phosphorus, where Ni_2P is seen as the only product (Figure 6.1). Initial SEM images were taken from the reaction of $Ni(acac)_2$ with yellow P_4, and reveals a morphology with larger voids as expected.

The morphology consists of large, smooth monoliths with holes (~ 1-5 μm). The smooth monoliths are perhaps due to the melting of the $Ni(acac)_2$ and the holes may be due to large volumes of gas evolution. These images can be seen in Figure 6.2.

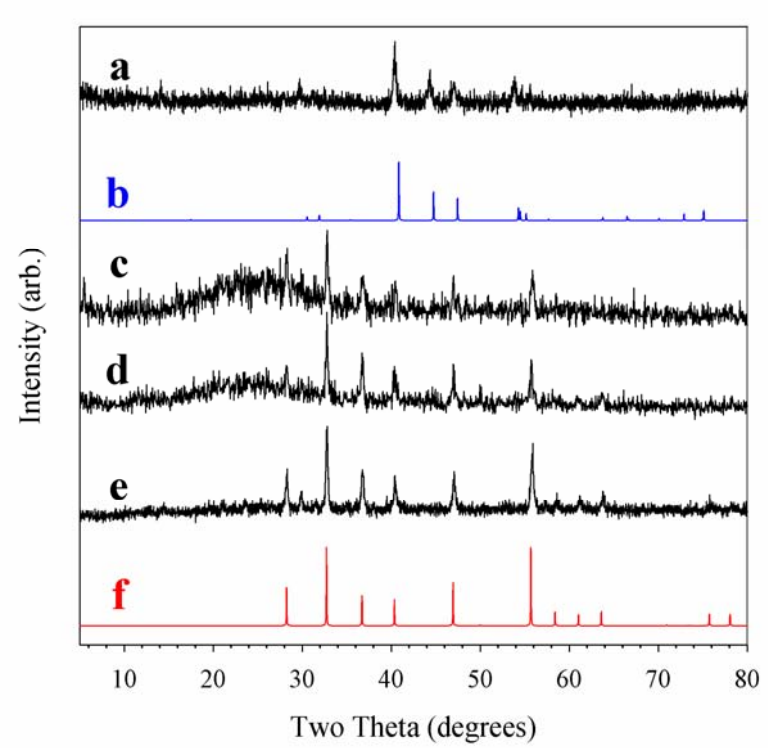

Figure 6.1 Experimental XRD of solid-state products from $Ni(acac)_2$ and red phosphorus (a), $Ni(acac)_2$ and yellow P_4 (c), $Ni(St)_2$ and yellow P_4 (d) and from $Ni(St)_2$ and red phosphorus (e). Calculated XRD patterns for Ni_2P and NiP_2 can be seen in (b) and (f) respectively.

The low melting point of $Ni(St)_2$ could be taken advantage of in targeting mixed metal polyphosphides as well. Synthesizing solid solutions is often difficult due to the inability to mix metal precursors. If a mixture of $Ni(St)_2$ (m.p. = 80 °C) and $Cu(St)_2$ (m.p. = 115 °C) powders were heated with stirring to temperatures above 115 °C, they could form an intimate mixture suitable for use in the synthesis of $Cu_{1-x}Ni_xP_2$. Proposals for mixed metal polyphosphide syntheses will be presented in the next section.

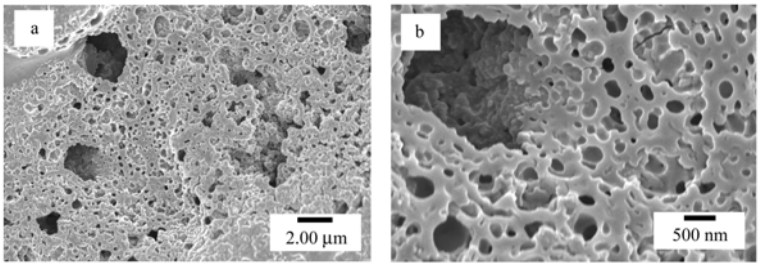

Figure 6.2 SEM images of solid-state products from $Ni(acac)_2$ and yellow P_4 (a and b).

6.2.2 Preliminary results: solid-state synthesis of transition-metal polysulfides

Attempts at extending our metal phosphide syntheses to other metal/non-metal binary phases led us to target metal polysulfides. There are many similarities between sulfur and phosphorus that led us to believe our synthesis could be translated to substitute sulfur for phosphorus. First, both phosphorus exist in the elemental state as discrete molecules (P_4 and S_8). Secondly, both have many allotropes in the elemental form, and can both form polymers from the aforementioned elemental monomers. This ability to catenate allows the formation of metal polyphosphides and polysulfides as the anions from P or S can form P_n^{x-} or S_n^{x-} polyatomic anions with direct P-P or S-S covalent bonding. We also noticed that CoS_2 and NiS_2 are cubic, pyrite-type structures just as our NiP_2 prouduct, as such these two phases were targeted.

In order to mimic our solid-state reactions producing MP_x phases from metal halides and phosphorus, which produced PCl_3 as a byproduct, a S_xCl_y byproduct was envisaged to dictate reaction stoichiometry. Sulfur monochloride (S_2Cl_2) is the most common (also commercially available) form of several sulfur chlorides (S_nCl_2) in which a polysulfide chain is terminated at each end with a Cl group, and was chosen as our targeted byproduct. In these reactions, as in red phosphorus reaction from Chapter 2,

either $CoCl_2$ or $NiCl_2$ was ground with S_8 (fine yellow powder) and pressed into a composite pellet, using molar ratios according to Equation 6.1.

$$MCl_2 + ½\ S_8 \rightarrow MS_2 + S_2Cl_2\ (M = Co \text{ or } Ni) \quad (6.3)$$

These pellets were loaded into ampoules and sealed under vacuum in the same manner as reactions from Chapter 2. These pellets were then heated over 3 h to 500 °C where they were held for 2 d in a tube furnace. In both of these reactions, minimal black powder could be seen at the pellet-containing end of the ampoule post-reaction, and sublimate could be seen at the other end. In both reactions a yellow sublimate, most likely S_8, could be seen along with an orange ($NiCl_2$) or blue ($CoCl_2$) sublimate.

The minimal black powder recovered in both reactions was washed with water and hexanes to remove any residual S_8 or MCl_2 before being examined by XRD. XRD results reveal the formation of both the targeted CoS_2 and NiS_2, albeit in small yields (~10% yields) and with no pellet shape retention (Figure 6.3). Initial results are promising, although different heating schemes may need to be employed to increase yields. This chemistry could also lend itself to solvothermal reactions as well. Elemental S_8 is very soluble in many non-polar organic solvents and may have better reactivity with an activated metal halide complex (e.g., $NiCl_2$-TOA).

An idea for future work stemming from this solid-state synthesis, is to try an target metal polyphosphosulfides ($M_xP_yS_z$). In these proposed syntheses a mixture of a metal halide, red phosphorus and S_8 could be pressed into a pellet and reacted in the solid-state as will be described in the next section.

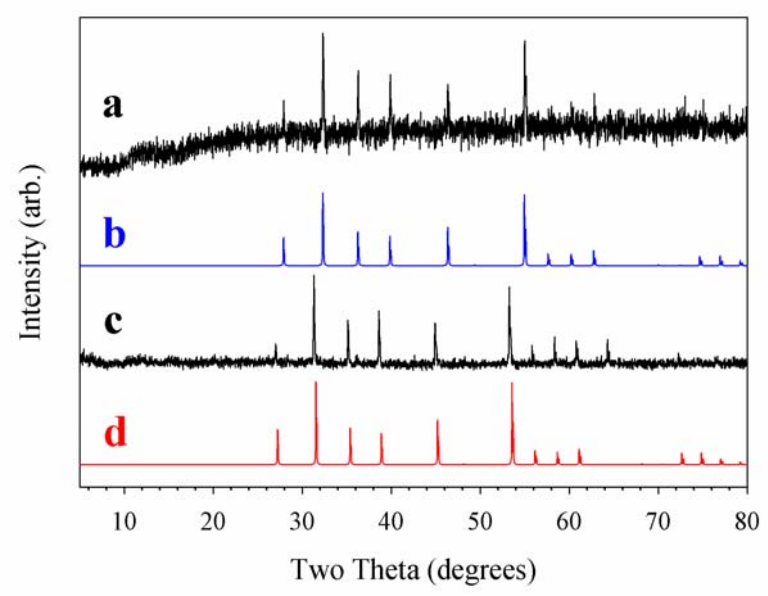

Figure 6.3 Experimental XRD patterns for washed products from the reactions between $CoCl_2$ and S_8 (a) and between $NiCl_2$ and S_8 (b). Calculated XRD patterns for cubic pyrite-type CoS_2 (b) and NiS_2 (d).

6.2.3 Preliminary results: synthesis of CuP_2 films fromCuCl$_2$ and Cu^0 film templates

Continuous thin films or coatings of metal/non-metal phases are often sought after for materials that are used in electronic and photovoltaic applications. Because of this, attempts at synthesizing thin films of CuP_2 were performed with a varying degree of success. In these reactions, a tared glass microscope slide (cleaned with pirhanha solution H_2SO_4/H_2O_2) was first coated with the copper source. For reactions using $CuCl_2$, $CuCl_2$ powder was heated (275 °C) under dynamic vacuum in a tube furnace, which caused the $CuCl_2$ to sublime and condense at the end of the tube furnace. A microscope slide was placed at this cool end, resulting in a slide coated with $CuCl_x$ sublimate. The $CuCl_2$ sublimate film was found to be a mixture of CuCl and $CuCl_2$ by XRD. This glass slide was reweighed and placed in a 1" diameter ampoule and sealed with an appropriate amount of yellow P_4 according to Equation 6.4. For reactions using

Cu^0, a tared microscope slide with a washer "mask" was sputter coated with Cu^0 until a reasonable mass of Cu^0 could be weighed. Cu^0 films made by sputter coating required long (20 min.) sputtering durations in order to obtain roughly 2 mg of Cu^0. These slides were then sealed with an appropriate amount of P_4 in a sealed ampoule according to Equation 6.5 and heated to 500 °C.

$$3\ CuCl_2 + 2\ P_4 \rightarrow 3\ CuP_2 + 2\ PCl_3 \quad (6.4)$$

$$Cu^0 + ½\ P_4 \rightarrow CuP_2 \quad (6.5)$$

In both of these reactions, the product XRD revealed the presence of CuP_2 as the major component along with Cu_3P as the minor component. Quantifying the amount of Cu in the precursor films was difficult due to unknown $CuCl/CuCl_2$ mixtures and low Cu^0 quantity. The inaccuracy of the stoichiometry used for these reactions may have contributed to the mixed phase product. SEM images of CuP_x films can be seen in Figure 6.4, and a photograph of the CuP_x film from Cu^0 is shown in Figure 6.5. The CuP_x films prepared from $CuCl_x$ did not remain adhered to the microscope slide through the reaction process. The SEM images of this product show a smooth, cracked top surface with shards of material underneath the top layer. These shards may be reminiscent of the sublimed $CuCl_x$ material. The effect of the washer "mask" can clearly be seen in the photograph and was implemented to show how patterned films may be prepared. The CuP_x film prepared from Cu^0 did remain adhered to the microscope slide through the reaction process.

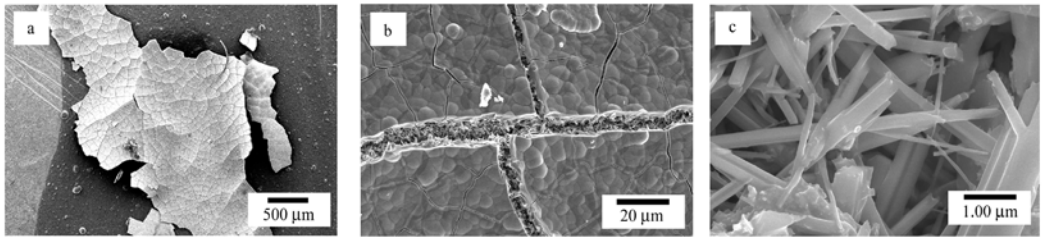

Figure 6.4 SEM images of a CuP_x film synthesized from $CuCl_x$ at progressively higher magnifications (a, b and c).

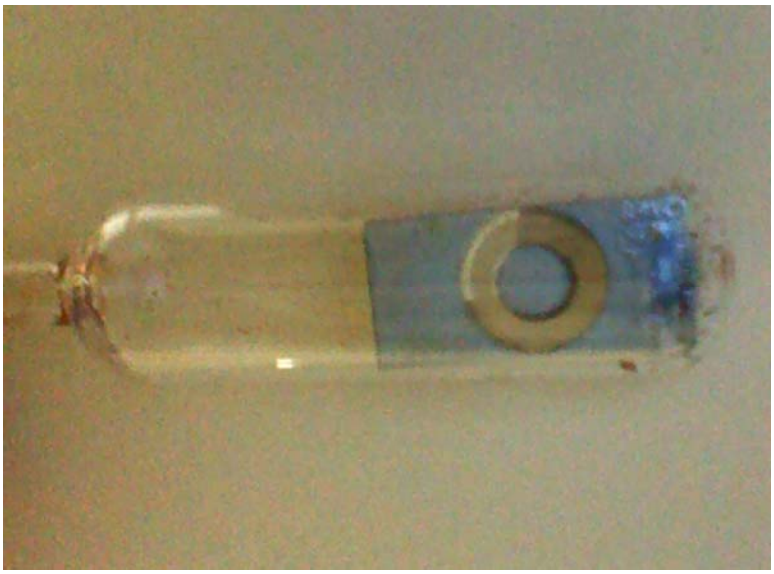

Figure 6.5 Photograph of a CuP_x film synthesized from Cu^0 still in the sealed ampoule used during the reaction.

6.2.4 Ideas for future research: synthesis of mixed metal polyphosphide solutions

Solid solutions of ternary phases consisting of two metals and a non-metal are often desirable as altering the relative amounts of each metal can tune a desired physical property such as the optical band gap. In solid solutions, it is often advantageous if the

individual binary metal/non-metal phases to be mixed have the same structure type so that there is no competition between structure types when mixing of the metals occurs. Syntheses attempting to produce mixed metal polyphosphides ($MM'P_x$) would be a logical next step in fully developing the chemistry presented in this thesis.

Envisaged ternary phases would include $Ni_{1-x}PdP_2$, $Co_{1-x}Ni_xP_3$ and $Cu_{1-x}Ag_xP_2$. There are two binary phases of NiP_2, a monoclinic phase and a cubic phase. We consistently produced the cubic phase, but the PdP_2 that we synthesized is a monoclinic phase with the same structure type as the monoclinic NiP_2. If mixing of these two phases could be achieved, it would be interesting to see if the monoclinic or cubic phase was obtained. Both CoP_3 and NiP_3 exist as cubic, skutterudite-type phases. We have successfully synthesized this phase for CoP_3 and the inclusion of Ni into this phase has been done before in elemental reactions[55] and may be attainable by our synthetic methods. The monoclinic phase of CuP_2 has a structure only shared by one other compound, AgP_2. For this reason, it would make sense to see if a mixture of these two phases could be achieved.

These mixed metal polyphosphides could possibly be synthesized by modifications to our solid state and solvothermal reactions. For solid state syntheses, a pellet could be pressed from an intimately ground mixture of metal halides and reacted with P_4 vapors, or a pellet comprised of intimately ground metal halides and red phosphorus could be reacted together directly. As was previously mentioned (Section 6.2.2) a melt of metal stearates could also be reacted with P_4 vapors. Using stearate melts may provide a more homogeneous mixture of metals compared to grinding a mixture of metal halides.

Solvothermal reactions targeting mixed metal polyphosphides could possibly be achieved using our synthetic methods as well. It may be possible to simply use a mixture of metal halides without further altering our reaction methods. This, however, would likely lead to a composite of single metal polyphosphides rather than a solid solution as

yellow P_4 would react with the more reactive halide first and, as the temperature was elevated, react with the second halide. To circumvent this problem, a mixture of metal halide complexes could be heated above the reaction onset temperatures of both metal halide complexes followed by the introduction of dissolved yellow P_4 via cannula transfer. For example, a mixture of $CuCl_2$-TOA (RT reaction onset) and $NiCl_2$-TOA (<50 °C reaction onset) could be heated to 80 °C prior to P_4 introduction, resulting in simultaneous MP_x nucleation.

6.2.5 Ideas for future research: synthesis of metal polyphosphosulfides

Solid solutions of ternary phases consisting of a metal, phosphorus and sulfur would be interesting synthetic targets. In our syntheses, P_4 or S_8 have been used, but we have never employed a phosphosulfide (P_xS_y). There are many P_xS_y compounds ranging from molecular to polymeric just as for phosphorus and sulfur. The most common form is P_4S_3, which is a molecular compound where S is inserted into half of the P-P bonds of the P_4 tetrahedron forming three P-S-P bonds. Another molecular form is $P_4S_{10,}$ where S is inserted into all 6 of the P-P bonds of the P_4 tetrahedron and then also attached terminally to each P, forming 6 P-S-P bonds and 4 P-S bonds.

If these compounds replaced yellow P_4 or red phosphorus in our reactions, perhaps they would promote the formation of homogeneous $M_xP_yS_z$ compounds. As was previously described, MP_x and MS_x with the same structure types would make for good first targets. We introduced the synthesis of the pyrite-type NiS_2 phase in this chapter, which has the same structure type as the NiP_2 we synthesized throughout this thesis. Because of this, the initial target phase would be $NiP_{2-x}S_x$. As previously mentioned (Chapter 1), NiP_2 is a diamagnetic material with a band gap of 0.73 eV while NiS_2 has a band gap of 0.30 eV and is antiferromagnetic with a Neel temperature (T_N) of 40 °K.[142] It may be possible to tune the band gap of $NiP_{2-x}S_x$ in the range of 0.30 to 0.73 eV, and it

would be interesting to see how the magnetic properties of NiS_2 would change upon P incorporation. Another intriguing phase would be CoP_xS_y as CoS_2 is reported as being metallic with a Curie temperature (T_C) of 120 °K while CoP_3 is diamagnetic, small band gap semiconductor (0.45 eV).

Synthetic approaches towards metal polyphosphosulfides could also include both solid-state and solvothermal routes. Pellets could be pressed from a mixture of a metal halide, red phosphorus and S_8 or from a mixture of a metal halide and P_4S_3 and reacted in the solid-state. Solvothermal routes could be performed by reacting dissolved metal halide complexes with a mixture of dissolved yellow P_4 and S_8. Dissolved metal halide complexes could also be reacted with P_4S_3 as it is also soluble in many non-polar organic solvents.

REFERENCES

(1) West, A. R. *Solid State Chemistry and its Applications*; John Wiley & Sons: New York, **1984**.

(2) Cox, P. A. *The Electronic Structure and Chemistry of Solids*; Oxford University Press: New York, NY, **1987**.

(3) Arora, S.; Manoharan, S. S. *Mater. Chem. Phys.* **2008**, *110*, 34-37.

(4) Green, M.; O'Brien, P. *Chem. Commun. (Cambridge)* **1999**, 2235-2241.

(5) Yoffe, A. D. *Advances in Physics* **2001**, *50*, 1-208.

(6) Esteves, A. C. C.; Trindade, T. *Curr. Opin. Solid State Mater. Sci.* **2002**, *6*, 347-353.

(7) Croll, S. *Prog. Org. Coat.* **2002**, *44*, 131-146.

(8) Carp, O.; Huisman, C. L.; Reller, A. *Prog. Solid State Chem.* **2004**, *32*, 33-177.

(9) O'Regan, B.; Graetzel, M. *Nature (London)* **1991**, *353*, 737-40.

(10) Fujishima, A.; Honda, K. *Nature (London)* **1972**, *238*, 37-8.

(11) Ohzuku, T.; Brodd, R. J. *J. Power Sources* **2007**, *174*, 449-456.

(12) Landi, B. J.; Castro, S. L.; Ruf, H. J.; Evans, C. M.; Bailey, S. G.; Raffaelle, R. P. *Sol. Energy Mater. Sol. Cells* **2005**, *87*, 733-746.

(13) Lee, K.-H. *J. Nucl. Med.* **2007**, *48*, 1408-1410.

(14) Biju, V.; Itoh, T.; Anas, A.; Sujith, A.; Ishikawa, M. *Anal. Bioanal. Chem.* **2008**, *391*, 2469-2495.

(15) D'Anna, E.; Leggieri, G.; Luches, A. *Thin Solid Films* **1992**, *218*, 219-30.

(16) Soignard, E.; McMillan, P. F.; Leinenweber, K. *Chem. Mater.* **2004**, *16*, 5344-5349.

(17) Halpin, T.; Byrne, G.; Barry, J.; Ahearne, E. *Proceedings of the Institution of Mechanical Engineers Part B-Journal of Engineering Manufacture* **2009**, *223*, 947-953.

(18) Haskell, B. A.; Nakamura, S.; DenBaars, S. P.; Speck, J. S. *Phys. Status Solidi B* **2007**, *244*, 2847-2858.

(19) Carvajal, J. J.; Aguilo, M.; Diaz, F.; Rojo, J. C. *Chem. Mater.* **2007**, *19*, 6543-6547.

(20) Furimsky, E. *Appl. Catal., A* **2003**, *240*, 1-28.

(21) Corbridge, D. E. C. *Phosphorus: An Outline of its Chemisty, Biochemistry and Technology*; Fourth Edition ed.; Elsevier: New York, **1990**.

(22) Von Schnering, H. G.; Hoenle, W. *Chem. Rev.* **1988**, *88*, 243-73.

(23) Schrey, F.; Boone, T.; Nakahara, S.; Robbins, M.; Appelbaum, A. *Thin Solid Films* **1987**, *149*, 303-11.

(24) Aronsson, B.; Lundstrom, T.; Rundquist, S. *Borides, Silicides, and Phosphides: A Critical Review of their Preparation, Properties, and Crystal Chemistry*; Ballantyn and Co.: Spottiswoode, U.K., **1965**.

(25) Ishida, S.; Asano, S.; Ishida, J. *J. Phys. F Met. Phys.* **1987**, *17*, 475-82.

(26) Ruehl, R.; Jeitschko, W. *Inorg. Chem.* **1982**, *21*, 1886-91.

(27) Motojima, S.; Haguri, K.; Takahashi, Y.; Sugiyama, K. *J. Less-Common Met.* **1979**, *64*, 101-6.

(28) Motojima, S.; Wakamatsu, T.; Sugiyama, K. *J. Less-Common Met.* **1981**, *82*, 379-83.

(29) Oyama, S. T.; Gott, T.; Zhao, H.; Lee, Y.-K. *Catal. Today* **2009**, *143*, 94-107.

(30) Senevirathne, K.; Burns, A. W.; Bussell, M. E.; Brock, S. L. *Adv. Funct. Mater.* **2007**, *17*, 3933-3939.

(31) Liu, S.; Qian, Y.; Xu, L. *Solid State Commun.* **2009**, *149*, 438-440.

(32) Lewkebandara, T. S.; Winter, C. H. *Chem. Vap. Deposition* **1996**, *2*, 75-7.

(33) Bihler, C.; Kraus, M.; Huebl, H.; Brandt, M. S.; Goennenwein, S. T. B.; Opel, M.; Scarpulla, M. A.; Stone, P. R.; Farshchi, R.; Dubon, O. D. *Phys. Rev. B Condens. Matter Mater. Phys.* **2007**, *75*, 214419/1-214419/9.

(34) Booth, R. A.; Majetich, S. A. *J. Appl. Phys.* **2009**, *105*, 07A926/1-07A926/3.

(35) Keller, L.; Fischer, P.; Furrer, A.; Doenni, A.; Li, D. X.; Suzuki, T. *Physica B (Amsterdam)* **1993**, *186-188*, 553-6.

(36) Burlet, P.; Quezel, S.; Rossat-Mignod, J.; Horyn, R. *Solid State Commun.* **1985**, *55*, 1057-61.

(37) Nozue, T.; Saito, A.; Kobayashi, H.; Yamagami, H.; Kamimura, T. *Physica B (Amsterdam)* **2000**, *284-288*, 1509-1510.

(38) Boyanov, S.; Bernardi, J.; Gillot, F.; Dupont, L.; Womes, M.; Tarascon, J. M.; Monconduit, L.; Doublet, M. L. *Chem. Mater.* **2006**, *18*, 3531-3538.

(39) Boyanov, S.; Womes, M.; Monconduit, L.; Zitoun, D. *Chem. Mater.* **2009**, *21*, 3684-3692.

(40) Odile, J. P.; Soled, S.; Castro, C. A.; Wold, A. *Inorg. Chem.* **1978**, *17*, 283-6.

(41) Ackermann, J.; Wold, A. *J. Phys. Chem. Solids* **1977**, *38*, 1013-16.

(42) Shirotani, I.; Takahashi, E.; Mukai, N.; Nozawa, K.; Kinoshita, M.; Yagi, T.; Suzuki, K.; Enoki, T.; Hino, S. **1993**, *32*, 294-6.

(43) Kim, M. G.; Lee, S.; Cho, J. *J. Electrochem. Soc.* **2009**, *156*, A89-A94.

(44) Pralong, V.; Souza, D. C. S.; Leung, K. T.; Nazar, L. F. *Electrochem. Commun.* **2002**, *4*, 516-520.

(45) Alcantara, R.; Tirado, J. L.; Jumas, J. C.; Monconduit, L.; Olivier-Fourcade, J. *J. Power Sources* **2002**, *109*, 308-312.

(46) Souza, D. C. S.; Pralong, V.; Jacobson, A. J.; Nazar, L. F. *Science* **2002**, *296*, 2012-5.

(47) Tirado, J. L. *Mater. Sci. Eng., R* **2003**, *R40*, 103-136.

(48) Yang, J.; Zhang, Z.-s.; Nuli, Y.-n. *Zhongguo Youse Jinshu Xuebao* **2004**, *14*, 341-344.

(49) Silva, D. C. C.; Crosnier, O.; Ouvrard, G.; Greedan, J.; Safa-Sefat, A.; Nazar, L. F. *Electrochem. Solid-State Lett.* **2003**, *6*, A162-A165.

(50) Wang, K.; Yang, J.; Xie, J.; Wang, B.; Wen, Z. *Electrochem. Commun.* **2003**, *5*, 480-483.

(51) Bernardi, J.; Lemoigno, F.; Doublet, M. L. *Solid State Ionics* **2008**, *14*, 197-202.

(52) Gillot, F.; Boyanov, S.; Dupont, L.; Doublet, M. L.; Morcrette, M.; Monconduit, L.; Tarascon, J. M. *Chem. Mater.* **2005**, *17*, 6327-6337.

(53) Park, C.-M.; Sohn, H.-J. *Chem. Mater.* **2008**, *20*, 6319-6324.

(54) Loevvik, O. M.; Prytz, O. *Phys. Rev. B: Condens. Matter* **2004**, *70*, 195119/1-195119/6.

(55) Shields, V.; Caillat, T.; Fleurial, J.-P.; Zoltan, A.; Zoltan, L.; Tuchscherer, M. *International Conference on Thermoelectrics* **2002**, *21st*, 64-67.

(56) Watcharapasorn, A.; DeMattei, R. C.; Feigelson, R. S.; Caillat, T.; Borshchevsky, A.; Snyder, G. J.; Fleurial, J. P. *J. Appl. Phys.* **1999**, *86*, 6213-6217.

(57) Muller, T. K., T.; Labardi, M.; LuxSteiner, M.; Marti, O.; Mlynek, J.; Krausch, G. *J. Vac. Sci. Technol., B* **1996**, *14*, 1296.

(58) Boda, G.; Stenstrom, B.; Sagredo, V.; Beckman, O.; Carlsson, B.; Rundqvist, S. *Phys. Scr.* **1971**, *4*, 132-4.

(59) Rundqvist, S. *Acta Chem. Scand.* **1961**, *15*, 451-3.

(60) Orishchin, S. V.; Babizhetskii, V. S.; Kuz'ma, Y. B. *Kristallografiya* **2000**, *45*, 974-975.

(61) Donohue, P. C.; Bither, T. A.; Young, H. S. *Inorg. Chem.* **1968**, *7*, 998-1001.

(62) Takacs, L.; Mandal, S. K. *Mater. Sci. Eng., A* **2001**, *A304-306*, 429-433.

(63) Hulliger, F. *Nature (London, U. K.)* **1963**, *200*, 1064-5.

(64) Van Wazer, J. R. *Phosphorus and its Compounds*; Interscience Publishers, Inc.: New York, NY, **1958**.

(65) Threlfall, R. E. *The story of 100 years of phosphorus making, 1851-1951*; Oldbury: Albright and Wilson, Ltd.: UK, **1951**.

(66) Kanatzidis, M. G.; Pottgen, R.; Jeitschko, W. *Angew. Chem. Int. Ed.* **2005**, *44*, 6996-7023.

(67) Shatruk, M. M.; Kovnir, K. A.; Shevelkov, A. V.; Popovkin, B. A. *Angew. Chem. Int. Ed.* **2000**, *39*, 2508-2509.

(68) Braun, D. J.; Jeitschko, W. *Z. Anorg. Allg. Chem.* **1978**, *445*, 157-66.

(69) Kloc, C.; Lux-Steiner, M. C.; Keil, M.; Baumann, J. R.; Doell, G.; Bucher, E. *J. Cryst. Growth* **1990**, *106*, 635-42.

(70) Zhang, Z.; Yang, J.; Nuli, Y.; Wang, B.; Xu, J. *Solid State Ionics* **2005**, *176*, 693-697.

(71) Jeitschko, W.; Donohue, P. C. *Acta Crystallogr., Sect. B: Struct. Sci* **1975**, *B31*, 574-80.

(72) Villars, P. *Pearson's handbook of crystallographic data for intermetallic phases*; ASM International: Materials Park, OH, **1991**.

(73) Zachariasen, W. H. *Acta Crystallographica* **1963**, *16*, 1253-5-.

(74) Ugai, Y. A.; Pshestanchick, V. R.; Anokhin, V. Z.; Gukov, O. Y. *Izvestiya Akademii Nauk SSSR, Neorganicheskie Materialy* **1974**, *10*, 405-8.

(75) Burdett, J. K.; Coddens, B. A. *Inorg. Chem.* **1988**, *27*, 418-21.

(76) Olofsson, O. *Acta Chem. Scand.* **1965**, *19*, 229-41.

(77) Olofsson, O. *Acta Chem. Scand.* **1972**, *26*, 2777-87.

(78) Xie, Y.; Su, H. L.; Qian, X. F.; Liu, X. M.; Qian, Y. T. *J. Solid State Chem.* **2000**, *149*, 88-91.

(79) Knausenberger, M.; Brauer, G.; Gingerich, K. A. *J. Less-Common Met.* **1965**, *8*, 136-48.

(80) Moser, J. B.; Kruger, O. L. *J. Less-Common Met.* **1966**, *10*, 402-7.

(81) Mughal, S. A.; Payne, A. J.; Ray, B. *J. Mater. Sci.* **1969**, *4*, 895-901.

(82) Kaner, R.; Castro, C. A.; Gruska, R. P.; Wold, A. *Mater. Res. Bull.* **1977**, *12*, 1143-7.

(83) Healy, M. D.; Laibinis, P. E.; Stupik, P. D.; Barron, A. R. *J. Chem. Soc., Chem. Commun.* **1989**, 359-60.

(84) Wells, R. L.; Aubuchon, S. R.; Kher, S. S.; Lube, M. S.; White, P. S. *Chem. Mater.* **1995**, *7*, 793-800.

(85) Xie, Y.; Su, H.; Li, B.; Qian, Y. *Mater. Res. Bull.* **2000**, *35*, 675-680.

(86) Kher, S. S.; Wells, R. L. *Chem. Mater.* **1994**, *6*, 2056-62.

(87) Buhro, W. E. *Polyhedron* **1994**, *13*, 1131-48.

(88) Carmalt, C. J.; Morrison, D. E.; Parkin, I. P. *Polyhedron* **2000**, *19*, 829-833.

(89) Su, H. L.; Xie, Y.; Li, B.; Liu, X. M.; Qian, Y. T. *Solid State Ionics* **1999**, *122*, 157-160.

(90) Aitken, J. A.; Ganzha-Hazen, V.; Brock, S. L. *J. Solid State Chem.* **2005**, *178*, 970-975.

(91) Davidson, F. M., III; Wiacek, R.; Korgel, B. A. *Chem. Mater.* **2005**, *17*, 230-233.

(92) Kawasaki, S.-i.; Yan, X.; Sue, K.; Hakuta, Y.; Suzuki, A.; Arai, K. *J. Supercrit. Fluids* **2009**, *50*, 276-282.

(93) Adschiri, T.; Hakuta, Y.; Sue, K.; Arai, K. *J. Nanopart. Res.* **2001**, *3*, 227-235.

(94) Mazurrider, B.; Chirico, P.; Hector, A. L. *Inorg. Chem.* **2008**, *47*, 9684-9690.

(95) Hashimoto, T.; Wu, F.; Speck, J. S.; Nakamura, S. *Jpn. J. Appl. Phys., Part 2* **2007**, *46*, L889-L891.

(96) Demazeau, G.; Goglio, G.; Largeteau, A. *High Pressure Res.* **2008**, *28*, 497-502.

(97) Dean, J. A. *Lange's Handbook of Chemistry*; 14th Edition ed.; McGraw-Hill, Inc.: New York, NY, 1992.

(98) Gregg, K. A.; Perera, S. C.; Lawes, G.; Shinozaki, S.; Brock, S. L. *Chem. Mater.* **2006**, *18*, 879-886.

(99) Park, J.; Koo, B.; Yoon, K. Y.; Hwang, Y.; Kang, M.; Park, J.-G.; Hyeon, T. *J. Am. Chem. Soc.* **2005**, *127*, 8433-8440.

(100) Henkes, A. E.; Schaak, R. E. *Chem. Mater.* **2007**, *19*, 4234-4242.

(101) Henkes, A. E.; Vasquez, Y.; Schaak, R. E. *J. Am. Chem. Soc.* **2007**, *129*, 1896-1897.

(102) Lukehart, C. M.; Milne, S. B.; Stock, S. R. *Chem. Mater.* **1998**, *10*, 903-908.

(103) Tebby, J. C. *Handbook of Phosphorus-31 Nuclear Magnetic Resonance Data*; CRC Press: Boca Raton, FL, **1991**.

(104) Krabbes, G.; Grosismann, G. *Z. Chem.* **1971**, *11*, 270-1.

(105) Li, S.; Cheng, Z.; Yuan, C.; Ma, Y.; Zhong, X. *Phosphorus Sulfur* **1988**, *36*, 53-9.

(106) Sharma, R.; Holland, G. P.; Solomon, V. C.; Zimmermann, H.; Schiffenhaus, S.; Amin, S. A.; Buttry, D. A.; Yarger, J. L. *J. Phys. Chem. C* **2009**, *113*, 16387-16393.

(107) Salavati-Niasari, M.; Dadkhah, M.; Davar, F. *Inorg. Chim. Acta* **2009**, *362*, 3969-3974.

(108) Manura, J. J.; Manura, D. J.; Scientific Instrument Services, Inc.: Ringoes, NJ, **1996-2003**.

(109) Villars, P. *Pearson's handbook of crystallographic data for intermetallic phases.* Materials Park, OH, **1991**; Vol. 1-3.

(110) Mazumder, B.; Hector, A. L. *J. Mater. Chem.* **2008**, *18*, 1392-1398.

(111) Perera, S.; Gillan, E. G. *Solid State Sci.* **2008**, *10*, 864-872.

(112) Choi, J.; Gillan, E. G. *J. Mater. Chem.* **2006**, *16*, 3774-3784.

(113) Zaitseva, N.; Dai, Z. R.; Grant, C. D.; Harper, J.; Saw, C. *Chem. Mater.* **2007**, *19*, 5174-5178.

(114) Thornton, G. *Science (Washington, DC, U. S.)* **2003**, *300*, 1378-1379.

(115) Bell, A. T. *Science* **2003**, *299*, 1688-1691.

(116) Valden, M.; Lai, X.; Goodman, D. W. *Science* **1998**, *281*, 1647-1650.

(117) Huynh, W. U.; Dittmer, J. J.; Alivisatos, A. P. *Science* **2002**, *295*, 2425-2427.

(118) Law, M.; Goldberger, J.; Yang, P. D. *Annu. Rev. Mater. Res.* **2004**, *34*, 83-122.

(119) Ruda, H. E.; Polanyi, J. C.; Yang, J. S. Y.; Wu, Z.; Philipose, U.; Xu, T.; Yang, S.; Kavanagh, K. L.; Liu, J. Q.; Yang, L.; Wang, Y.; Robbie, K.; Yang, J.; Kaminska, K.; Cooke, D. G.; Hegmann, F. A.; Budz, A. J.; Haugen, H. K. *Nanoscale Research Letters* **2006**, *1*, 99-119.

(120) Jeong, U.; Wang, Y.; Ibisate, M.; Xia, Y. *Adv. Funct. Mater.* **2005**, *15*, 1907-1921.

(121) Trindade, T.; Obrien, P. *Adv. Mater.* **1996**, *8*, 161-&.

(122) Trindade, T.; Obrien, P.; Zhang, X. M. *Chem. Mater.* **1997**, *9*, 523-530.

(123) Murray, C. B.; Norris, D. J.; Bawendi, M. G. *J. Am. Chem. Soc.* **1993**, *115*, 8706-8715.

(124) Manna, L.; Wang, L. W.; Cingolani, R.; Alivisatos, A. P. *J. Phys. Chem. B* **2005**, *109*, 6183-6192.

(125) Zhou, X. L.; El Khoury, J. M.; Qu, L. T.; Dai, L. M.; Li, Q. *J. Colloid Interface Sci.* **2007**, *308*, 381-384.

(126) Rogach, A. L.; Franzl, T.; Klar, T. A.; Feldmann, J.; Gaponik, N.; Lesnyak, V.; Shavel, A.; Eychmuller, A.; Rakovich, Y. P.; Donegan, J. F. *J. Phys. Chem. C* **2007**, *111*, 14628-14637.

(127) Barker, A. J.; Cage, B.; Russek, S.; Stoldt, C. R. *J. Appl. Phys.* **2005**, *98*, 7.

(128) Chen, S.; Liu, W. M. *Mater. Chem. Phys.* **2006**, *98*, 183-189.

(129) Lee, S. Y.; Harris, M. T. *J. Colloid Interface Sci.* **2006**, *293*, 401-408.

(130) Barrett, C. A.; Dickinson, C.; Ahmed, S.; Hantschel, T.; Arstila, K.; Ryan, K. M. *Nanotechnology* **2009**, *20*, 8.

(131) Schreuder, M. A.; McBride, J. R.; Dukes, A. D.; Sammons, J. A.; Rosenthal, S. J. *J. Phys. Chem. C* **2009**, *113*, 8169-8176.

(132) Kwon, C. W.; Yoon, T. S.; Yim, S. S.; Park, S. H.; Kim, K. B. *J. Nanopart. Res.* **2009**, *11*, 831-839.

(133) Yin, Y.; Alivisatos, A. P. *Nature* **2005**, *437*, 664-670.

(134) Brock, S. L.; Perera, S. C.; Stamm, K. L. *Chem. Eur. J.* **2004**, *10*, 3364-3371.

(135) Koo, J. P. B.; Hwang, Y.; Bae, C.; An, K.; Park, J. G.; Park, H. M.; Hyeon, T. *Angew. Chem. Int. Ed.* **2004**, *43*, 2282-2285.

(136) Barry, B. M.; Gillan, E. G. *Chem. Mater.* **2008**, *20*, 2618-2620.

(137) Charles D. Wagner, A. V. N., Anna Kraut-Vass, Juanita W. Allison, Cedric J. Powell, John R. Rumble, Jr. *NIST X-ray Photoelectron Spectroscopy Database.* http://srdata.nist.gov/xps/Default.aspx. **2003**.

(138) Klemm, W. *Proceedings of the Chemical Society of London* **1958**, 329-341.

(139) Nefedov, V. I.; Salyn, Y. V.; Domashevskaya, E. P.; Ugai, Y. A.; Terekhov, V. A. *J. Electron. Spectrosc. Relat. Phenom.* **1975**, *6*, 231-238.

(140) Fitzmaurice, J. C.; Hector, A.; Parkin, I. P. *J. Mater. Sci. Lett.* **1994**, *13*, 1-2.

(141) Park, C. M.; Kim, Y. U.; Sohn, H. J. *Chem. Mater.* **2009**, *21*, 5566-5568.

(142) Fujimori, A.; Mamiya, K.; Mizokawa, T.; Miyadai, T.; Sekiguchi, T.; Takahashi, H.; Mori, N.; Suga, S. *Phys. Rev. B Condens. Matter* **1996**, *54*, 16329-16332.